TECHNISCHE UNIVERSITÄT WIEN
Vienna University of Technology

D I P L O M A R B E I T

Selective Oxidation of Ethanol on TiO_2 supported bimetallic Au Ag Catalysts: Kinetics and Characterization

ausgeführt am

Institut für Materialchemie

der Technischen Universität Wien

unter der Anleitung von

Assoc. Prof. Dipl.-Ing. Dr.techn. Karin Föttinger

durch

Melanie Riess

Grundsteingasse 18

1160 Wien

Wien, 29 April 2020

Danksagung

An dieser Stelle möchte ich allen herzlich danken, die mich bei der Erstellung dieser Diplomarbeit unterstützt haben.

Prof. Karin Föttinger danke ich für die Möglichkeit in ihrer Forschungsgruppe zu arbeiten sowie für die Betreuung dieser Diplomarbeit. Zudem möchte ich hier ein Kompliment aussprechen: Der Balance-Akt zwischen zielgerichteten, respektvollen Richtungsweisungen sowie dem Überlassen von genügend Freiheit um persönliches Wachstum zu ermöglichen, erfordert jede Menge Fingerspitzengefühl. Prof. Föttinger hat diese Aufgabe mit jeder Menge Fachwissen in Kombination mit erfrischend viel Geduld und Empathie gemeistert.

Weiters gilt mein Dank meinen Kollegen und Kolleginnen: Dr. Nevzat Yigit, für die häufige Unterstützung bei praktischen Arbeiten im Labor und die vielen einhergehenden Diskussionen. Katharina Rauchenwald, für ihre tatkräftige, praktische Unterstützung sowie das motivierte, tiefgehende Hinterfragen unterschiedlicher Aspekte der Arbeit. DI Markus Latschka, für den vielseitigen fachlichen Input sowie das geduldige Aufmuntern, wenn die Versuche mal doch nicht so liefen, wie erhofft. Dr. Klaus Dobrezberger, für seine Zeit und Expertise im Bereich der Elektronenmikroskopie, die er großzügig geteilt hat. DI Gernot Pacholik dafür, dass auch er stets ein offenes Ohr für mich hatte, fachliche Diskussionen nie scheute und obendrein noch gute Laune versprühte. DI Lorenz Lindenthal, für seine Bemühungen, mir die diskrete Fourier-Transformation verständlicher zu machen und die zuverlässige, konstante Versorgung mit Schokolade. Zuletzt danke ich dem Vorgänger des Projekts: Dr. Andreas Nagl, welcher mir viele seiner Unterlagen und Daten überlassen hat und sich Mühe gab, trotz anderweitiger Verpflichtungen für mich erreichbar zu sein.

Bei meinen Freunden möchte ich mich für die Ablenkung vom Ernst des Studiums durch gemeinsame sportliche und kulturelle Aktivitäten bedanken. Jenen, die mit mir das Studium absolviert haben, danke ich besonders für die Motivation und Hilfe.

Der größte Dank gilt jedoch meiner Familie: meiner Schwester und besonders meinen Eltern, die mich stets unterstützen und mir das Studium überhaupt erst ermöglicht haben.

Abstract

The aim of this thesis was to better understand and further optimize bimetallic Au Ag nanoparticles (NP) supported on TiO_2 as catalyst for the selective gas-phase partial oxidation of ethanol (EtOH) to acetaldehyde (CH_3CHO). The greater goal behind the work is to find a green alternative to fossil based CH_3CHO production.

0.8, 2.5, 4.2 and 7.3 wt% Ag were added onto a commercial 0.8 wt% Au TiO_2 catalyst using incipient wetness impregnation. Kinetic measurements, IR spectroscopy with CO and EtOH as probe molecules, operando DRIFTS measurements and oxygen chemisorption measurements allowed insight into the catalysts' adsorption properties, surface composition and reactivity.

Silver addition leads to an increase in catalytic activity, selectivity towards acetaldehyde, apparent activation energy and ethanol reaction order and a decrease in oxygen reaction order. Effects of the silver addition flatten out with higher loadings: from 0.8 wt% Au 4.2 wt% Ag TiO_2 to 0.7 wt% Au 7.3 wt% Ag TiO_2 hardly any performance alterations are detected. At 400 °C, an ethanol conversion of 99.7 % with a selectivity towards acetaldehyde of 99 % is achieved with 0.8 wt% Au 4.2 wt% Ag TiO_2.

In accordance with literature reports, our oxygen chemisorption and FTIR results of CO adsorption suggest a coverage of the Ag by TiO_{2-x}. Owing to the bimetallic character of the particles, Au is also affected by the migration of TiO_{2-x}.

FTIR measurements with EtOH as probe molecule reveal that more ethoxy groups adsorb bidentate on Au Ag TiO_2 than on TiO_2 and Au TiO_2, likely due to a locally high concentration of oxygen vacancies in the TiO_{2-x} regions around the Au Ag bimetallic NP.

Zusammenfassung

Ziel dieser Arbeit war es, bimetallische Au Ag Nanopartikel (NP) auf TiO_2 als Katalysator für die selektive partielle Gasphasenoxidation von Ethanol zu Acetaldehyd besser zu verstehen und weiter zu optimieren. Eine nachhaltigere Alternative zur heutzutage üblichen Acetaldehyd Produktion auf Erdölbasis wird angestrebt.

Ein kommerzieller 0.8 m% Au TiO_2 Katalysator wurde mit 0.8, 2.5, 4.2 und 7.3 m% Ag imprägniert. Kinetische Messungen, IR-Spektroskopie mit CO und EtOH als Sondenmoleküle, Operando-DRIFTS-Messungen und O_2-Chemisorptionsmessungen ermöglichten Einblicke in die Adsorptionseigenschaften, die Oberflächenzusammensetzung und die Reaktivität der Katalysatoren.

Die Zugabe von Silber führt zu einer Zunahme der katalytischen Aktivität, Selektivität zu Acetaldehyd, Aktivierungsenergie und Ethanol-Reaktionsordnung und einer Abnahme der Sauerstoff-Reaktionsordnung. Die Effekte der Silberzugabe flachen ab: von 0.8 m% Au 4.2 m% Ag TiO_2 zu 0.7 m% Au 7.3 m% Ag TiO_2 werden kaum Veränderungen festgestellt. Bei 400 ° C wird mit 0.8 m% Au 4.2 m% Ag TiO_2 eine Ethanolumwandlung von 99.7 % mit einer Acetaldehyd Selektivität von 99 % erreicht.

In Übereinstimmung mit Literaturberichten legen unsere Ergebnisse der Sauerstoffchemisorption und der FTIR überwachten CO-Adsorption eine Bedeckung des Ag durch TiO_{2-x} nahe. Aufgrund des bimetallischen Charakters der NP wird auch Au von der Migration des TiO_{2-x} betroffen.

FTIR-Messungen mit EtOH als Sondenmolekül zeigen, dass mehr Ethoxygruppen bidentat an Au Ag TiO_2 adsorbieren als an TiO_2 und Au TiO_2, was auf eine lokal hohe Konzentration von Sauerstoffleerstellen in den TiO_{2-x}-Filmen rund um die bimetallischen Au Ag NP zurückzuführen ist.

Table of Contents

1. Introduction

Importance of acetaldehyde as platform chemical in the past, present and future

Two million tons of acetaldehyde are produced per year, owing to its versatile use in industry: acetaldehyde serves as precursor in the production of pyridine derivatives, pentaerythritol, crotonaldehyde, ethylidene diacetate (which is a precursor to vinyl acetate). [1]

On industrial scale, acetaldehyde is generated by oxidation of ethylene – which is manufactured in large scale by the petroleum industry by steam cracking of naphtha. Substituting fossils with bio-feedstock (preferably second-generation biomass to avoid competition with food industry) is indisputably crucial for the present and future generations. Thus, working solvent-free, using (bio)ethanol as renewable feedstock and molecular oxygen as non-hazardous, safe oxidant conforms with the *Green Chemistry* approach. Finding a cost-effective way to produce acetaldehyde sustainably from ethanol opens the path to a versatile, biomass-based, sustainable platform chemical, which therefore has the potential to outplay different fossil-based platform chemicals and may therefore even increase the industrial demand for acetaldehyde. [1] [2]

One potential application may be returning to the traditional production of acetic acid from acetaldehyde. Acetic acid is in use as solvent, and for production of vinyl acetate monomer, cellulose acetate, acetic anhydride, acetate esters, terephthalic acid, monochloroacetic acid, and more – over 80 % of produced acetic acid are used in the polymer industry. Demand of acetic acid totals up to 13 million tons annually (per 2015), whereas it used to be generated by oxidation of acetaldehyde, nowadays, due to cost-efficiency, it is manufactured in the Monsanto process (using a Rh-complex catalyst) or the Cavita process (using an Ir-complex catalyst), by oxidation of methanol. Both processes rely on fossil-based carbon and require toxic and corrosive additives, like HI as co-catalyst. [3] Likewise, n-butyraldehyde used to be manufactured from acetaldehyde, is nowadays however mainly generated by hydroformylation of propylene. Acetaldehyde moreover occurs as intermediate in many more processes, e.g. in the production of ethyl acetate, peracetic acid, butanol, 2-ethylhexanol, chlorinated acetaldehydes (chloral),

glyoxal, alkyl amines, and more. Potential applications therefore exist in great quantities. [1]

2. Theoretical Background

2.1. Gold catalysts and their role in ethanol oxidation

Ever since the discovery of gold nanoparticles' (NP) catalytic activity and selectivity in the 1980s, numerous reactions over Au have been studied thoroughly and demonstrated exceptional catalytic properties of Au, mainly for nanoparticles below 10 nm in size (Zheng et al. and Guan et al. reported gold nanoparticles of 6 nm in size are more active than smaller or larger particles, in a range of 1.7 to 15 nm [4] [5]). Au nanoparticles show promising catalytic performance for example in CO oxidation, the water gas shift reaction, selective hydrogenation (hydrogenation of dienes or alkynes to alkenes), direct synthesis of vinyl chloride from ethyne with hydrogen chloride, conversion of propene with molecular oxygen to propene oxide, direct production of hydrogen peroxide ($H_2 + O_2 \rightarrow H_2O_2$), oxidation of cyclohexane to cyclohexanol and cyclohexanone and epoxidation of propylene – and that often at lower temperatures than other commercial catalysts. A reducible support is beneficial in many cases. [2] [6] [7] [8]

In previous work done in the research group, Nagl et al. (2019) investigated the selective gas-phase partial oxidation of ethanol to acetaldehyde: (bimetallic) gold catalysts on different supports were examined. Au on TiO_2 (both anatase and rutile), ZnO, Al_2O_3 and C were tested, whereas gold supported on rutile delivered the most promising results with highest activity and highest selectivity (> 97 %) towards acetaldehyde. Ag, Ru and Pt were tested as promoter metals, whereof Ag exhibited the best performance improvements. XAS at the Au LIII edge showed that gold remains in its metallic form during the reaction, while for the Ag K edge it was found that around 50 % of Ag in 5 wt% Au 1 wt% Ag Rutile and 40 % in 1 wt% Ag Rutile are oxidized under reaction conditions. With NAP-XPS, however, a depletion of Ag from the surface was monitored and under dehydrogenation conditions, an increased amount of Ti^{3+} was revealed. [2]

In ethanol oxidation, the presence of gold nanoparticles facilitates the rate limiting β-H elimination of adsorbed ethoxy groups. [7] Biella et al. reported in 2003, that for both primary and secondary alcohols, oxidation over Au nanoparticles on silica in gas-phase delivers the respective aldehyde or ketone, while oxidation in liquid phase produces carboxylates. [9] This was confirmed for ethanol oxidation over Au nanoparticles on TiO_2 by respective gas-phase investigation from Nagl et al. and research performed in liquid-phase by Mostrou-Moser et al.. [2] [3]

A possible explanation for the different performances can be found in work published in 2010 by Zope et al., who proposed, that selective oxidation of alcohols in liquid-phase over various gold and platinum catalysts is promoted by high-pH conditions. Using $^{18}O_2$ and $H_2{}^{18}O$ and confirming the results by density functional theory (DFT) calculations, Zope et al. reported, that during ethanol oxidation in liquid-phase, not the oxygen atoms from dissociated O_2, but instead the oxygen atoms from hydroxide ions are incorporated into the alcohol, while the molecular oxygen instead regenerates the hydroxide ions. [10]

In gas-phase, on the other hand, DFT calculations carried out by J. E. de Vrieze, resulted in the conclusion, that O-H scission and proton transfer from ethanol to atomic oxygen, surface hydroxyl species (which are formed in the mentioned proton transfer from ethanol to atomic oxygen), molecular oxygen, and hydroperoxyl species are all taking place and are all rate-limiting. [2]

The conclusion that different reaction mechanisms dominate the liquid- and the gas-phase reaction is supported by the conclusions drawn for the most-suitable promoter metal: Nagl et al. reported silver to be the most promising promoter metal (compared to Ru and Pt, whereas Au Ru performs better than Au Pt) for selective ethanol oxidation in gas-phase over Au on TiO_2. [2] Mostrou-Moser et al. investigated the liquid-phase reaction and concluded that for performance enhancement, Au Pt is preferred over Au Ru, while Au Ag delivered the worst results. [2] [3]

2.2. Oxygen activation and the role of titanium oxide and silver

Whether gold nanoparticles activate molecular oxygen or not, has been a controversially discussed topic. However, research done in the last two decades seems to agree that gold indeed is able to promote O_2 dissociation – at least once atomic oxygen is present on the

Au(111) facet. However, even then, activation of molecular oxygen happens on Au in a much less efficient manner than e.g. on Ag or Cu. [11] [12] Often, the oxygen activation is ascribed to a metal oxide support. [2] [13]

2.2.1. Au-assisted Mars-van Krevelen mechanism

Widmann et al. introduced the term "Au-assisted Mars-van Krevelen mechanism" in 2011, proposing the following mechanism for CO oxidation on Au TiO_2 catalysts at temperatures above 80 °C: firstly, CO adsorbs on the Au NP, which then reacts with activated surface lattice oxygen species at the perimeter of the Au TiO_2 interface. At last, those interface sites get replenished by dissociative adsorption of O_2. [14] Kim et al. worked with Au nanoclusters on $CeO_2(111)$ and reported in 2013 the CO_2 desorption to be the rate-limiting step. [15] Widmann et al. reported the removal of the activated surface lattice oxygen by CO to be the rate-limiting step in 2018 (again working on Au TiO_2). [16] Schlexer et al. published a work in 2018, confirming a significant reduction of the oxygen vacancy formation energies by up to 2.2 eV at the Au Anatase (101) interface perimeter compared to the gold-free anatase surface (atomistic reaction models based on DFT calculations). Au NP's ability to accommodate excess electrons stabilizes the vacancies, or in other words, charge transfer from the vacancy to the Au NP occurs and is ascribed to be the reason for the decrease of the vacancy formation energies. Moreover, Schlexer et al. agreed (based on calculations) that the reactive removal of surface lattice oxygen is the rate determining step and measurements concluded that the re-oxidation process of TiO_{2-x} proceeds barrierless. Computational results demonstrate that a high vacancy concentration is needed for a barrierless re-oxidation: two adjacent vacancies at the perimeter enable the O_2 molecule to split spontaneously and refill both vacancies. Replenishment of a single oxygen vacancy (including formation of one oxygen adatom O_{ad}), however, leads to a significantly increased barrier for the re-oxidation process. [17]

2.2.2. Strong metal support interaction

In 2005, Goodman -after publications had reported a strong bonding between Au and reduced Ti atoms, resulting in electron-rich Au and stressing the importance of reduced Ti defect sites- drew a connection between exceptionally active Au on titania and the SMSI (strong metal support interaction) effect. Goodman thereby focused on electronic effects:

charge transfer and therefor activation of both the metal NP component and the transition metal oxide support show reason to consider the highly active Au TiO_2 in context of the extensively studied SMSI. However, Goodman stressed, that there is no migration of a TiO_x layer onto the Au NP, arguing, that this could be a feature of Group VIII noble metals on reducible transition metal oxide, but not of Au on reducible transition metal oxide. [18]

The SMSI effect was first introduced in the late seventies, when CO and H_2 chemisorption suppression on titania supported metals was correlated with the temperature of their reduction: high temperature reduction (HTR) above 300 °C was noted to suppress chemisorption abilities of Group VIII noble metals on TiO_2, while low temperature reduction (LTR) does not affect chemisorption properties. Soon the SMSI effect was known to affect many catalytic reactions – e.g., increasing methanation and decreasing hydrogenolysis activity. It is ascribed to electron transfer from the reduced transition metal oxide support (TiO_2, CeO_2) to the metal. However, many phenomena cannot only be explained by charge-transfer, but in combination with the geometrical factor of encapsulation of the metal nanoparticle by the support. For TiO_2, that means migration of suboxide TiO_{2-x} onto the metal NP/clusters. The encapsulation is reversible under oxidative conditions. However, initial formation of the suboxide phase on the metal NP is needed, for it to reach an altervalent state of being reduced and oxidized by different reaction partners. [19] Fu et al. suggested that the encapsulation is thermodynamically driven and occurs, when the metals work function and surface energy are large and the surface energy can be minimized by encapsulation. Encapsulation by TiO_{2-x} has been reported numerous times for Fe, Co, Rh, Ir, Ni, Pd, and Pt, however, to the authors best knowledge, not for Au. [19] [20] [21] [22] [23]

Silver NP, on the other hand, have been reported to be encapsulated by TiO_{2-x}. Claus et al. published a report in 1999, that included HRTEM images showing already a partly coverage of the Ag NP on the Ag TiO_2 LTR catalyst (reduced at 200 °C) and complete encapsulation by amorphous layers at the HTR catalyst (reduced at 500 °C). The LTR Ag NP are reported to have a mean diameter of 2.8 ± 1.9 nm, while the HTR Ag NP show a higher dispersion with a mean diameter of 1.4 ± 0.5 nm. However, oxygen chemisorption measurements resulted in a 30 % decrease from the LTR to the HTR catalyst due to extended coverage of the Ag NP. Claus et al. worked with 7 wt% Ag on TiO_2 (P25 Degussa), prepared by incipient wetness technique. LTR and HTR treatments did not result in

textures changes: identical BET surface areas (35 $m^2 g^{-1}$), pore volumes (0.24 $cm^3 g^{-1}$) and pore diameters (24 nm) were obtained. [24] [25]

Grabchenko et al. [20] and Mamontov et al. [26] worked on ethanol dehydrogenation over Ag CeO_2 SiO_2 catalysts and reported the following: a) Ag NP facilitate surface reduction of CeO_2, leading to an increased amount of oxygen vacancies in CeO_2. The Ce-O bond energy is reduced, while the positive charge on $Ag^{\delta+}$ is increased. b) Thus, the charge transfer moreover provides increased charge of Lewis sites ($Ag^{\delta+}$), and facilitates adsorption of ethanol as ethoxy intermediate, and breakage of the β-C-H bond. Therefore, both described effects of the charge-transfer promote the reaction. Under oxidative conditions, a spillover of active oxygen species from ceria to the silver NP may also contribute to the increase of activity.

Liu et al. reported in 2005 about the exceptionally high activity of Au Ag alloy nanocatalysts (supported on mesoporous aluminosilicate) in CO oxidation. The size of the metal nanoparticles is reported to no longer be a critical factor. A synergistic effect is assumed, whereas silver is believed to play a key role in oxygen activation. [27]

2.3. The reaction mechanism of partial ethanol oxidation over gold catalysts

Numerous studies agree that the initial step in the ethanol oxidation reaction is the formation of ethoxy via O-H bond cleavage. [28] [29] [30] [31] [32]

The potential counterpart of the ethoxy pathway - the alkyl pathway - was calculated (by DFT calculations for ethanol oxidation on Au(111)) to have a higher energy barrier of 171 kJ mol^{-1} in contrast to 144 kJ mol^{-1} for the ethoxy pathway. Once atomic oxygen is available, however, the energy barrier for ethoxy formation drops down to 15 kJ mol^{-1}, and for the alkoxy pathway down to 73 kJ mol^{-1}. [2]

For liquid-phase partial oxidation of ethanol over Au TiO_2, Jørgensen et al. proposed the mechanism depicted in Figure 1 in 2007. Ethanol dehydrogenation forms ethoxy, which then either oxidizes to CO_2 or forms acetaldehyde. Further oxidation of acetaldehyde leads to acetic acid. Furthermore, ethyl acetate forms due to esterification of acetic acid with ethanol. Further oxidation of acetic acid to CO_2 was neglected. Ethanol dehydrogenation (k1) is thought to be the rate-limiting step. [29]

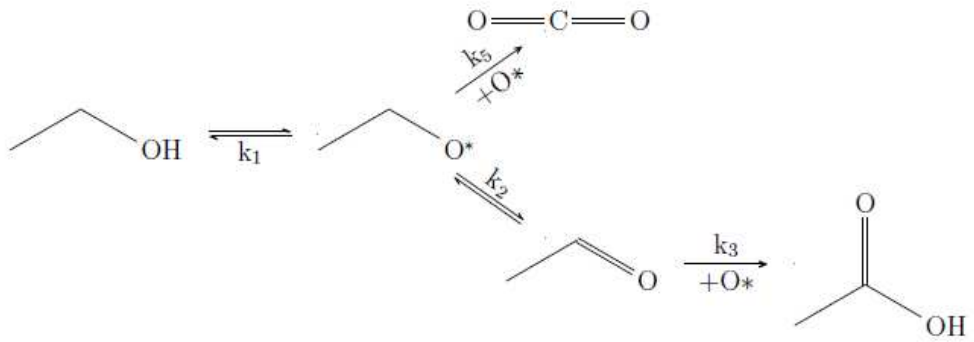

Figure 1 (Partial) ethanol oxidation as proposed by Jørgensen et al. [29]

Liu et al., who also worked on partial ethanol oxidation over Au catalysts, proposed the mechanism shown in Figure 2, and included further oxidation of acetic acid to CO_2 and linked esterification, oxidative dehydrogenation to acetaldehyde, acetic acid production, and combustion: Ethanol adsorbs as ethoxy species, (releasing H_2O in presence of oxygen) which then reacts to acetaldehyde. Adsorbed acetaldehyde then may react either with adsorbed ethoxy to gas-phase ethyl acetate, or with oxygen to adsorbed acetate species. Adsorbed acetate species may form gas-phase acetic acid or are oxidized to gas-phase CO_2. [30]

$$2CH_3CH_2OH + O_{(a)} \rightarrow 2CH_3CH_2O_{(a)} + H_2O \quad (1)$$

$$CH_3CH_2O_{(a)} \rightarrow CH_3CHO_{(a)} + H_{(a)} \quad (2)$$

$$CH_3CHO_{(a)} + CH_3CH_2O_{(a)} \rightarrow CH_3COOCH_2CH_{3(g)} + H_{(a)} \quad (3)$$

$$CH_3CHO_{(a)} + O_{(a)} \rightarrow CH_3COO_{(a)} + H_{(a)} \quad (4)$$

$$2H_{(a)} + O_{(a)} \rightarrow H_2O_{(a)} \rightarrow H_2O_{(g)} \text{ (fast)} \quad (5)$$

$$2CH_3COO_{(a)} \rightarrow CH_2{=}C{=}O_{(g)} + CH_3COOH_{(g)} + O_{(a)} \quad (6)$$

$$2CH_3COO_{(a)} + 7O_{(a)} \rightarrow 4CO_{2(g)} + 3H_2O_{(g)} \quad (7)$$

Figure 2 (Partial) ethanol oxidation as proposed by Liu et al., whereas (a) marks adsorbed species and (g) species in gas phase. [30]

2.4. Titanium dioxide – Rutile versus Anatase

Nagl et al. concluded rutile to be significantly more active in ethanol oxidation than anatase or P25 (which usually consists of 70-90 % anatase and 10-30 % rutile). Adding metal onto the different TiO_2 modifications results in the same trend. [2]

In photocatalytic processes, anatase generally is the more active TiO_2 modification, due to it being a stronger oxidant. The more stable rutile, however, shows a better oxygen adsorption at the surface: in anatase, oxygen vacancies (where molecular oxygen primarily interacts with the TiO_2 surface) are located beneath its most stable (101) facets. This is not the case for rutile's most stable facet (110), where oxygen vacancies are more accessible and molecular oxygen therefore interacts more strongly. Increased oxygen adsorption and a lower redox potential of the excited electron lead to rutile being particularly useful for activation of molecular oxygen. Adsorption of molecular oxygen leads to electron transfer from the surface defects, resulting in the formation of superoxide anion. Rutile is therefor often used for partial oxidation reactions that involve superoxide radicals or singlet oxygen. [19] [23] [33]

3. Experimental

3.1. Catalyst synthesis

Gold nanoparticles on titanium dioxide extrudates named Aurolite™ Au TiO_2 are commercially available from Strem Chemicals (CAS number: 7440-57-5). Laser ablation in liquids leads to ligand-, surfactant- and reactant-free catalysts.

For this thesis Aurolite™ Au TiO_2 with a metal loading of 0.8 wt% Au TiO_2 was used as starting material. Subsequently, silver was added using incipient wetness impregnation: Silver nitrate $AgNO_3$ (puriss., K15600412, purchased from Merck KGaA, Darmstadt, Germany) was diluted in deionized water and carefully dripped onto Aurolite. Around 2 mL of water were used per gram Aurolite to fill its pore volume. The wet powder was then stirred at 50 °C for 4 hours, and afterwards dried at 100 °C for around 18 hours. Both of those steps were carried out in the dark. The so prepared catalysts were stored in the dark at 25 °C.

For the preparation of non-Aurolite references, either rutile or anatase or the commercially available P25 (a mixture of both modifications) was used. TP Hombikat Mikrorutil (Venator, BET surface area 105 m^2/g), anatase nanopowder (Sigma Aldrich, 45-55 m^2/g), and AEROXIDE® P25 TiO_2 (35-65 m^2/g with an anatase/rutile ratio of approximately 80/20, Evonik Industries) were obtained for this reason. The TiO_2 was calcinated at 450 °C for 4 hours before the metals were added.

For addition of gold, deposition-precipitation with urea was chosen as suitable method. Under vigorous stirring $HAuCl_4 \cdot 3\ H_2O$ (Sigma Aldrich, LOT#MKBX5428V) was added to 0.84 M urea (puriss., LOT# K16691086, purchased from Merck KGaA, Darmstadt, Germany) at 80 °C in 100 mL deionized water per gram catalyst. The calcinated TiO_2 support was added. The reaction mixture was kept under stirring, in the dark, for 4 hours. The product was then separated by centrifugation (4500 rpm/3260 RFC) and washed with deionized water five times. An overnight drying step at 110 °C concluded the synthesis. Eventually, silver was added with the above described incipient wetness method.

3.2. Catalyst pretreatment

In previous work of the group and also in this work (unless stated otherwise) the Au Ag TiO_2 catalysts were pretreated as follows:

Pretreatment starts with an oxidative cleaning step. For that, under 20 % O_2 in He the catalysts are heated up to 400 °C with a heating ramp of 10 °C min^{-1}. Afterwards, the catalyst is cooled down and held at 300 °C for 30 min under 5 % H_2 in He to activate the metals. It was shown for Au TiO_2 catalysts, that removing either the oxidative step or the reductive step resulted in significantly reduced catalytic activity. [2] [8] [34]

However, in 2012 it was reported by M. Rothensteiner et al., who tracked XANES spectra of a 4 wt% Au 1 wt% Ag P25 catalyst during a temperature programmed reduction, that the reduction of Ag is completed at 140 °C and reduction of Au at 180 °C respectively. [8]

3.3. TEM Measurements

The particle size distributions were established by STEM-HAADF imaging using a non-aberration corrected FEI Tecnai F20 FEG-TEM instrument (operated at 200 kV) equipped

with an EDAX Octance SDD EDX system and a GATAN GIF Tridiem spectrometer and a high-brightness XFEG. Samples were imaged on lacey carbon grids.

The particle size distributions were evaluated with the image processing programs Gatan Digital Micrograph and ImageJ. By differentiating the contrast in the HAADF images the program determines particles and their area and subsequently mean diameters were calculated by assuming spherical particles.

3.4. Kinetic Screenings

Kinetic measurements were carried out in a fixed bed quartz reactor with continuous flow under atmospheric pressure. Ethanol was introduced by bubbling He through a liquid-vapor saturator that was kept at different temperatures. A flow diagram of the setup is shown in Figure 3. The mass flow controllers, mks 247 (MKS Instruments), were controlled by a microcontroller Arduino Leonardo ETH (Arduino) in combination with a 16 bit AD5696 DAC (Analog Devices) with a custom software allowing automated programming of the gas flows, making them highly reproducible measurements.

The furnace was controlled by a Eurotherm 3216 PID (Eurotherm/Schneider Electric) controller, with the type K thermocouple located inside the reactor.

The quantitative analysis of the exhaust gas flow was conducted using an Agilent 7890A GC (equipped with an FID and a TCD detector) setup for two column-use (Agilent HP PLOT-Q and an HP-PLOT Molsieve). On-line monitoring of the reaction was done by mass spectrometry (Pfeiffer Vacuum OmniStar GSD 320 O mass spectrometer).

The reproducibility of the kinetic experiments was tested by screening one spot sample of two catalysts 6 times in a row. The standard deviations (STD) for the ethanol conversion was calculated for each measured temperature, the mean relative standard deviation (RSTD) results in 7.5 ± 3.3 %. Those deviations could be caused by fluctuations of the gas flows, the cooling of the EtOH saturator or the furnace temperature.

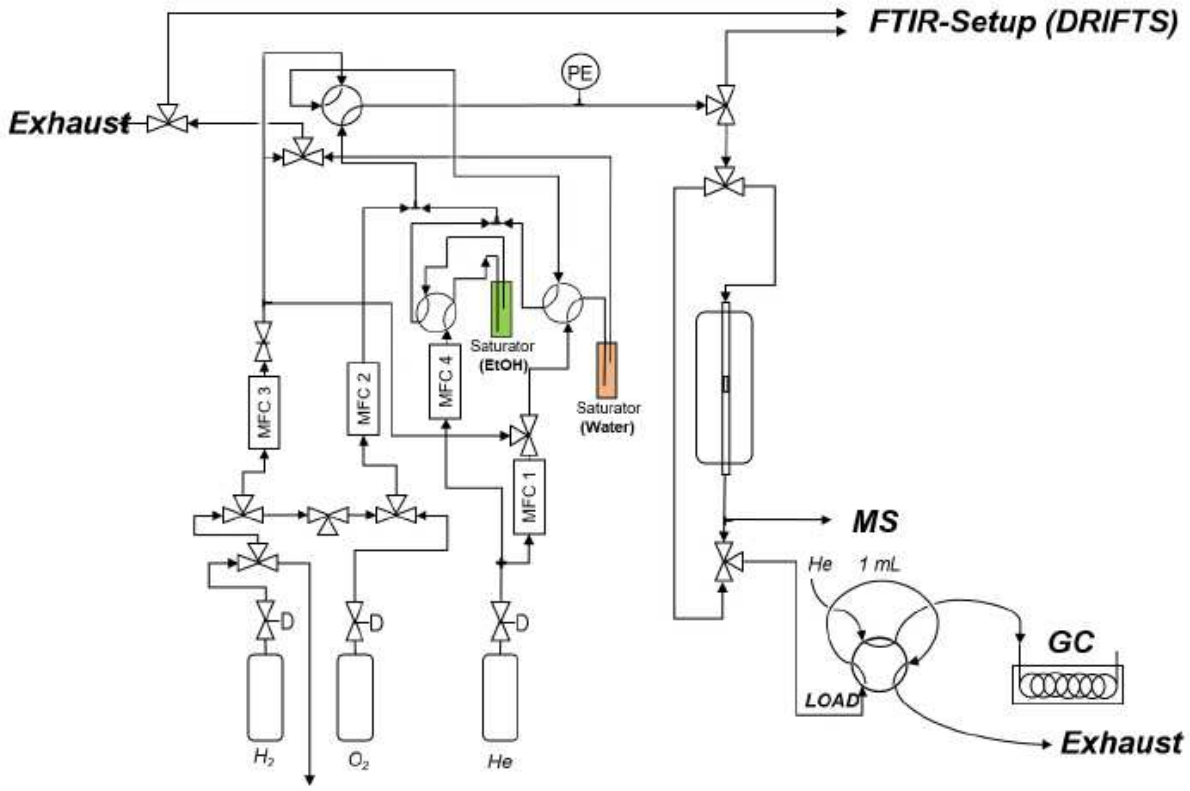

Figure 3 Flow diagram of the kinetic setup. Four mass flow controllers, two for He, one for H_2 and one for O_2 allow the dosage of the gases at the defined flow rates. Two saturators allow dosing of liquids (as vapors). For the reactions, one was used for EtOH whereas the other one (for H_2O) was not used within this thesis. Effluent gases are analyzed by an Agilent 7890A GC (equipped with an FID and a TCD detector) with two columns (Agilent HP PLOT-Q and an HP-PLOT Molsieve). On-line-monitoring was done by mass spectrometry (Pfeiffer Vacuum OmniStar GSD 320 O mass spectrometer). Gas-flows can be directed to the FTIR setup to conduct operando DRIFTS measurements.

3.4.1. Determination of Catalytic Activities and Selectivities

The catalysts were diluted with quartz sand to avoid mass and heat transfer limitations. Catalytic activity evaluation was usually done with 1 mg of the catalysts diluted with quartz sand to up to 100 mg. EtOH was introduced by bubbling 49.0 mL min^{-1} He through a liquid-vapor saturator, filled with absolute ethanol and kept at 5 °C. A total flow of 51.2 mL min^{-1} with 1.1 mL min^{-1} EtOH and 1.1 mL min^{-1} O_2 diluted in He, was employed, resulting in a partial pressure of 2.2 kPa each and therefore a 1:1 ratio of the educts. All used gases had a ≥ 99.9990 Vol% purity and were provided by the Messer group. Temperatures between 150 and 300 °C (in steps of 25°C) were applied, starting with the highest temperature of 300 °C and randomly choosing the order of the following, lower reaction temperatures. An irreversible deactivation at higher temperatures was reported by M. Rothensteiner et al. [35] (probably due to morphological changes of the metal

particles. Sintering as the reason was excluded due to results of TEM measurements). Therefor it was chosen to consistently start with the highest temperature of 300 °C.

3.4.2. Determination of Reaction Orders

Reaction order measurements were performed by keeping one educt stream constant while varying the second educt stream. For the O_2 reaction order, the O_2 partial pressure was varied between 1.1 kPa and 8.2 kPa, starting with the lowest value and increasing the flow in a slightly randomized order. Meanwhile, the EtOH partial pressure was kept constant at 2.2 kPa. The EtOH reaction orders were established with EtOH partial pressures ranging from 0.5 kPa to 4.5 kPa, again starting with the lowest value and increasing it in a slightly randomized order, while the O_2 partial pressure was kept constant at 10 kPa. In both cases, the total flow was kept at approx. 51 mL min^{-1}. The detailed flow settings are listed in the appendix on pages 102 and 103. Samples were measured in a conversion regime below 20% (unless stated otherwise) to ensure that the system was in differential conversion regime.

3.5. Ex-situ Vacuum Transmission Cell Infrared Spectroscopy

Transmission FTIR measurements were carried out on a Bruker Vertex 70 spectrometer with a resolution of 4 cm^{-1}. The instrument is constantly purged with dry air and equipped with a globar light source and a mercury cadmium telluride (MCT) detector. Typically, for a good signal/noise ratio, 128 or 256 scans were added to a spectrum.

The FTIR vacuum cell is equipped with CaF_2 windows. A pressure of approximately 10^{-6} mbar can be reached with a rotary vane pump and a Pfeiffer Vacuum turbomolecular pump. A pellet of the sample is prepared and introduced into the cell in a sample holder that is equipped with a heating wire and a type K NiCr/NiAl Thermocoax thermocouple that are connected to a Eurotherm 902 temperature controller. The sample holder can be cooled down via a cooling loop. Gases and vapors can be introduced into the cell via a leak valve. The pressure in the chamber is monitored by a MKS Baratron type 626 pressure gauge for pressures above 1 mbar.

It must be mentioned that absolute intensities of absorption peaks are hardly comparable when different pellets are used due to their varying thicknesses. In addition, the

temperature in the pellet may deviate from the temperature measured on the sample holder.

After mounting the sample, temperature programmed oxidation in 20 % O_2 in He at 400 °C for 30 min was followed by temperature programmed reduction in 5 % H_2 in He at 300 °C for 30 min. The cell was evacuated and cooled down to room temperature.

3.5.1. Ethanol Adsorption and Desorption

For EtOH adsorption, the cell was cooled down to 20 °C. Absolute EtOH was cleaned from dissolved gases by freeze-pump-thaw procedure carried out three times in a row. Subsequently 5 mbar EtOH vapor were introduced into the cell and held for 10 min. After evacuation the heating ramp of 10 °C min^{-1} up to 600 °C was started. Spectra were taken before and during pretreatment, EtOH adsorption and EtOH desorption during heating.

3.5.2. CO Adsorption

For CO adsorption, the FTIR transmission cell was cooled down to below -100 °C by purging the cooling loop with liquid nitrogen. Subsequently 5 mbar CO were introduced and held in the cell for 10 min, afterwards the cell was evacuated and the desorption of the CO was tracked. Spectra were taken before and during pretreatment, during cooling down, CO adsorption and CO desorption.

3.6. In-situ DRIFTS Measurements

Diffuse reflectance infrared Fourier transform spectroscopy (DRIFTS) measurements were carried out on a Bruker Vertex 70 FTIR equipped with a MCT detector and a Pike DiffuseIR, including a heatable environmental chamber with gas-flow capabilities and a CaF_2 window.

The undiluted, powdered catalysts were placed into an Al_2O_3 sample cup and the powders' surface was smoothed. The sample cup is equipped with a porous bottom, allowing gases to traverse. Therefore, reactant gases enter the chamber, traverse through the powdered sample, through the bottom of the sample cup and exit the chamber to be monitored by mass spectrometry (Pfeiffer Vacuum OmniStar GSD 320 O mass spectrometer). The

exhaust flow was then forwarded to an Agilent 7890A GC (equipped with an FID and a TCD detector) setup for two column-use (Agilent HP PLOT-Q and an HP-PLOT Molsieve).

The same flows as for the catalytic activity evaluation described in section 3.4.1 were applied: EtOH was introduced by sending the He flow of 49 mL min^{-1} through a saturator filled with EtOH, set to 5 °C. Both EtOH and O_2 partial pressures amount to 2.2 kPa = 1.1 mL min^{-1} each, resulting in a total flow of approximately 51 mL min^{-1}. Spectra were taken before, during and after the pretreatment. Afterwards, the desired reaction temperature was employed. Heating was done under He. Spectra were taken before the reaction (under He), under EtOH only, under EtOH & O_2 and after the reaction (under He) at the respective temperatures. Each step was only completed as soon as the taken IR spectra and MS signals confirmed steady state was reached. Once steady state was reached, a GC measurement was carried out.

As background, the cell equipped with an Al-alignment mirror purged with He, was used. Spectra were taken from 4000 to 900 cm^{-1} with a resolution of 4 cm^{-1}.

3.7. Modulation excitation Spectroscopy (MES)

3.7.1. Theory behind MES

When exposing a reaction to a periodic variation of a limiting parameter, reversibly formed products of that reaction will oscillate in the same frequency as that parameter. There may be a phase delay between stimulation and reaction in the time-resolved spectrum. Information about the kinetics of the reaction and potential intermediates can be obtained from that phase delay. However, as can be seen in Figure 4, it should be noted that the system only reaches a quasi-steady state after a few periods after beginning the modulation. [36]

One speaks of Modulation Excitation Spectroscopy (MES). The stimulation can occur by varying the temperature, pH, concentration or other parameters. With many variable parameters and ideally high-resolution spectra, MES becomes a powerful tool. [37]

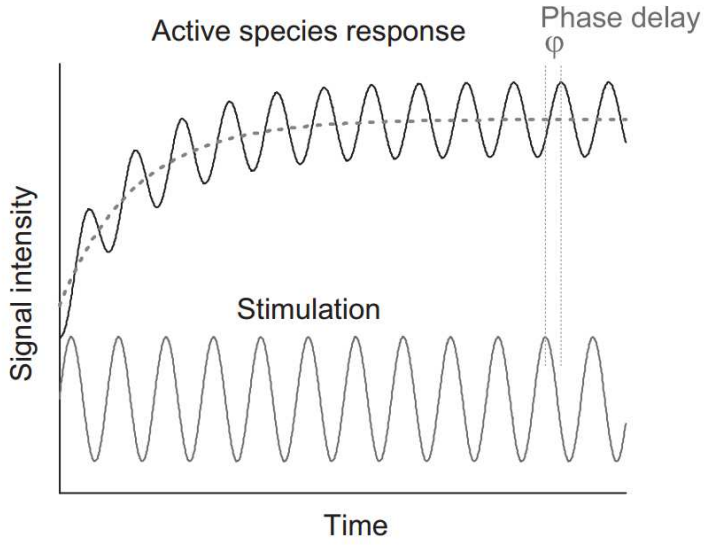

Figure 4 Reaching a quasi-stationary state of the response signals after the start of the stimulation and qualitatively drawn phase shift between the stimulation and response signals. Image taken from Urakawa et al. (2003). [37]

A mathematical tool called phase sensitive detection (PSD), is used for data evaluation and sensitivity improvement, which uses the averaged response signals to separate or demodulate the spectra dependent on their phase shifts. The underlying formula can be found in the following equation:

$$A_k\left(\phi_k^{PSD}\right) = \frac{2}{T}\int_0^T (A(t)\sin(k\omega t + \phi_k^{PSD})dt \qquad \text{with } k=1,2,\ldots$$

A_k represents the mean absolute amplitude and $\phi_k{}^{PSD}$ the mean phase shift in the spectroscopic modulation experiment.

In IR spectroscopy, reactions are usually tracked and depicted as time-resolved spectra: spectra are taken and compared to one another, as it is portrayed in Figure 5 a). If the signals are weak or overlay one another, they will not be noticed in traditional time-resolved spectra. Also, short-lived intermediates might not be measured at all. Often, difference spectra are used for tracking slight differences (as seen in Figure 5 b)). However, highly complex difference spectra might be the result, which are difficult (to impossible) to interpret due to being highly sensitive to the slightest changes and background noise. However, the phase-resolved absorption spectrum (as depicted in Figure 5 c)) portrays the intensity versus the wavenumber for different phase shifts. PSD is a so-called narrow-band technique. Only periodic signals are amplified. In contrast, strong, static signals are deleted. This allows to i) highlight signals that might usually go

by unnoticed, ii) distinguish overlaying peaks if they occur with different phase delays. Therefore, more information about the kinetics of a reaction become accessible. [36]

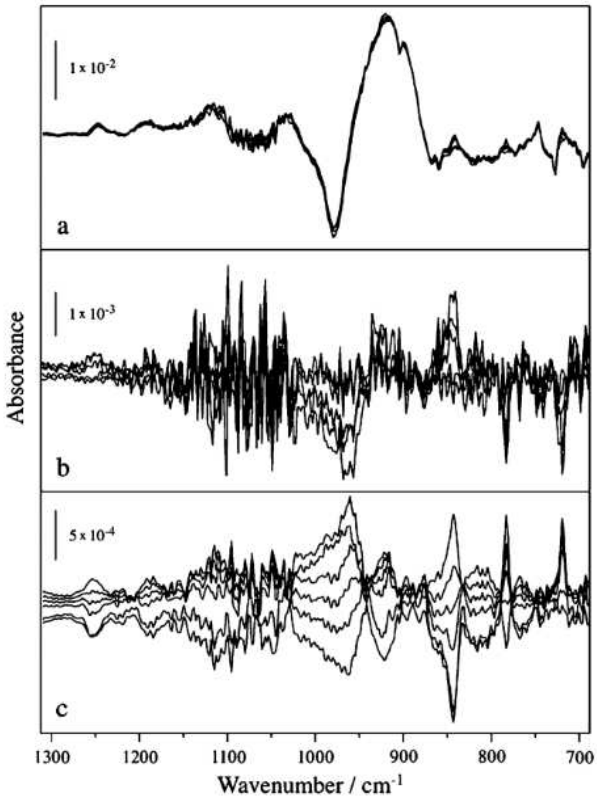

a) Time-resolved spectrum

b) difference spectrum

c) Phase-resolved spectrum

Figure 5 Example of a modulation of the cyclohexane concentration in the epoxidation of cyclohexane with a Ti-Si airgel catalyst with TBHP as the oxidizing agent, taken form Bürgi et al. [36].

The principle of modulated excitation and phase-sensitive detection can be applied to many different measurement and signal detection methods, whereby DRIFTS and transmission IR spectroscopy were used in this work.

3.1.1. Methodology

Modulation Excitation Spectroscopy (MES) measurements were carried out in transmission-mode on a Bruker Vertex 70 FTIR equipped with a MCT detector and a resolution of 2 cm^{-1}. The respective undiluted catalyst was pressed into a pellet and introduced into an environmental chamber, equipped with a heating wire, a thermocouple, gas flow-capabilities and CaF_2 windows.

After the pretreatment, the catalysts were heated under He to the desired temperature with a heating ramp of 10 °C/min, at which a background spectrum was taken. EtOH (He bubbled through a liquid-vapor saturator filled with absolute EtOH, kept at 5 °C) and O_2 were added to the He stream (1.1 mL min^{-1} each). Once steady-state was reached (as

determined by in-situ monitoring with a Pfeiffer Vacuum OmniStar GSD 320 O mass spectrometer and observation with FTIR spectra), the modulation was started. During the first half-period, EtOH, diluted in He, and O_2 were introduced into the cell, followed by the second half-period, during which EtOH, diluted in He, and H_2 were introduced. Each half period lasted 101 s, 12 scans were used for each interferogram and 64 interferograms were taken during each half-period. For the sake of time-efficiency, the interferograms were converted to spectra after the measurements were finished. One modulation experiment consisted of 20 periods, whereas only the last 10 periods were used for result evaluation.

3.8. O_2 Chemisorption

O_2 pulse chemisorption was performed with the MicrotracBEL Catalyst Analyzer Belcat-II and was used as an easy accessible method to determine whether or not the reduction temperature has impact on chemisorption properties of the respective catalyst. For that, 60 to 120 mg of catalyst were weighed into the sample holder and stabilized with quartz wool. For the samples with a smaller silver loading, a higher net weight was necessary than for the samples with higher silver loading.

The pretreatment was carried out as usual, afterwards the gas pulses were dosed at 170 °C with 5 % O_2 in He with a total flow of 50 mL min^{-1}. The amount of adsorbed gas was measured with a TCD detector.

3.9. XRD Measurements

XRD measurements were performed using a PANalytical X'Pert (PANalytical B.V., almelo, the netherlands) PRO powder diffractometer in Bragg-Brentano geometry. A Cu LFF X-ray tube was used, with CuKα λ1 = 1.5406 Å and λ2 = 1.5444 Å. 45 kV at 40 mA were applied. A Ni-Kβ-Filter, θ/θ goniometer: PW3050/60; goniometer radius 200 mm; fixed divergence slit 0.4354°; fixed anti scatter slit 2°; detector: X´Celerator; scanning length 2.546°, fixed anti scatter slit 5.5°; max. diffraction angle 2θ, 20-90°, step size 0.0200°, time per step 99.700 s.

4. Results and Discussion

4.1. Characterization of Catalysts

To determine whether the oxidation temperature of 400 °C with a hold time of 30 min (as it has been used in previous work) was sufficient for cleaning the catalysts surface, a temperature programmed oxidation (TPO) with 20 % O_2 in He and a heating ramp of 10 °C min^{-1} was carried out, as it is presented in Figure 6. Nitrates as residues from the synthesis and carbonates from air exposure are expected to desorb from the catalysts surface during heating and were tracked by mass spectrometry (m/z 44 for carbonates and m/z 30 for nitrates). The TPO shows that the vast majority of nitrates desorb at 180 °C, 262 °C and at 400 °C. Majority of carbonates desorbs at 277 °C and 400 °C. However, there is also a small peak of nitrates desorbing at 474 °C and a rather large signal of CO_2 desorbing at 560 °C, which can most likely be attributed to the oxidation of carbon residues.

Additionally, the progress of the pretreatment was tracked in the FTIR vacuum transmission cell. As it is presented in Figure 7, before pretreatment (green line), plenty carbonates and nitrates species are attached to the catalysts surface, which cause absorption in the 1200 – 1650 cm^{-1} region. The broad signal between 3000 and 3500 cm^{-1} is caused by weakly bound hydroxyl groups on the TiO_2 surface (physisorbed water). During the oxidative step of the pretreatment, the carbonates, nitrates and hydroxyl groups desorb from the surface and the spectra taken afterwards show a clean sample surface. The elevation of background absorbance during the reductive step (blue line) has been reported in the past and is ascribed to production of conduction band electrons under reducing atmosphere. The extent of accumulation of electrons can be increased by adsorbed hole-scavengers like methanol, and decreased by adsorbed electron-scavengers such as gasphase O_2 or adsorbed –OH or H_2O. The weak signals between 3550 and 3800 cm^{-1} are due to isolated Ti-OH groups from dissociated water, which have been reported to be present on the anatase surface even after evacuation at 700 °C. [38] [39] [19] [31]

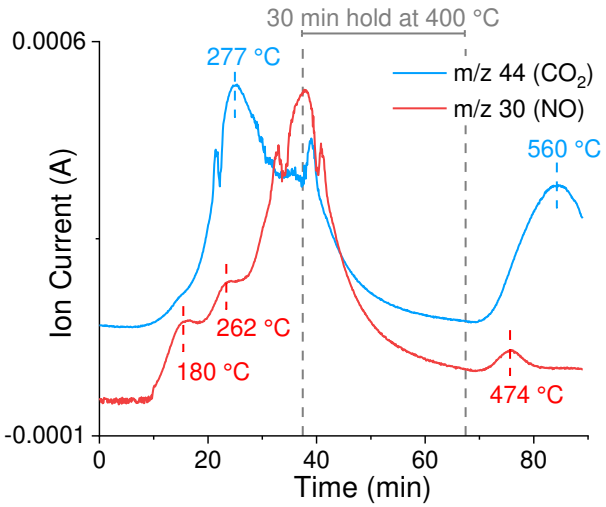

Figure 6 Temperature programmed oxidation of 20 mg 0.7 wt% Au 7.3 wt % Ag Aurolite tracked with mass spectrometry. 20 % O_2 in He with a total flow of 50 mL min^{-1} in a continuous-flow fixed bed quartz reactor. Heating with 10 °C min^{-1} up to 600 ° with a 30 min hold at 400 °C.

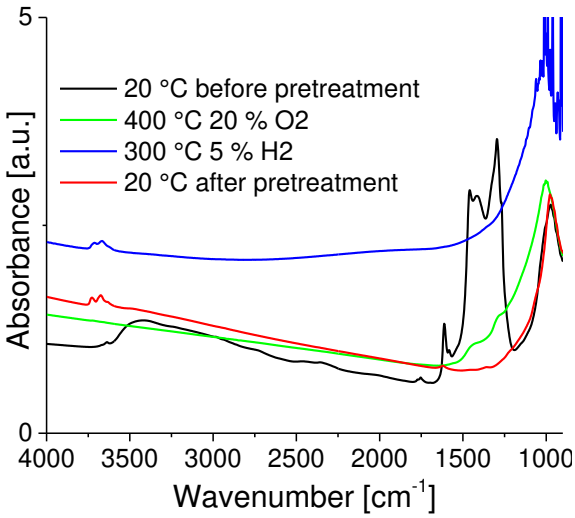

Figure 7 IR Absorbance spectra of the 0.7 wt% Au 7.3 wt% Ag Aurolite catalyst in the FTIR transmission cell before pretreatment (in lack), during pretreatment (in green and blue) and after pretreatment (in red)

Taking both the TPO and the IR spectra into account, the pretreatment consisting of 400 °C oxidation for 30 min under 30 % O_2 in He is sufficient for removing surface species from the catalyst. The further CO_2 and NO peak in the TPO might be caused by carbon and nitrates trapped in the TiO_2 bulk.

4.1.1. Mean particle size and metal distribution

Prior work done in the research group analyzed particle size distribution with STEM-HAADF images and concluded there was no significant difference in the mean diameter between the monometallic catalyst Au Rutile and the bimetallic counterpart Au Ag Rutile. The catalysts were reported to have mean diameters of 3.3 ± 1.0 nm (particles observed n = 292) for 2.8 wt% Au Rutile and 3.6 ± 1.2 nm (n = 252) for 2.8 wt% Au 1.0 wt% Ag Rutile. Also, there was reported to be no significant difference in particle size distribution whether the self-synthesized (by deposition-precipitation with urea) Au Rutile (3.3 ± 1.0 nm; n = 292) or the commercially available Aurolite (3.2 ± 0.6 nm; n = 147) was used. [40]

In later work, ageing effects were determined: freshly bought Aurolite was determined to have a mean diameter of 2.6 ± 0.3 nm (n = 370) while Aurolite stored at 250 K in the dark for a few months was reported to have a mean diameter of 4.9 ± 0.4 nm (n = 212). [3]

In figures Figure 8 STEM-HAADF images of the 0.8 wt% Au 4.2 wt% Ag Aurolite catalyst, synthesized and pretreated as described in the chapter *3.2 Catalyst pretreatment*, are shown. The mean diameter of 5.0 ± 2.6 nm (n = 485) is therefore in agreement with the already reported results.

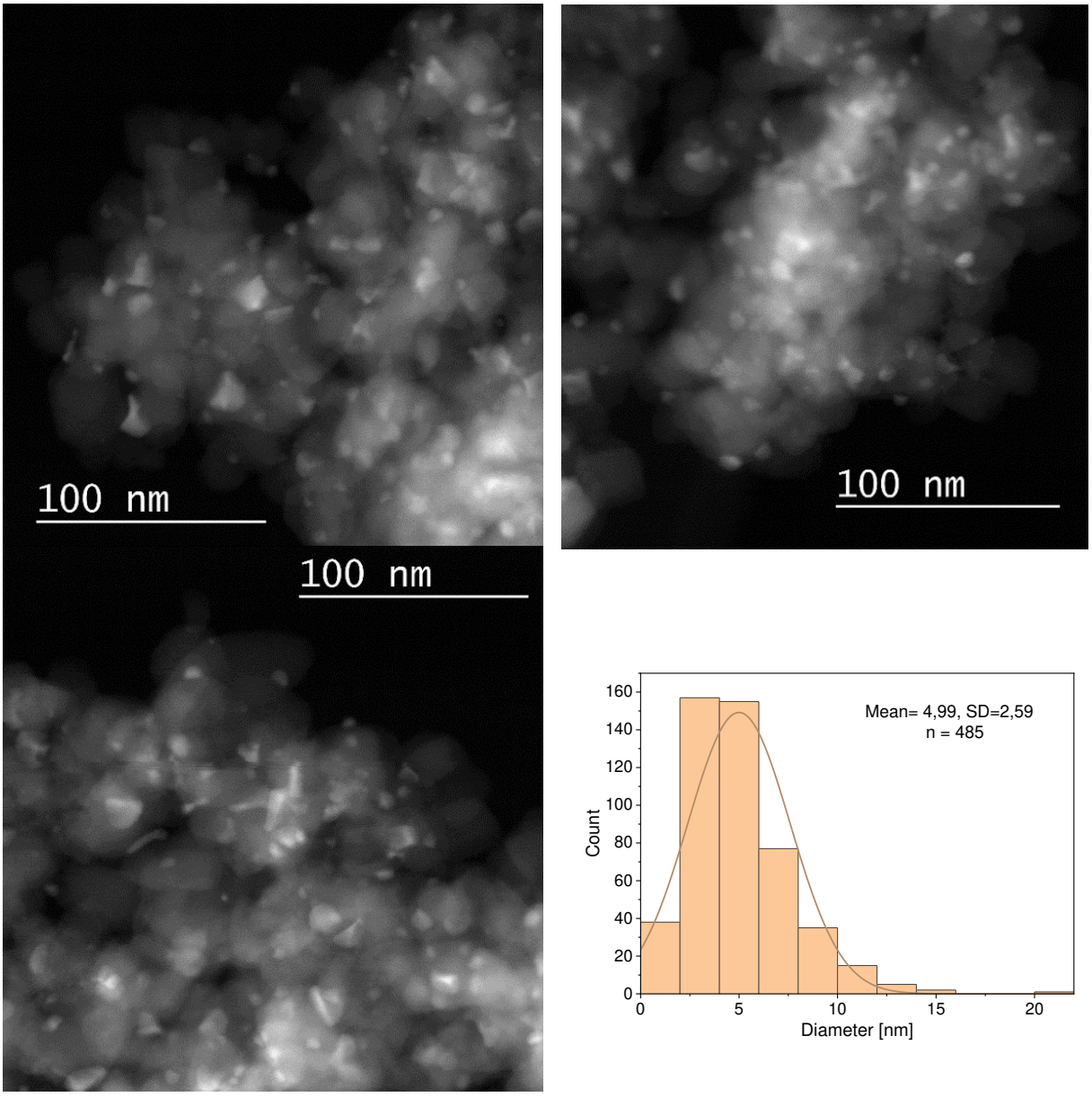

Figure 8 STEM-HAADF images of 0.8 wt% Au 4.2 wt% Ag on Aurolite

Additionally, EDX images were taken of the 0.8 wt% Au 4.2 wt% Ag Aurolite catalyst and are depicted in Figure 9. They demonstrate, where there is silver (grey spots), there is also gold (orange spots) on TiO_2 (blue/ turquoise area) – meaning that the metal particles are of bimetallic character.

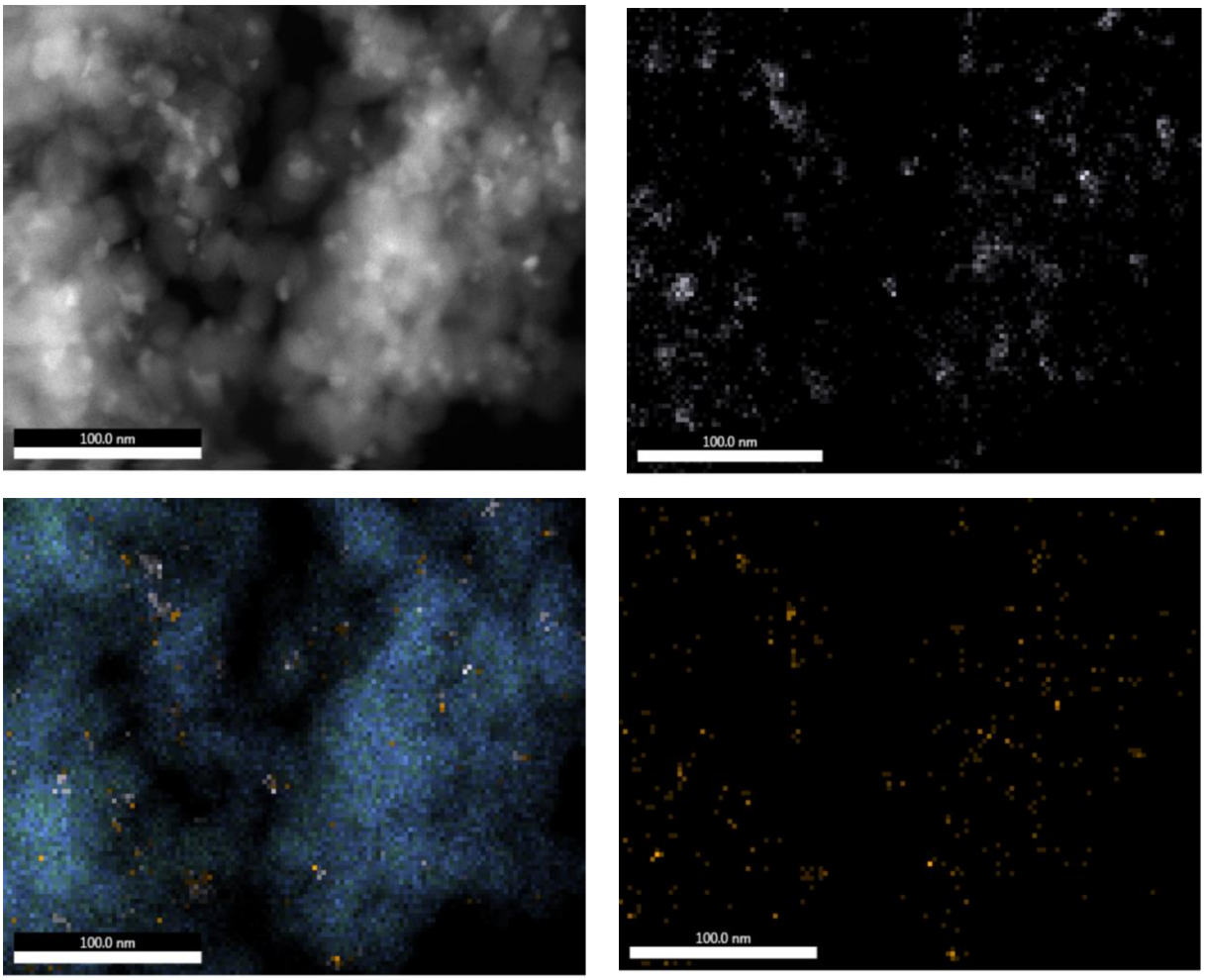

Figure 9 all images were taken of the same spot of the 0.8 wt% Au 4.2 wt% Ag Aurolite catalyst (after pretreatment):
top left: HAADF image,
top right: EDX image: Ag L signal in silver,
bottom left: EDX image: Ag L in silver, Au L in gold, O K in blue, Ti K in turquoise
bottom right: EDX image Au L in gold.

4.2. Catalytic Performance dependent on silver loading

4.2.1. Catalytic Activities

For characterization of the catalysts activities, each catalyst was screened five to six times over the course of six months For each screening, a new catalyst-quartz sand-mixture was weighed in, filled into the quartz glass capillary reactor and mounted into the furnace. Mean reaction rates and (R)STDs were calculated for each catalyst at each reaction temperature, respectively. The mean RSTD for the reaction rates (calculated from the RSDs of each catalyst at each measured temperature separately) is calculated to be

39 ± 20 %. (for the setup itself it is 7.5 ± 3.3 %). These deviations can for example be caused by gas leakage due to insufficient mounting of the capillaries or filling the catalyst bed unevenly. However, they are most likely due to inhomogeneity of the samples themselves. Since the catalysts are highly catalytically active and only 1 mg of catalyst was used for each kinetic screening, those screenings can be seen as spot samples. The metal loadings of the produced batches were inbetween 1 and 8 wt%. Slight statistical variations in the actual metal loading of each spot sample will have a high effect on the catalytic activity in the screening.

No performance impairment over the course of six months was noted. In Figure 10 the mean reaction rates per gram catalyst ± STDs are plotted over the respective reaction temperature, whereas in Figure 11 the mean reaction rates per gram metal ± STDs are displayed.

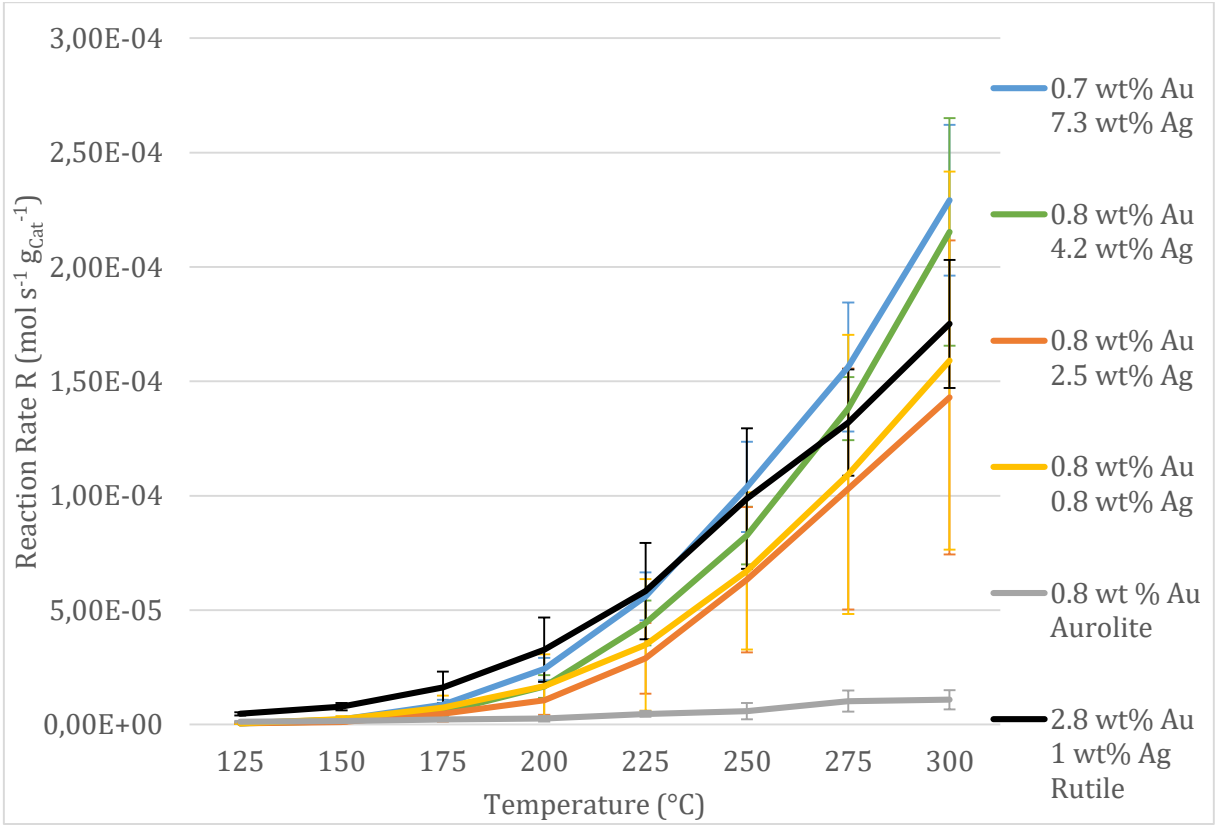

Figure 10 Reaction Rate R per gram catalyst. Mean values and STDs were calculated from at least 5 measurements, error bars depict STDs.

The activity of the catalysts synthesized in this thesis (Au Ag Aurolite batch) can compete with the ones that had been used in the working group before (2.8 wt% Au 1 wt% Ag Rutile). That is one remarkable outcome, considering the significantly lower gold loadings

of 0.7-0.8 wt% compared to 2.8 wt%, which leads to cheaper catalysts. In detail, the 2.8 wt% Au 1 wt% Ag Rutile catalyst shows a higher activity at low temperatures (125 – 200 °C), but only a shallow increase of activity with rising temperature. The Au Ag Aurolite batch shows a much steeper slope: it starts with lower activity at low temperatures, catches up at around 225 °C and then out-performs the Rutile catalyst at higher temperatures. Silver appears to impact the reaction rate primarily at elevated temperatures.

Comparing the within this thesis synthesized catalysts (Au Ag Aurolite batch) between themselves, it appears that the reaction rate per gram catalyst increases with the silver loading, while there might be a saturation or flattening of the beneficial properties between 4.2 wt% Ag and 7.3 wt% Ag. However, taking the overlapping STDs of the mean reaction rates into account, a direct comparison between the catalysts with varying silver loadings must be regarded with suspicion, since they are prone to statistical errors. Nevertheless, the most active catalysts (with 4.2 wt% Ag and 7.3 wt% Ag loadings) deliver a mean reaction rate at 300 °C around 20 times higher than Aurolite without Ag. 1 wt% Ag P25 delivered even lower values than Au Aurolite and is therefore not plotted in the diagram.

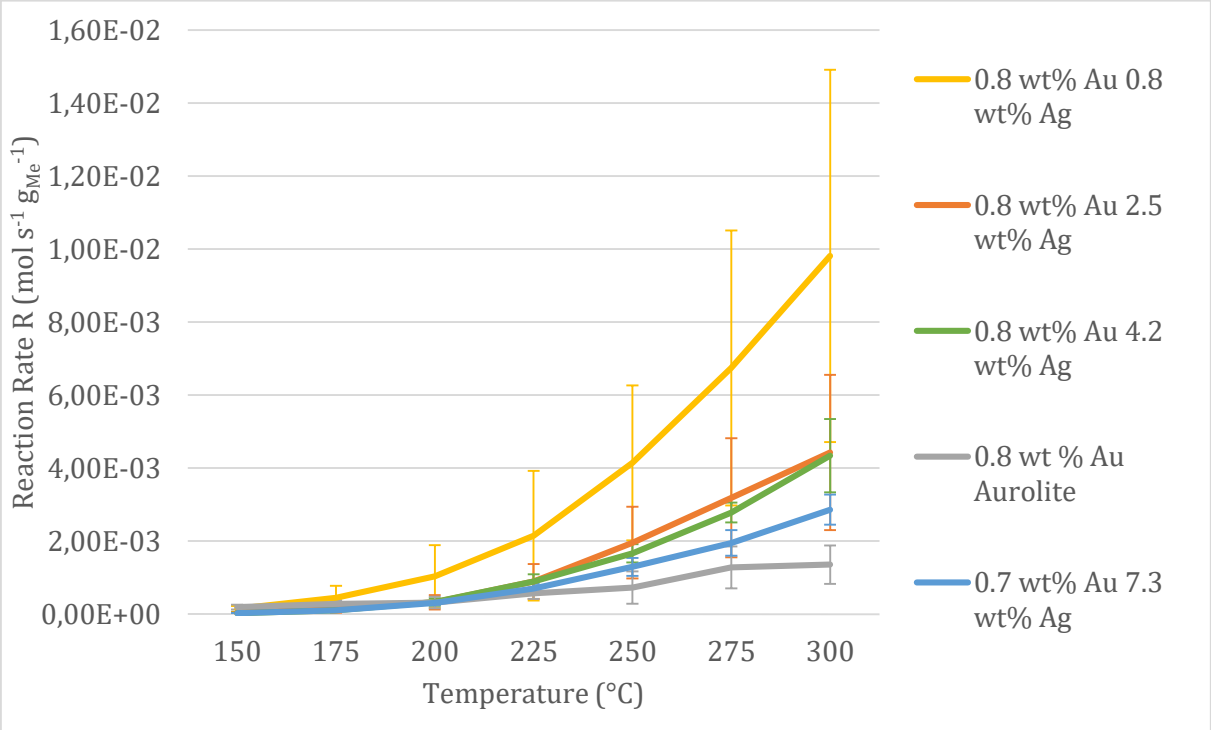

Figure 11 Reaction Rate R per gram metal. Mean values were calculated from 5 measurements, the error bars depict STDs.

When comparing the reaction rates per gram metal within the Au Ag Aurolite batch, it becomes clear that the 0.8 wt% Au 0.8 wt% Ag Aurolite catalyst clearly delivers the highest results – remarkably almost 10x higher than for the Aurolite sample with 0.8 wt% Au alone. However, when more silver is added, the promotional effect is flattened. The correlation is non-linear. The more silver is added, the smaller is the impact of that added silver on the reaction rate.

In conclusion, for using the metals most effectively, the 0.8 wt% Au 0.8 wt% Ag Aurolite catalyst delivered the best results (reaction rate per gram metal). For receiving the highest catalytic activity in total (reaction rate per gram catalyst), the 0.8 wt% Au 7.3 wt% Ag Aurolite is the best choice.

4.2.2. Catalytic Selectivities

For the direct comparison of product selectivities of the different catalysts, similar ethanol conversions of around 20 % were aspired to achieve. Therefore, between 0.9 mg to 1.1 mg of the respective Au Ag Aurolite catalysts was used for each screening. For the Au Aurolite reference, 10 mg were used, which still resulted in a significantly lower ethanol conversion of around 10 % at 300 °C.

The Au Ag Aurolite batch shows a drastic improvement from the pure Au Aurolite: remarkably high selectivity of > 95 % towards acetaldehyde are monitored at all temperatures. Further addition of silver leads to a steady increase of the selectivity towards acetaldehyde. Formation of the side products CO_2, acetic acid and ethyl acetate start at progressively higher temperatures.

Similar to the catalytic activity in 4.2.1, the performance-wise improvement from the catalyst with 4.2 wt% Ag loading to the catalyst with 7.3 wt% Ag loading is with 0.5 % rather small.

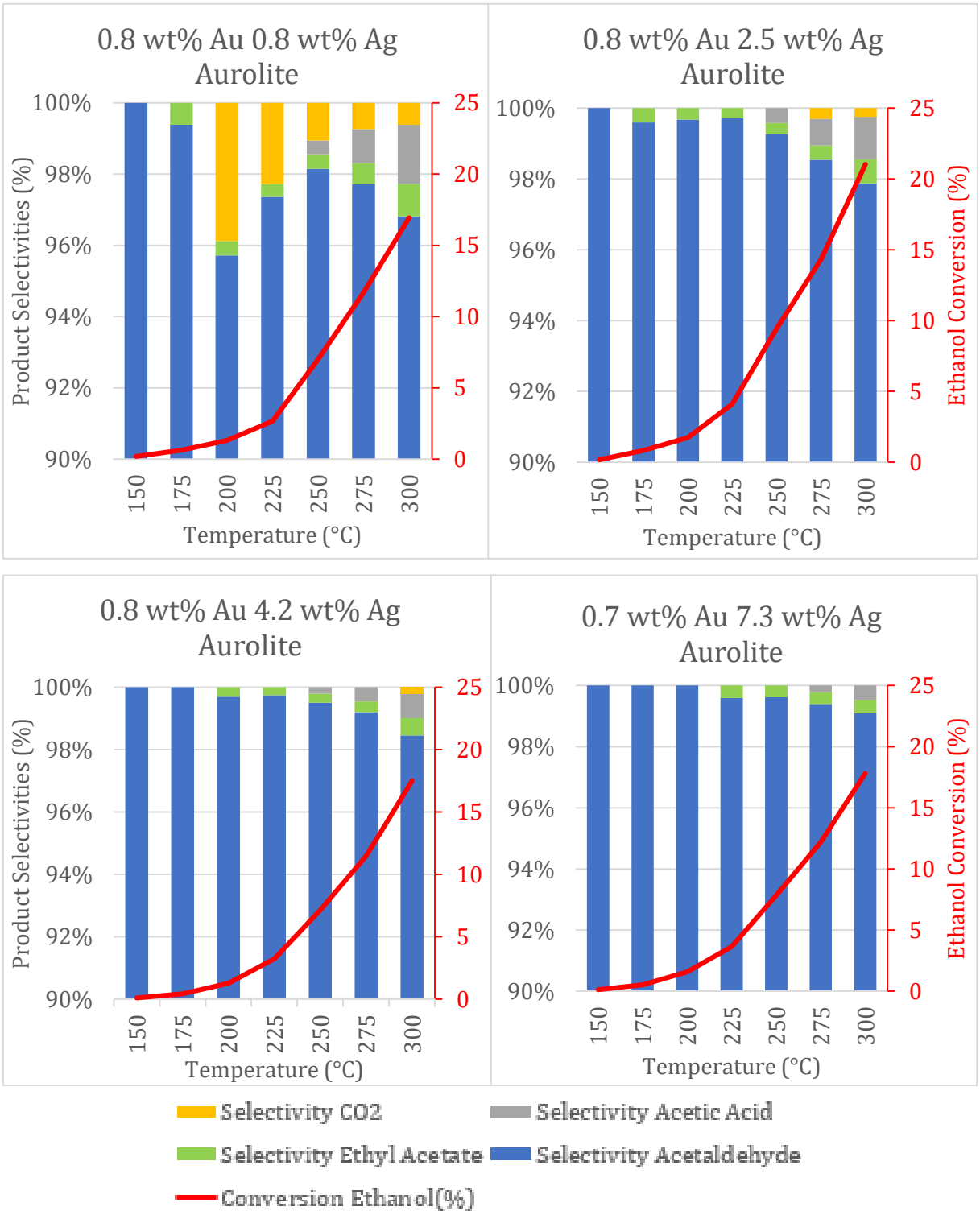

Figure 12 Catalytic selectivities towards acetaldehyde, ethyl acetate, acetic acid and CO_2 at the respective reaction temperature and ethanol conversion of the 0.8 wt% Au and 0.8/ 2.5/ 4.2/ 7.3 wt% Ag Aurolite catalysts

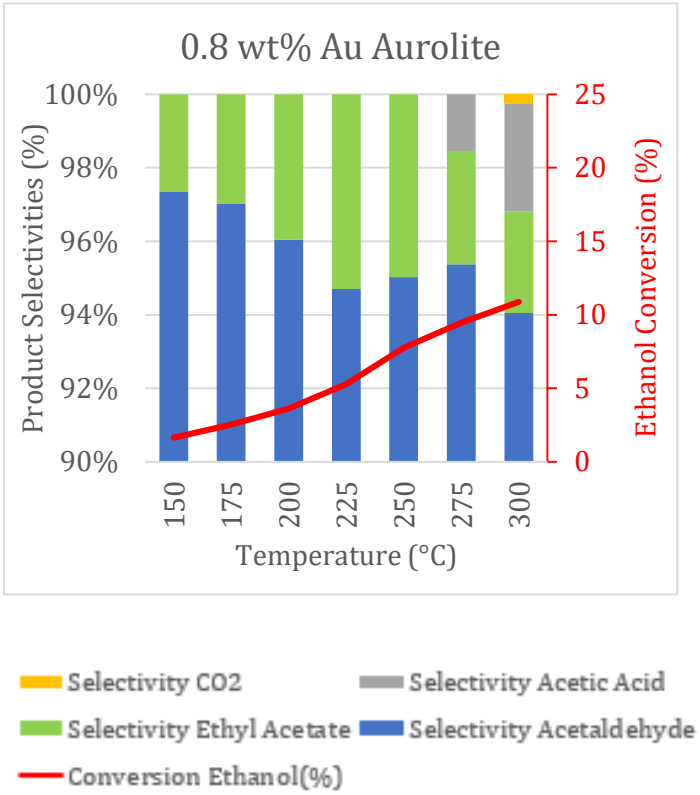

Figure 13 Catalytic selectivities towards acetaldehyde, ethyl acetate, acetic acid and CO_2 at the respective reaction temperature and ethanol conversion of the 0.8 wt% Au Aurolite catalyst.

4.2.3. Catalytic performance at high temperatures and high conversion regimes

So far, catalytic studies were consistently carried out in conversion regimes below 30 %. In the following measurements, larger amounts of catalysts were used and higher temperatures were reached to study catalytic performance at higher conversion regimes.

For the 0.8 wt% Au 4.2 wt% Ag Aurolite catalyst, 2 mg were diluted with quartz sand to 100 mg and a kinetic screening was started out as usual (starting at 300 °C and then going down in temperature), followed by measurements at 350 °C and 400 °C. The results is depicted in Figure 14Figure 16 and impressively show 99.7 % ethanol conversion while maintaining the excellent selectivity towards acetaldehyde of 99 %.

Selectivity towards acetic acid likewise ethyl acetate decreases at high temperatures, which is possibly simply due to reduced surface adsorption of acetaldehyde to the catalysts surface and therefore reduced probability of further reaction to acetic acid or ethyl acetate. This is supported by an ethanol TPD (see Figure 27 on page 49), which

shows that the vast majority of acetaldehyde desorbs from Au Ag Rutile at < 187 °C and only an easily overlooked portion remains until 410 °C.

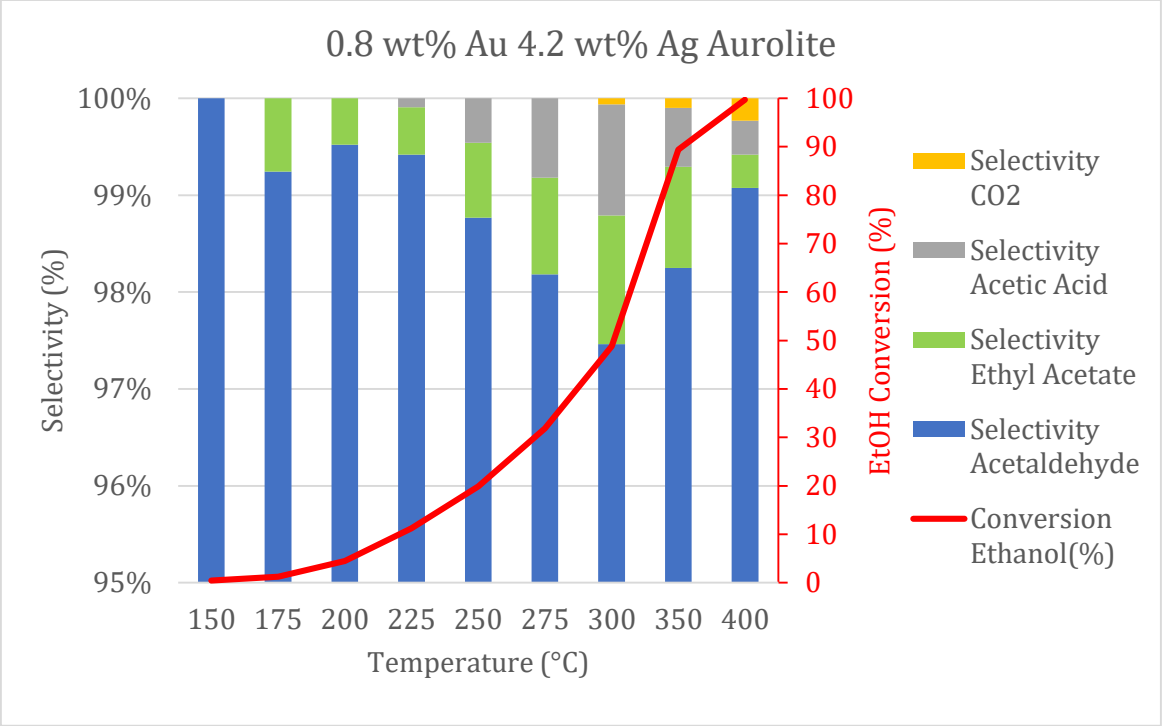

Figure 14 Results of a kinetic screening of 2 mg 0.8 wt% Au 4.2 wt% Ag Aurolite diluted with quartz sand to 100 mg. The screening was started as usual with 300 °C, following 150 – 275 °C in intervals of 25 °C in random order. Afterwards, measurements at 350 °C and 400 °C followed, held for 10 h each, ensuring steady states were reached.

10 mg Aurolite catalyst was diluted with quartz sand to 100 mg as well before starting the same modified kinetic screening as already described above. The results are depicted in Figure 15 and demonstrate a conversion of up to 60 % with a selectivity towards acetaldehyde of 94 %. Clearly, more side products are formed, at all measured temperatures. Taking the ethanol TPD into account (see Figure 27 on page 49), and comparing the Au Ag Rutile and the Au Rutile TPDs, it becomes clear, that on Au Rutile, a grander portion of acetaldehyde remains adsorbed on the surface until up to 365 °C. The respective peak in the Au Ag Rutile diagram is significantly smaller. The desorption behavior of acetaldehyde does accordingly impact the formation of acetic acid and ethyl acetate both on pure Rutile and P25 (anatase and rutile mixture, similarly as used for Aurolite).

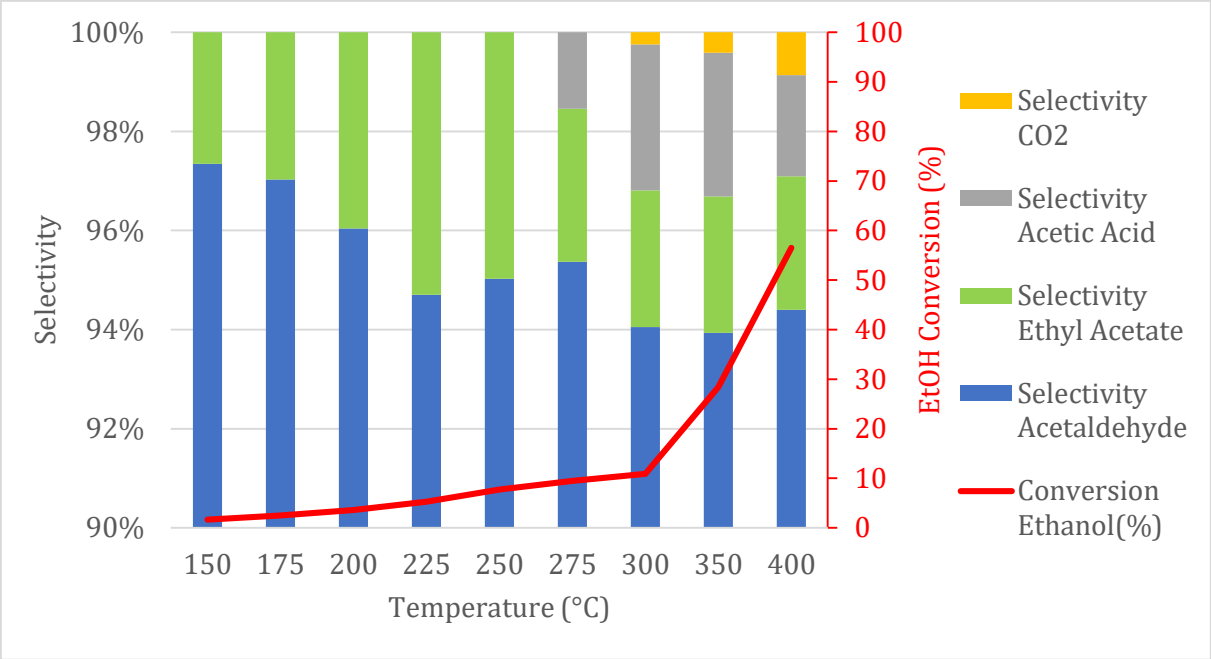

Figure 15 Results of a kinetic screening of 10 mg Aurolite diluted with quartz sand to 100 mg. The screening was started as usual with 300 °C, following 150 – 275 °C in intervals of 25 °C in random order. Afterwards, measurements at 350 °C and 400 °C followed, held for 10 h each, making sure steady states were reached.

4.2.4. Activation Energies

Activation energies are investigated by Arrhenius plots. When flattening of the slope occurs at higher temperatures, then that is a sign for diffusion or transportation limitations and those values are not taken into account (mostly at 300 °C, few times at 275 °C). The results are calculated from five kinetic screenings for each catalyst. 67 % of the Arrhenius plots delivered a Pearson factor of > 0.99. All Arrhenius plots are above $R^2 > 0.91$. The apparent activation energy rises with the silver loading, which agrees with the observations made in 4.2.1, where the Rutile catalyst containing a higher fraction of Au is more active at lower temperatures than the Au Ag Aurolite batch.

Table 1 Calculated Apparent Activation Energies from Arrhenius plots

Catalyst	mean apparent activation energy ± STD (kJ/mol)
0.8 wt% Au (Aurolite)	23.51 ± 2.29
2.8 wt% Au 1 wt% Ag Rutile	38.18 ± 2.14
0.8 wt% Au 0.8 wt% Ag Aurolite	63.14 ± 1.42
0.8 wt% Au 2.5 wt% Ag Aurolite	71.64 ± 3.71
0.8 wt% Au 4.2 wt% Ag Aurolite	72.27 ± 2.76
0.7 wt% Au 7.3 wt% Ag Aurolite	72.40 ± 8.21

4.2.5. Reaction Orders of EtOH and O_2

Reaction Orders of EtOH and O_2 in the ethanol oxidation on the Aurolite catalysts are displayed in Table 2. Few measurements exceeded a conversion of 15 %, the respective values are marked with *. The Pearson factors are depicted with a colour code – most values display in green, therefore deliver $R^2 > 0.90$.

All values are between 0 and 1. The interpretation of the absolute values listed in Table 2 is challenging, however one trend is eye-catching and of high interest: With the addition of silver, the O_2 reaction order steadily decreases until it reaches zero.

The decrease of the O_2 reaction order can be attributed to a higher availability of reactive oxygen species and supports the postulation that silver plays a key role in oxygen activation.

An O_2 reaction order of 0.0 to 0.1 at all temperatures is reached with the 0.8 wt% Au 4.2 wt% Ag Aurolite, which suggests that for the Aurolite catalyst, a silver addition of 4.2 wt% is sufficient for oxygen activation.

Ethanol reaction orders, in contrast, increase with silver loading.

Table 2 Reaction Orders of EtOH and O_2 in Ethanol Oxidation over Au Ag TiO_2 catalysts

	0.8%Au0.8%Ag Aurolite		0.8%Au2.5%Ag Aurolite		0.8%Au4.2%Ag Aurolite		0.7%Au7.3%Ag Aurolite	
	EtOH Order	O_2 Order	EtOH Order	O_2 Order	EtOH Order	O_2 Order	EtOH Order	O_2 Order
150 °C	0.18	0.50	0.25	0.18	0.30	0.11	0.34	0.09
200 °C	0.30	0.62	0.62	0.02	0.38	-0.00	0.37	0.05
250 °C	0.46	0.23	*0.71**	0.10	0.62	0.05	0.62	0.05
300 °C	0.51	*0.46**	*0.78**	0.27	0.85	*0.12**	*0.60**	*0.01**

$0.98 < R^2 < 1.00$	$0.90 < R^2 < 0.98$	$0.70 < R^2 < 0.90$	$0.50 < R^2 < 0.70$	$0.00 < R^2 < 0.50$

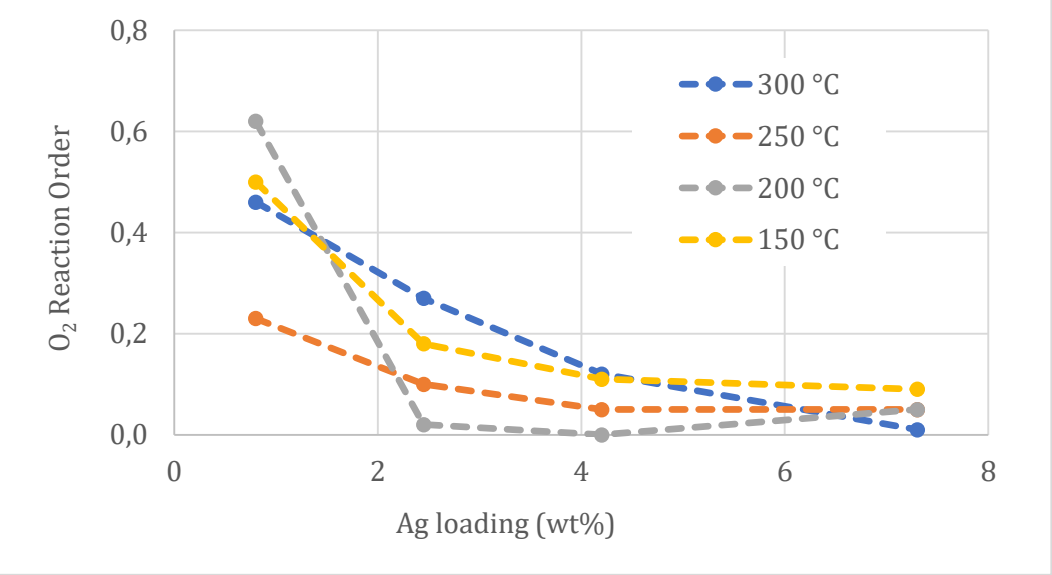

Figure 16 O_2 Reaction Order for the Au Ag Aurolite batch over the different Ag loadings for 300 °C, 250 °C, 200 °C and 150 °C

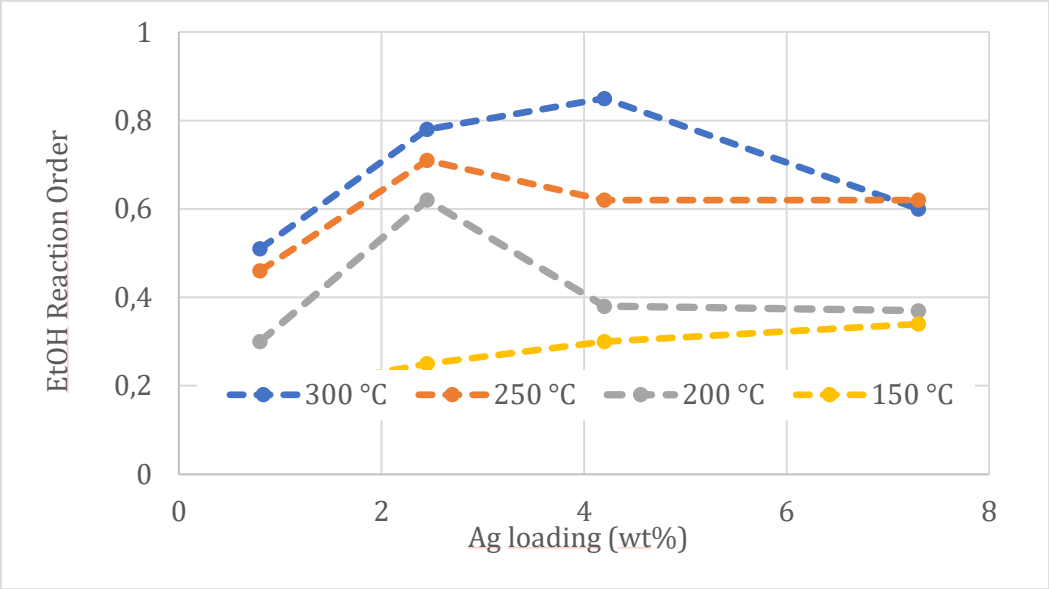

Figure 17 EtOH Reaction Order for the Au Ag Aurolite batch over the different Ag loadings for 300 °C, 250 °C, 200 °C and 150 °C

4.2.6. Conclusion

The catalytic screening of catalysts with varying silver content resulted in the same trends for catalytic activity (for the reaction rates per gram catalyst) as well as for the catalytic selectivity towards acetaldehyde: addition of silver is beneficial. Total catalytic activity (reaction rate per gram catalyst) as well as selectivity towards acetaldehyde increases with silver addition.

The Au Ag Aurolite catalysts perform superb also at high temperatures (400 °C) and high conversion regimes: at 99.7 % ethanol conversion, 99 % selectivity towards acetaldehyde was monitored.

However, it also becomes clear, that the catalytic performance does not benefit from silver addition in a linear correlation. The reaction rate per gram metal decreases with further addition of silver, which means that further addition of silver becomes less and less efficient – the benefits brought by silver addition flatten out. To underline this statement, the reaction rate per gram catalyst/ metal and the selectivity towards acetaldehyde at 300 °C are plotted over the catalysts silver loading in Figure 18. Trend lines show the best fit (highest R^2) as power functions.

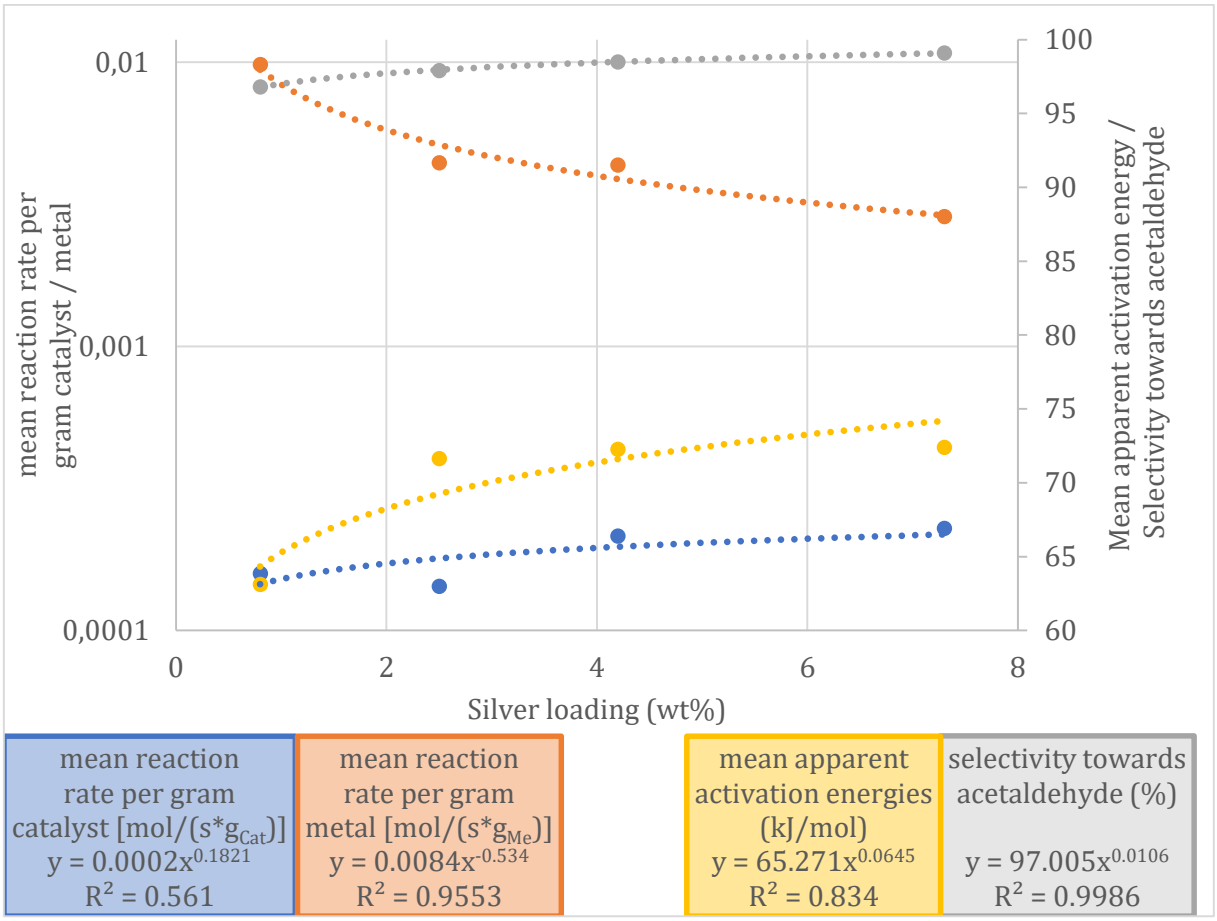

Figure 18 Mean reaction rates on the primary y-axis and selectivity towards acetaldehyde & mean apparent activation energies on the secondary y-axis of the Au Ag Aurolite batch plotted over the silver loading

Improvement in catalytic activity and selectivity from the catalyst with 4.2 wt% Ag to 7.3 wt% is little. Furthermore, the measured reaction orders for O_2 decrease with Ag addition -which can be attributed to a higher availability of reactive oxygen species- and reach zero for 0.8 wt% Au4.2 wt% Ag Aurolite, which means that oxygen is activated sufficiently.

Surprisingly, addition of silver leads to an increase of the apparent activation energy. Silver seems to have a negative contribution to ethanol activation, which is corroborated by the increase in ethanol reaction orders and is possibly caused by coverage of some of the gold. While Aurolite (0.8 wt% Au TiO_2) shows an apparent activation energy of 23.5 kJ/mol, 0.8 wt% Au 4.2 wt% Ag TiO_2 results in 72.3 kJ/mol activation energy.

In conclusion, addition of silver increases the activation energy, which leads to lower activity at reaction temperatures of < 225 °C (compared to the 2.8 wt% Au 1 wt% Ag Rutile catalyst). However, due to silver playing a key role in oxygen activation, catalytic activity

rises drastically with increasing temperatures. Once an amount of silver, that allows to sufficiently activate oxygen is added, no further performance improvement is possible by adding more silver, which explains the flattening of the benefits.

Silver addition also leads to an increase in selectivity towards acetaldehyde formation, by impacting the desorption behavior of acetaldehyde from the catalyst. The formation of side-products is hindered.

4.3. Effects of Silver on EtOH Adsorption and Desorption: ex-situ IR studies

4.3.1. EtOH Adsorption Sites

The examined samples were the following: Rutile, Au Rutile (Nagl et al. confirmed by LA-ICP-MS measurements a gold loading of 2.8 wt% Au Rutile [40], even though the nominal value was thought to be 5 wt% Au) and Au Ag Rutile (nominal metal loadings of 1 wt% Au 2 wt% Ag Rutile, no LA-ICP-MS results available). The BET surface area of the Rutile was reported to be 103 $m^2\ g^{-1}$, while the used Au Rutile catalyst resulted in 28 $m^2\ g^{-1}$ and Au Ag Rutile in 29 $m^2\ g^{-1}$. [2]

After introducing 5 mbar of EtOH vapor at 20 °C into the transmission cell, the spectra shown in Figure 19 were taken. Spectra taken shortly before EtOH adsorption were used as background. The peak assignments are listed in Table 3.

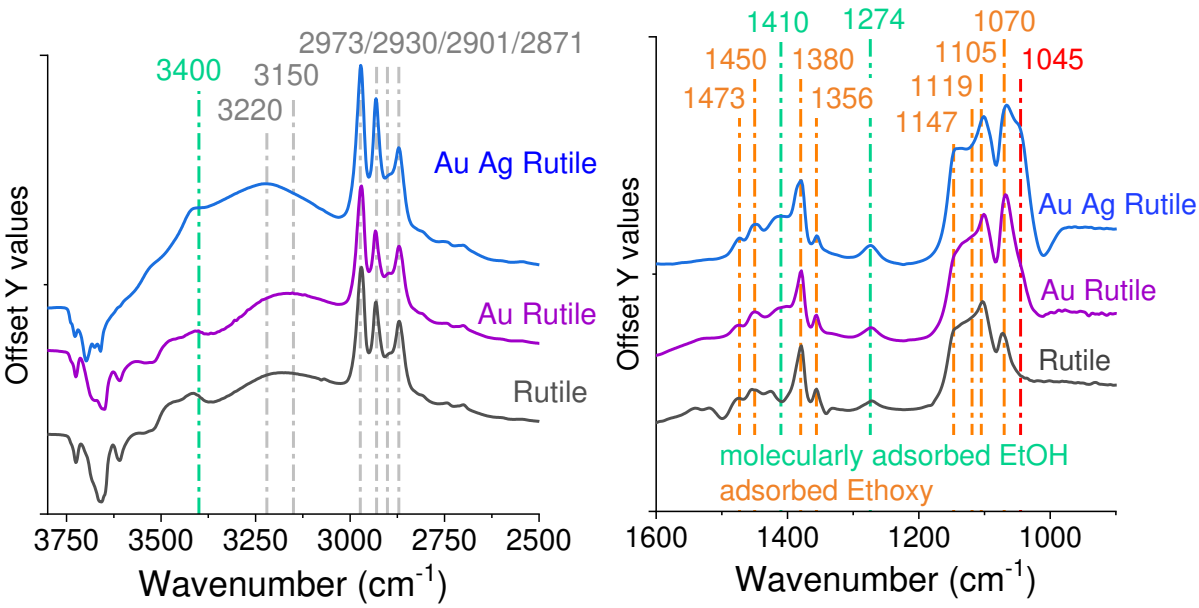

Figure 19 EtOH and ethoxy species adsorbed Rutile, 5 wt% Au Rutile and 1 wt% Au 2 wt % Ag Rutile - after pretreatment, at 20 °C EtOH vapor was introduced into the vacuum cell until 5 mbar pressure was observed

Multiple peaks between 1600 cm^{-1} and 1000 cm^{-1} show a pattern typical for ethoxy adsorbed to TiO_2. Observing the area below 1100 cm^{-1} makes one remarkable trend become clear: Addition of silver leads to a significantly stronger signal at 1042 cm^{-1}, which is assigned to bidentate adsorbed ethoxy on TiO_2. The spectra of Rutile and Au Rutile instead show a stronger signal at 1119 cm^{-1}, which is assigned to ethoxy adsorbed monodentate to TiO_2. On all catalysts, molecularly adsorbed ethanol is present as well. [41] [28] [42] [43]

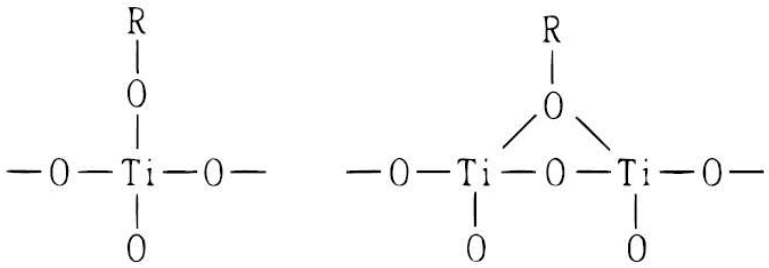

Figure 20 Schematic drawing of monodentate and bidentate adsorbed ethoxy on TiO_2, taken from Wu et al. [41]

Panayotov et al. reported that the broad signal between 3000 and 3500 cm^{-1} is caused by weakly bound hydroxyl groups on the TiO_2 surface. The maximum at around 3400 cm^{-1}

represents asymmetric OH stretching (ν_3) of randomly oriented molecules while a shoulder at around 3200 cm^{-1} is thought to be due to "ice-like structures", caused by symmetric OH stretching (ν_1) of tetrahedrally coordinated molecules.

The decrease of the ν(OH) at around 3700 cm^{-1} while the broad band at 3400 cm^{-1} increases during exposure to ethanol vapour indicates H-bonding of ethanol with isolated surface –OH groups. Both signals are more pronounced on Rutile and Au Rutile than on Au Ag Rutile, suggesting either i) H-bonding plays a less significant role on the Au Ag Rutile catalyst or ii) the number of isolated –OH groups was smaller on the Au Ag Rutile in the first place. [19] [44]

Table 3 Peak assignments of ethoxy and ethanol species adsorbed on TiO_2

Meas. Wavenumber in this work (cm^{-1})	Vibrational mode / Species / Reference(s)	Assigned Species for this work
1042	ν(C-O) / EtO_{ad} bidentate/ 1042 [41]/ 1049 [28]/1052 [32]	EtO_{ad} bidentate
1070	ν(C-C)/ EtO_{ad} / 1074 [41] ν_s(CCO)/ EtO_{ad} /1070 [42] [28]	EtO_{ad}
1105	ν(C-O)/EtO_{ad} / 1100, 1105 [42]	EtO_{ad}
1119	ν(C-O)/ EtO_{ad} monodentate/ 1113 [32]/ 1119 [41]	EtO_{ad} monodentate
1147	ν(C-O)/EtO_{ad} / 1150, 1160 [42] ν(C-O)/ EtO_{ad} monodentate/ 1147 [32]	EtO_{ad}
1274	δ(OH)/ $EtOH_{ad}$/ 1270 [42]/ 1274 [32]	$EtOH_{ad}$
1350	δ(CH)/ CH_3CHO_{ad}/ 1350 [44]	CH_3CHO_{ad}
1356	wagging (CH_2)/ EtO_{ad}/ 1352 [32] / 1356 [41]	EtO_{ad}
1380	δ_s(CH_3)/ EtO_{ad}/ 1379 [41] [32]/ 1380 [32]	EtO_{ad}
1410	δ_s(CH_3)/ $EtOH_{ad}$/ 1400 [32]	$EtOH_{ad}$
1450	δ_a(CH_3)/ EtO_{ad}/ 1447 [41] δ_a(CH_2)/ EtO_{ad}/ 1450 [32]	EtO_{ad}
1473	scissoring (CH_2)/ EtO_{ad}/ 1473 [41]	EtO_{ad}
1625	δ (H_2O)/ H_2O_{ad}/ 1600 [19]/ 1622-1626 [38]	H_2O_{ad}

2700 2744	ν(CH)/ CH_3CHO_{ad} / in gas phase: 2716; adsorbed on TiO_2: 2759 [44]	CH_3CHO_{ad}
2871 2973 2901	ν_s (CH_3) /2870 [41]/ 2872 [32]/ 2875 [42] ν_a (CH_3)/ 2969 [43]/ 2971 [41] [32]/ 2975 [42] ν_s (CH_3) / $EtOH_{ad}$/ 2901 [32]	$EtOH_{ad}$, EtO_{ad}
2901 2930	ν_s (CH_2) / 2901 [28] ν_a (CH_2) / 2931 [41] [32]/2930 [42]/	$EtOH_{ad}$, EtO_{ad}
3200	ν_s(OH)/ H_2O_{ad}/ tetrahedrally coordinated water molecules [38]	H_2O_{ad}
3400	ν(HO· · ·H)/ $EtOH_{ad}$/ 3400 [32] ν_a(OH)/H_2O_{ad}/ below 3500, maximum at 3417 due to randomly orientied water molecules [38]	$EtOH_{ad}$ H_2O_{ad}
3550 – 3800	ν(OH) isolated Ti–OH groups, that have little interaction with other hydroxyl groups – present on the various adsorption sites on the surface [38] [45] Residual hydroxyl groups that are present even after evacuation at 700 °C [19]	OH (Dissociated water)

4.3.2. EtOH Desorption

After the EtOH adsorption in the FTIR transmission cell as discussed in 4.3.1, the samples were heated up with a heating rate of 10 °C min^{-1}. Spectra were taken at 20 °C, 100 °C, 200 °C, 300 °C, 350 °C and 400 °C. The results are depicted in Figure 21, Figure 24 and Figure 26. The peak assignments and their literature references are listed in Table 3.

4.3.2.1. EtOH Desorption from Rutile

The negative signals around 3400 cm^{-1} and at 1625 cm^{-1} are due to residual hydroxyl groups of physisorbed water, that must have been present before taking the background spectra and desorb during heating.

Ethoxy groups remain adsorbed until the end of the measurements: 400 °C. The $-CH_3$ and $-CH_2$ stretching modes between 2870 and 2975 cm^{-1} remain present until 400 °C, even though they lose intensity during heating. The mentioned loss of intensity is caused by desorption of the molecularly adsorbed ethanol.

Molecularly adsorbed EtOH remains adsorbed up to 100 °C, which is visible from the signals at 1410 and 1274 cm^{-1} (in turquoise), that vanish during heating. In addition –as already discussed in 3.2- elevation of background absorbance of TiO_2 is ascribed to production of conduction band electrons. The extent of accumulation of electrons can be increased by adsorbed hole-scavengers like methanol, and decreased by adsorbed electron scavengers such as gasphase O_2 or adsorbed –OH or H_2O. [31] Therefore, the rising background signal between 2000 and 1100 cm^{-1} (better visible in Figure 22) must be due to the loss of an electron-scavenging specimen, as e.g. –OH groups are – agreeing the mentioned desorption of molecularly adsorbed ethanol.

Unfortunately, the rising background absorbance makes it impossible to fully recognize the characteristic ethoxy signals between 1070 and 1150 cm^{-1} at higher temperatures.

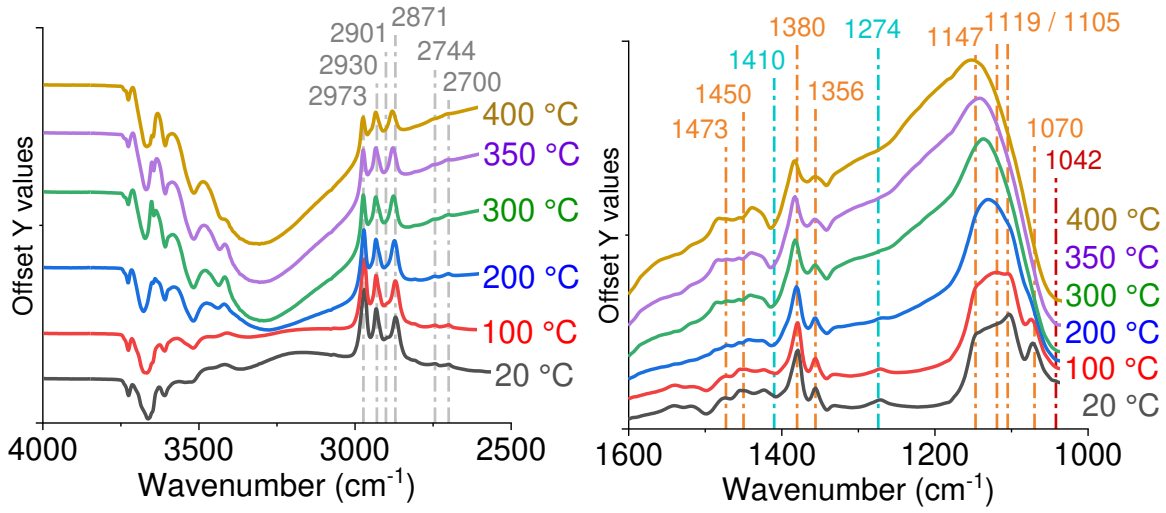

Figure 21 EtOH Desorption from Rutile carried out and monitored in FTIR transmission cell with a resolution of 4 cm^{-1}.

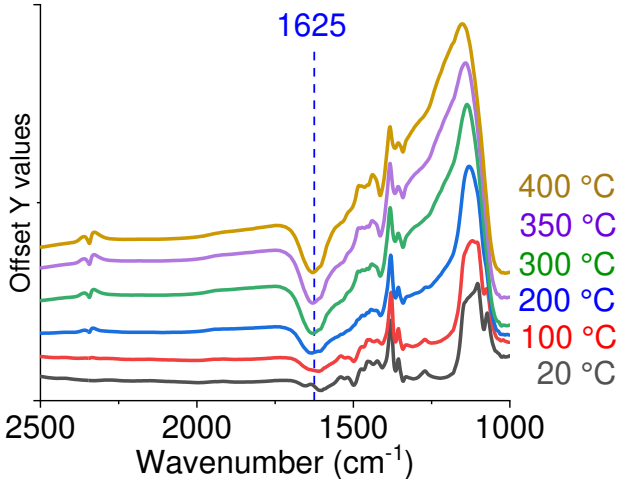

Figure 22 EtOH Desorption from Rutile carried out and monitored in FTIR transmission cell with a resolution of 4 cm^{-1}.

4.3.2.2. EtOH Desorption from Au Rutile

Again, negative signals around 3400 cm^{-1} and at 1625 cm^{-1} are due to residual hydroxyl groups of water, that were present whilst taking the background spectra and desorb during heating.

Just like on plain Rutile, molecularly adsorbed EtOH remains adsorbed until up to 100 °C, which is firstly visible from the signals at 1410 and 1274 cm^{-1} (in turquoise), that vanish during heating. Secondly, again, there is rising background absorbance between 2000 and 1100 cm^{-1}, which again makes it hard to track the ethoxy signals between 1050 and 1150 cm^{-1} during heating.

Ethoxy groups remain adsorbed until 300 – 350 °C, the $-CH_3$ and $-CH_2$ stretching modes between 2870 and 2975 cm^{-1} are significantly lowered by reaching 300 °C, and almost completely vanished by 350 °C. This loss of intensity is not to be ascribed to desorption of ethoxy, but instead to reaction of ethoxy species to acetaldehyde (and formation of crotonaldehyde) and acetic acid, as it is described in more detail in 4.3.2 from page 43 onwards. There are prominent signals arising from 200 °C on, marked in blue at 1530 and 1445 cm^{-1}, originating from adsorbed acetaldehyde and acetate species**.** A peak at 1350 cm^{-1} –which is depicted in Figure 25, and must not be confused with the one at 1356 cm^{-1} from ethoxy– arises simultaneously, and according to Singh et al., is to be ascribed to adsorbed acetaldehyde to TiO_2. [44] The weak shoulder at 1644 cm^{-1} rising up from the negative, dominant water-peak at 1625 cm^{-1} indicates the presence of crotonaldehyde. However, neither are signals found in the for ν(C=O) of acetaldehyde characteristic 1725 cm^{-1} region, nor in the for crotonaldehyde typical 3060-3030 cm^{-1} region.

Direct comparison of the IR region between 1300 and 1400 cm^{-1} of Rutile to the same region in the Au Rutile spectra, (as depicted in Figure 25) underlines that the peak at 1356 cm^{-1} effectively differs from the one at 1350 cm^{-1}.

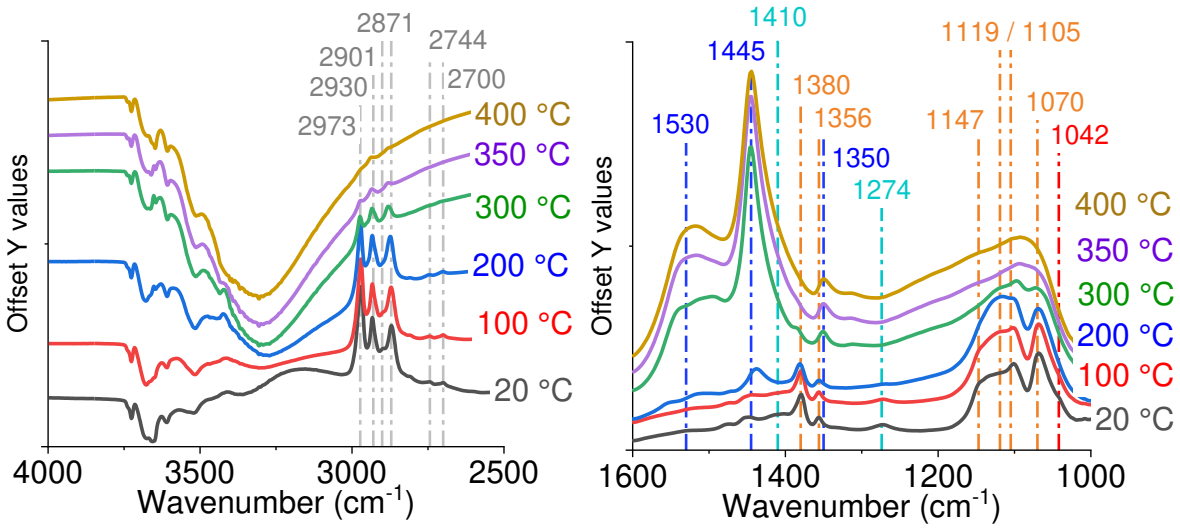

Figure 23 EtOH Desorption from 2.8 wt% Au Rutile carried out and monitored in FTIR transmission cell with a resolution of 4 cm^{-1}.

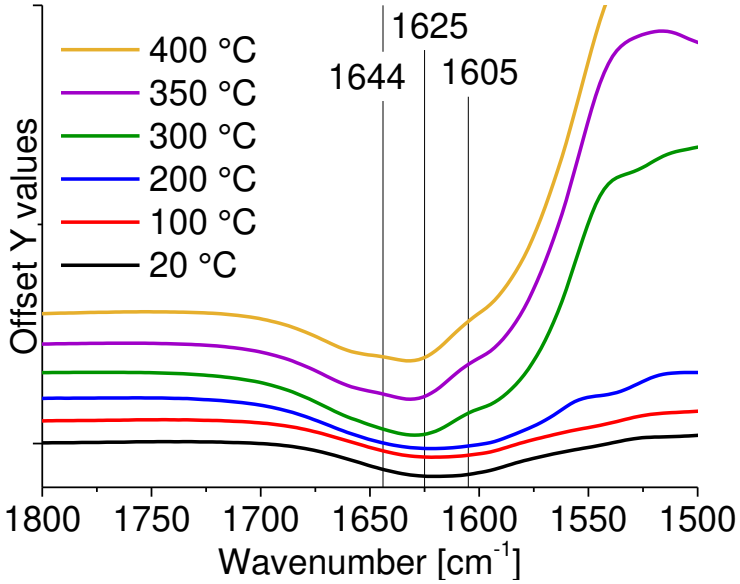

Figure 24 EtOH Desorption from 2.8 wt% Au Rutile carried out and monitored in FTIR transmission cell with a resolution of 4 cm^{-1}. 1800 – 1500 cm^{-1} in detail.

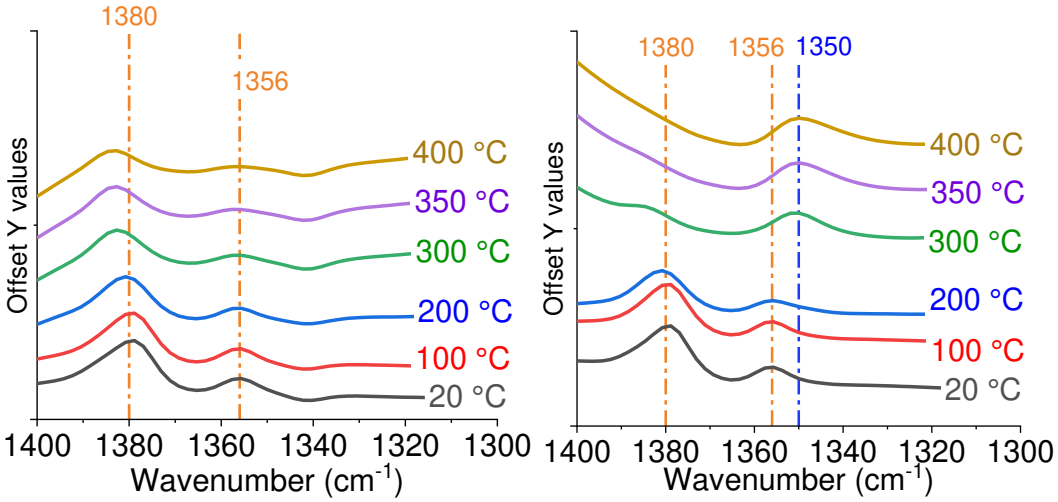

Figure 25 EtOH Desorption from Rutile (left) and 2.8 wt% Au Rutile (right) carried out and monitored in FTIR transmission cell with a resolution of 4 cm^{-1}. Direct comparison of the region 1400 cm^{-1} – 1300 cm^{-1}.

4.3.2.3. EtOH desorption from Au Ag Rutile

Molecularly adsorbed EtOH remains adsorbed up to 200 °C, as opposed to 100 °C for both Rutile and Au Rutile. Background absorbance rises with desorption of molecularly adsorbed ethanol but does not completely overlay the ethoxy species in the respective region of 1150 to 1050 cm^{-1}.

Ethoxy groups remain adsorbed until the end of the measurements: 400 °C. The -CH_3 and -CH_2 stretching modes between 2870 and 2975 cm^{-1} remain present until 400 °C, even though they lose intensity during heating. The mentioned loss of intensity is most likely caused by desorption of the molecularly adsorbed ethanol.

The ethoxy signals between 1500 and 1200 cm^{-1} remain relatively constant, while there are changes in the peak shapes for the signals below 1150 cm^{-1}, most likely due to rising background absorbance. However, the shoulder at 1042 cm^{-1} (bidentate ethoxy) remains visible even up to 400 °C.

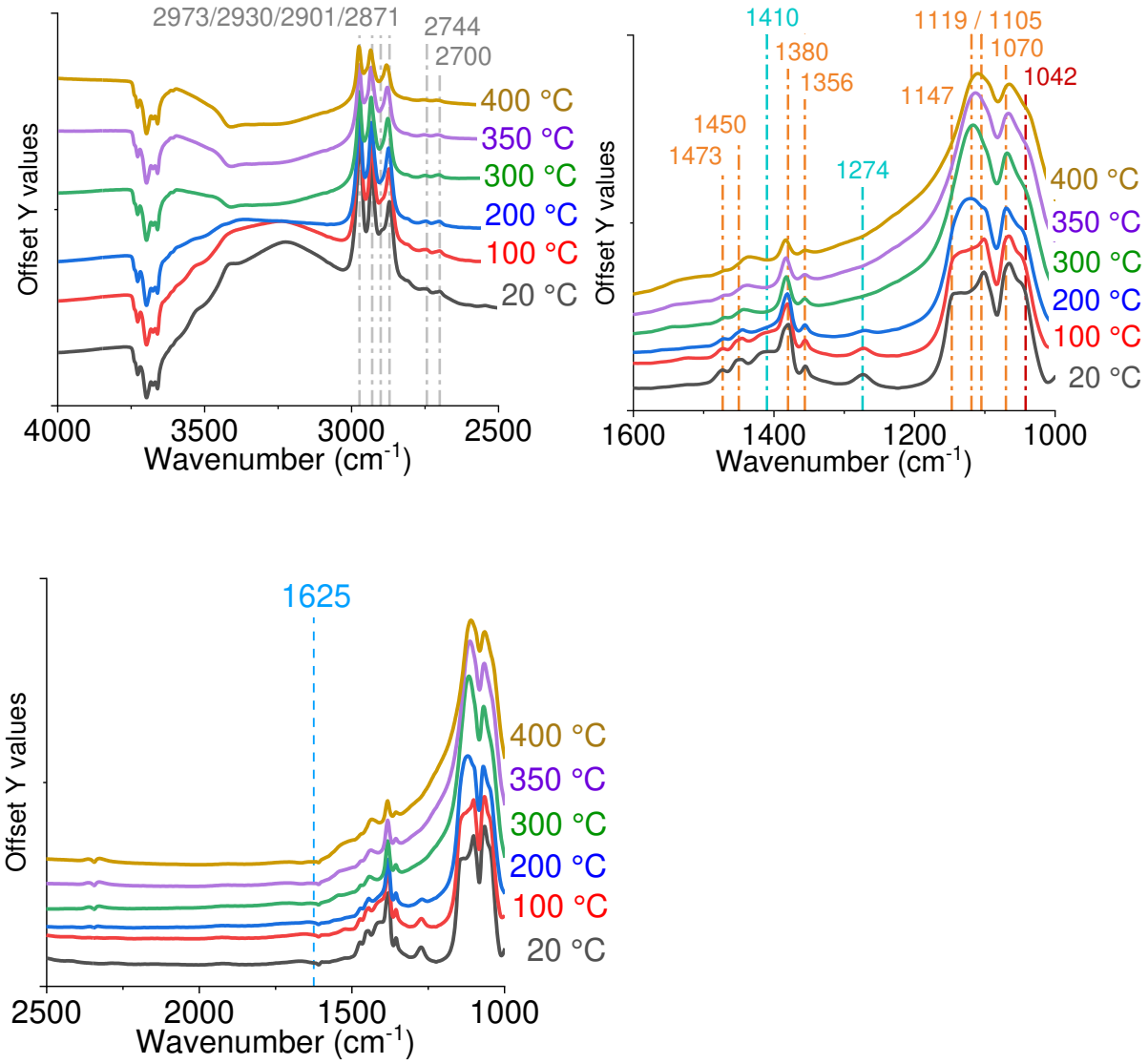

Figure 26 EtOH Desorption from 1 wt% Au 2 wt% Ag Rutile carried out and monitored in FTIR transmission cell with a resolution of 4 cm^{-1}.

4.3.3. Discussion

Ethanol adsorption and desorption take place differently on all three tested catalysts:

On Rutile, ethanol adsorbs i) molecularly, which desorbs at around 100 °C and ii) as ethoxy monodentate, which remains adsorbed up until measurements stopped (400 °C).

On Au Rutile, ethanol adsorbs i) molecularly, which desorbs at around 100 °C and ii) as ethoxy monodentate with slightly more bidentate species than there were found on Rutile. Acetaldehyde and acetate species start to form from ethoxy at around 250 °C and by reaching 300 °C the ethoxy signals have vanished.

On Au Ag Rutile, ethanol adsorbs i) molecularly, which desorbs at around 200 °C and ii) as ethoxy monodentate as well as ethoxy bidentate, showing a significantly stronger signal for the bidentate species than on Rutile or Au Rutile. The ethoxy groups remain adsorbed up until measurements stopped (400 °C), no formation of acetaldehyde or acetate species is observed - presumably due to the more stable bidentate bond or due to less Au on the surface (partial coverage of Au by Ag).

4.4. Effects of Silver on the Reaction Mechanism: In-situ IR measurements

The catalysts were pretreated as usual, and heated up aiming for temperatures at which Nagl et al. detected desorption of acetaldehyde CH_3CHO during ethanol TPD measurements (see Figure 27): 66 °C or 87 °C, 174 or 187 °C, 324 °C and 365 °C. [2] Unfortunately, for Au Ag Rutile, after reaching 325 °C, the spectral signal lowered significantly and it was not possible to take IR spectra at 365 °C or 410 °C.

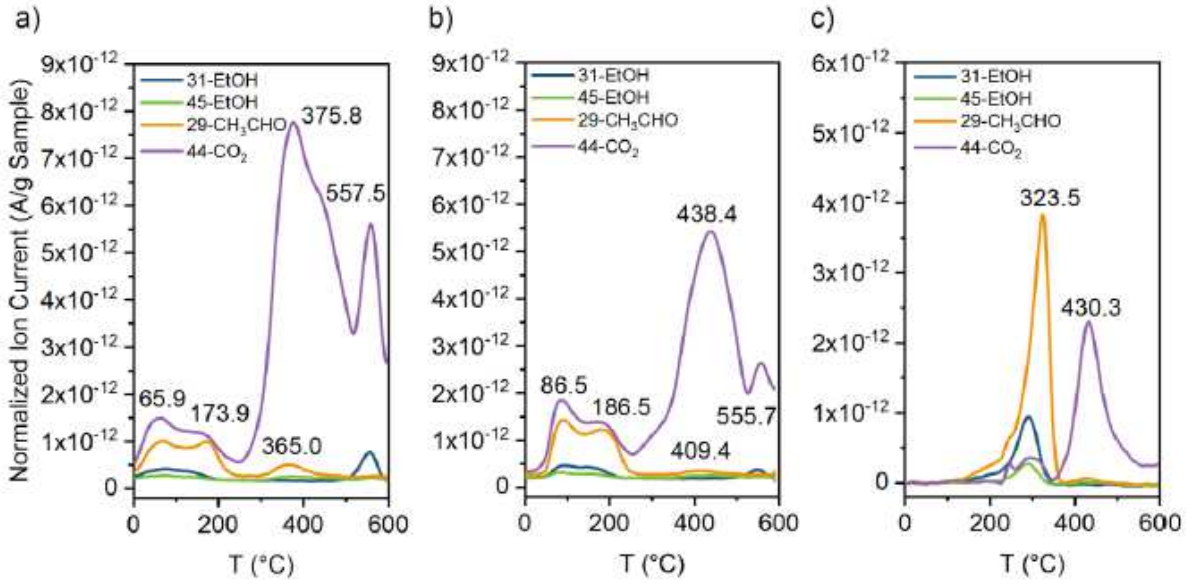

Figure 27 Ethanol TPD experiments for (a) Au Rutile (b) Au Ag Rutile (c) Rutile reference sample, m/z signals of 31 and 45 were used for the EtOH detection, whereas 29 was used for acetaldehyde (CH_3CHO) and 44 for CO_2. Taken from Nagl et al. [2]

Besides water, acetaldehyde (CH_3CHO) is monitored as the main product of ethanol oxidation over the used catalysts. Adsorbed acetaldehyde can further be oxidized into surface acetate. Total oxidation of ethanol (eventually adsorbed as ethoxy) and further oxidation of acetic acid lead to CO_2 - surface carbonates may occur. Ethyl acetate is formed

by coupling of adsorbed acetaldehyde or acetic acid/surface actetates with ethoxy species. It is reported in literature numerous times, that crotonaldehyde (CrCHO) is formed by aldol condensation of acetaldehyde on the surface of TiO_2. [44] [46] The mechanism for aldol condensation proposed by Singh et al. in 2008 is depicted in Figure 28. Rekoske et al. studied acetaldehyde adsorption on TiO_2 thoroughly in 1999 and reported that the CH_3CHO aldolization is strongly dependent on the exposure time to acetaldehyde: exposure to 10 Torr of acetaldehyde at 40 °C delivers strong signals of crotonaldehyde after 5 min. However, continuing exposure leads to displacement of crotonaldehyde: after 15 min crotonaldehyde signals are weakened and after 30 min of exposure they vanished completely. A poisoning of the active sites was suggested from the authors to be the reason for the phenomenon. [46]

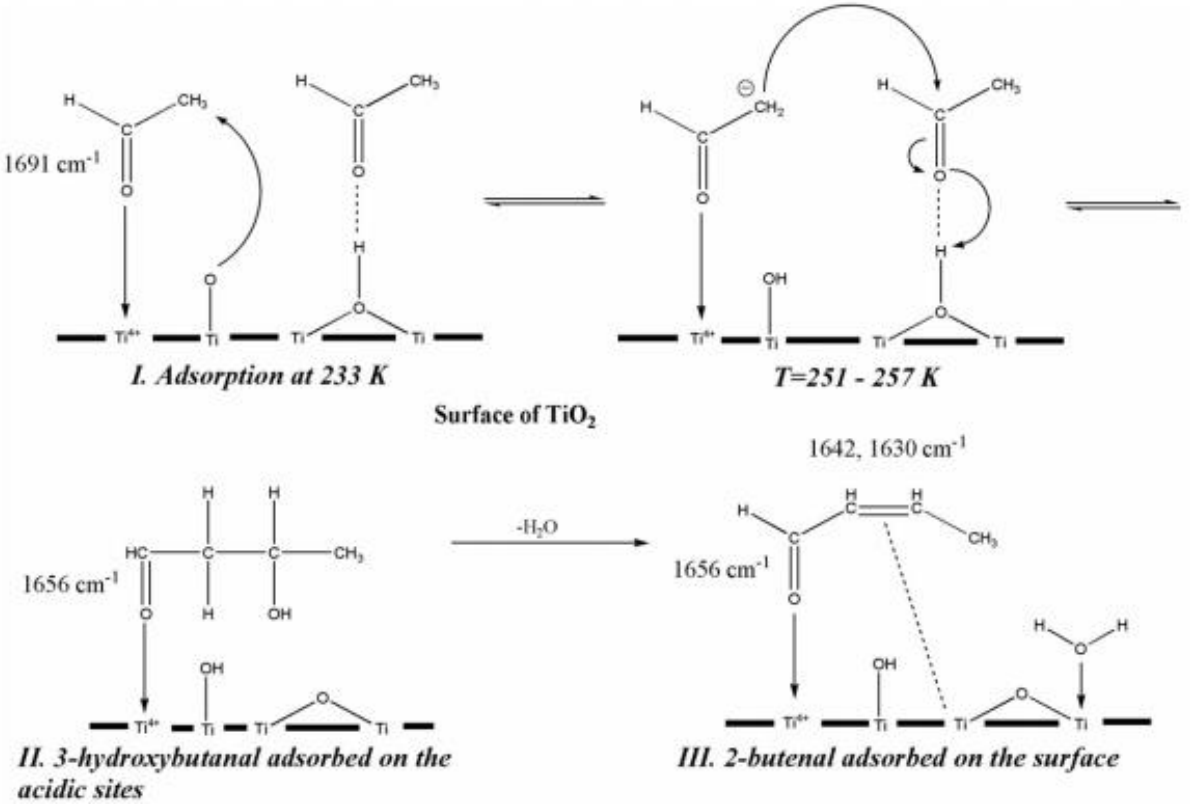

Figure 28 Schematic mechanism of aldol condensation of acetaldehyde on TiO_2, taken from Singh et al. [44]

Altogether, adsorption of ethanol, ethoxy, hydroxyl groups, acetaldehyde, crotonaldehyde, acetate species and surface carbonates onto anatase and rutile proceed through a rich set of numerous adsorbed forms, transient surface species, shifts of band positions due to interactions of the groups with one another and changing exposure times.

Peak assignments are listed in Table 3 (for the ethoxy and ethanol signals) and Table 4 (for intermediate and reaction products).

Table 4 IR signals of reaction products and intermediate species

Wavenumber (cm^{-1}) meas. in this work	Vibrational mode / species / reference	Ascribed Species for this work
1120	$\gamma(CH_3)$, ν (C–C)/ CH_3CHO_{ad}/ 1120 [47]	CH_3CHO_{ad}
1167	ν (CC) / ads. Crotonaldehyde ($CrCHO_{ad}$)/ 1167 [47]	$CrCHO_{ad}$
1260	η^2(CO) / CH_3CHO_{ad} / 1259 [44] δ(CH) / $CrCHO_{ad}$ / 1259 [47]	CH_3CHO_{ad} $CrCHO_{ad}$
1345, 1350	$\delta_s(CH_3)$/ CH_3CHO_{ad}/ 1338 [47] $\delta_s(CH_3)$ + δ(CH)/ CH_3CHO_{ad}/ 1350 [44] $\delta(CH_3)$, δ(CH)/ CH_3CHO_{ad}/ 1355 (anatase, high exposure), 1348 (rutile), 1342 (anatase, low exposure) [46]	CH_3CHO_{ad}
1365	$\delta_s(CH_3)$ / CH_3CHO_{ad} / 1377 [44] δ(CH) / CH_3CHO_{ad} / 1376 [47]	CH_3CHO_{ad}
1445	ν_a / surface carbonate CO_3^{2-} / 1437 $\delta_{as}(CH_3)$/ CH_3CHO_{ad}/ 1443, 1420 [44]; 1442 [47] ν_s (COO) / Adsorbed acetates bidentate /1435 [48]	Carbonates, CH_3CHO_{ad} $CH_3COO^-_{ad}$
1520	ν_a (COO)/ Adsorbed acetates bidentate /1530 [48] ν_a (COO)/ acetate/ 1562 (anatase), 1544 (rutile) [46] ν_a (COO)/ adsorbed carboxyl species / 1517 [49] ν_a (COO)/ surface acetate / 1526 [47]	CH_3COOH_{ad} $CH_3COO^-_{ad}$
1590	ν_a (COO)/ adsorbed carboxyl species / 1568 [49] ν (C=C) / $CrCHO_{ad}$ / 1594 [47]	CH_3COOH_{ad} $CrCHO_{ad}$
1625	δ (H_2O)/H_2O_{ad}/ 1600 [19]/ 1622-1626 [38] δ(HOH) / water /1629 [49]	H_2O_{ad}
1652	ν (C=O) / $CrCHO_{ad}$ / 1645 – 1629 [47] ν (C=O) / $CrCHO_{ad}$ / 1656 [44] ν (C=C) / $CrCHO_{ad}$ / 1642, 1630 [44]	$CrCHO_{ad}$
1680	ν(C=O) / surface acyl / 1680 [48]	CH_3CHO_{ad}

	ν(C=O) / adsorbed acetaldehyde on TiO_2/ 1691 [44] ν_a(C=O) / adsorbed carbonyl species / 1667 [49]	
1685-1722	ν(C-O)/ CH_3CHO_{ad}/ 1722-1685 [47]	CH_3CHO_{ad}
1725	ν(C=O) / CH_3COOH_{ad} / 1725 [48] ν(C=O) / CH_3CHO_{ad} / 1723, 1721, 1718 [32] ν(C=O) / CH_3CHO_{ad} / 1725 (anatase), 1718 (rutile), 1703 (anatase) [46] ν(C=O) / CH_3CHO (gasphase) / 1735 [46] ν_a(C=O) / CH_3CHO_{ad} / 1725 [49]	CH_3COOH_{ad} CH_3CHO_{ad}
1770	ν_a(CO) / CH_3COOH_{ad} / 1750 [49]	CH_3COOH_{ad}
2700 2744	ν(CH)/ CH_3CHO_{ad} / 2759 [44] [46] ν(CH)/ CH_3CHO_{ad} / 2730 [47] ν(CH)/ $CrCHO_{ad}$ / 2745 (anatase), 2740 (rutile) [46]	CH_3CHO_{ad} $CrCHO_{ad}$
3064	υ(C=C–H)sp2 / $CrCHO_{ad}$ / 3017 [44] υ(C=C–H)sp2 / $CrCHO_{ad}$ / 3038 (anatase), 3036 (rutile) [46] $\nu(CH_3)$/ $CrCHO_{ad}$ / 3035 [46] ν(CH)/ $CrCHO_{ad}$ / 3023 [48]	$CrCHO_{ad}$

4.4.1. Steady state in-situ DRIFTS difference spectra

In the following Figure 29 to Figure 30, in-situ IR studies under ethanol and oxygen flow are depicted as difference spectra, whereat the respective catalyst under He after pretreatment was taken as background. Therefore, adsorbed ethanol, ethoxy, intermediates and reaction products are accountable for the signals, while background signals from TiO_2 are cancelled out. While Figure 29 gives an overview over the entire region of 4000 – 1000 cm^{-1} of all catalyst at all measured temperatures, Figure 30 shows the regions of interest in more detail. Ethanol and ethoxy signals (as they are extensively discussed in 4.3.1 from page 40 onwards) are marked in orange, while reaction products or intermediates are marked in green.

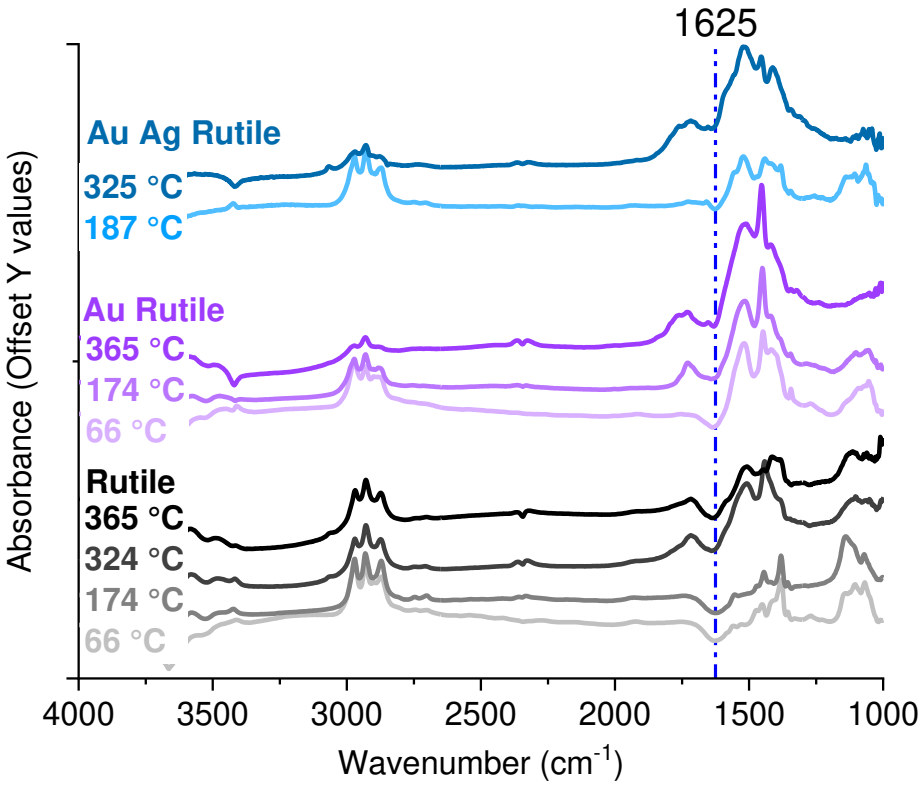

Figure 29 DRIFTS Difference spectra of Rutile, Au Rutile and Au Ag Rutile under EtOH and O_2 (Background = Respective catalyst under He flow)

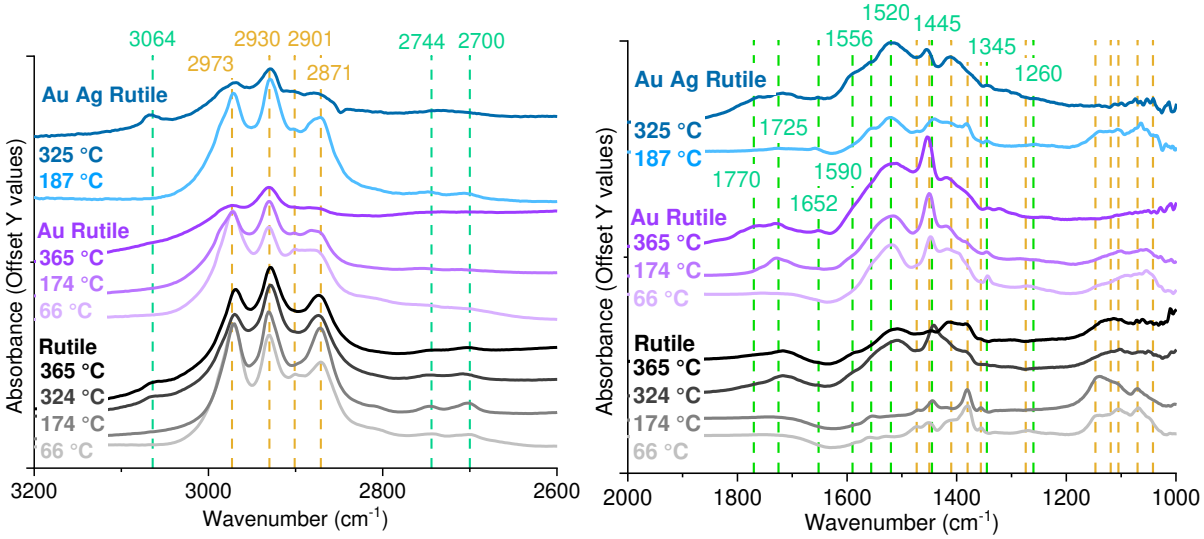

Figure 30 DRIFTS Difference spectra of Rutile, Au Rutile and Au Ag Rutile under EtOH and O_2, 3200 – 2600 and 2000 - 1000 cm^{-1} in detail, peak assignments are listed in Table 4 (Background = Respective catalyst under He flow after pretreatment)

For Rutile, at 66 °C and 174 °C, the positive signals originate mainly from ethoxy and EtOH adsorbed to TiO_2, however, there are also weak signals at 2744 and 2700 cm^{-1} visible, which are ascribed to –CH stretching vibrations of acetaldehyde adsorbed to TiO_2 (either as CH_3CHO_{ad} or $CrCHO_{ad}$). The negative signal at 1625 cm^{-1} is ascribed to desorption of

water due to heating. In contrast to the ex-situ measurements, signals at 1450 cm^{-1} and the 1590-1510 cm^{-1} region strongly increase at 324 °C – which is accounted to an overlay of signals originating from crotonaldehyde, molecularly adsorbed acetic acid and acetate species, indicating oxidation of ethanol to acetaldehyde and further oxidation to acetate species, their protonation and desorption – and therefore agreeing with the ethanol TPD (see Figure 27). At 324 °C, there is also a small peak arising at 3064 cm^{-1}, which is ascribed to CrCHO as well, even though in literature the respective peak is reported to be found between 3040 - 3020 cm^{-1}. When heated up further to 365 °C, the crotonaldehyde, acetic acid and acetate signals decrease, however the ethoxy groups remain on the surface (during reaction conditions at least).

The quantitative analysis of the effluent gases is depicted in Figure 31 (results of 66 °C are not shown due to the ethanol conversion of 0.05 % hitting the limits of detection). It demonstrates that even though the respective signals are found merely very weakly in the IR spectra, the reaction of ethanol to acetaldehyde, acetic acid and ethyl acetate has not come to a halt. On the contrary, EtOH conversion rises from 12.6 % at 324 °C to 23.9 % at 365 °C. This leads to the conclusion, that at 365 °C ethoxy species are, more than ever, oxidized to acetaldehyde, which simply immediately desorbs, so that the respective signals are found merely very weakly in the IR spectra.

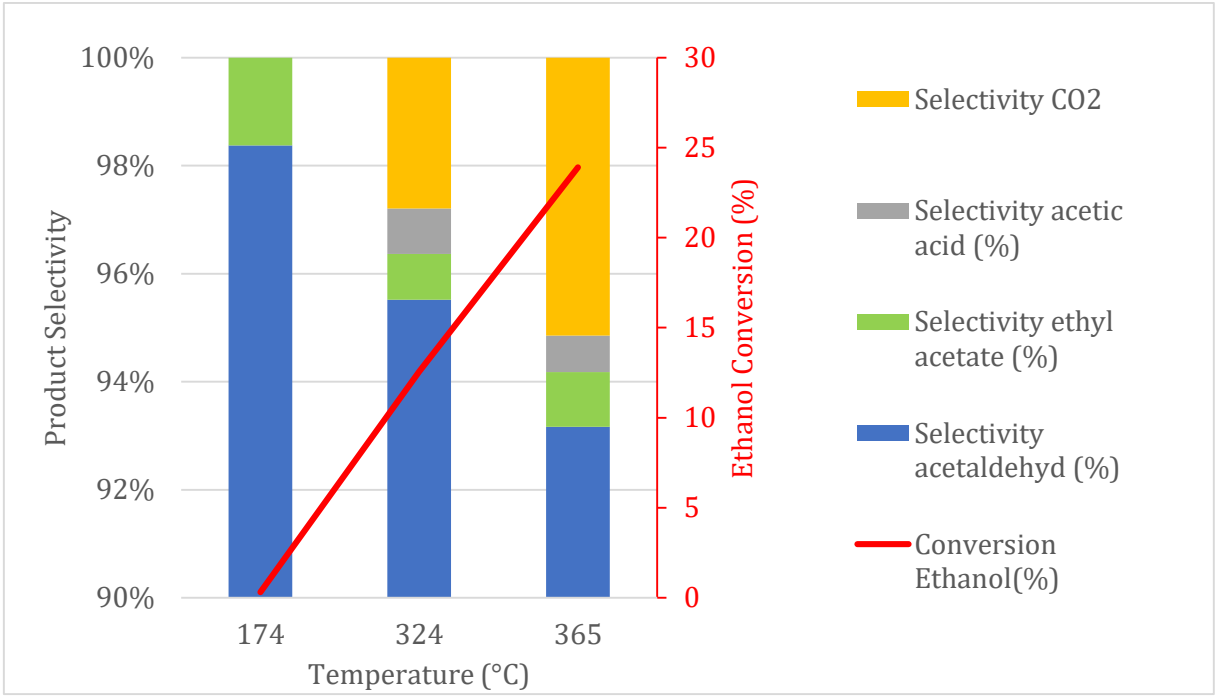

Figure 31 Quantitative analysis of the effluent gases during DRIFTS measurements over Rutile

Au Rutile shows a similar behavior as it did in the ex-situ measurements with EtOH only, as discussed in 4.3.2 from page 43 onwards. Ethoxy species are consumed, therefore the C-H stretching vibrations weaken significantly. In the meantime, there is a strong rise in acetaldehyde, crotonaldehyde, acetic acid and acetate species documented, which remain adsorbed up until 365 °C. The small peaks at 3064 and 1652 cm^{-1} are ascribed to crotonaldehyde and were not found in the ex-situ measurements.

The behavior of Au Ag Rutile in the in-situ measurements differs significantly from its behavior in the ex-situ measurements. The spectra taken at 187 °C resemble the spectra of Rutile taken at 365 °C, suggesting the desorption temperature of acetaldehyde had already been reached at that point, and contradicting the TPD (see Figure 27). At 325 °C, C-H stretching vibrations are significantly weaker than what they were at 187 °C, suggesting the decline of ethoxy species from the surface. Meanwhile, a peak at 3064 cm^{-1} (crotonaldehyde) arises and the signals between 1560 and 1515 cm^{-1} (ascribed to acetic acid and acetate species) increase strongly. The peak at 1445 cm^{-1} however, (which is partly ascribed to acetaldehyde) does not rise in the same manner, leading to the conclusion, that in the other spectra, acetaldehyde contributed strongly to the 1445 cm^{-1} peak. The signals between 1770 – 1720 cm^{-1} however must be primarily ascribed to acetic acid, owing to them rising proportionally with the signals between 1560 and 1515 cm^{-1}.

4.4.2. Steady state in-situ DRIFTS difference spectra: stepwise addition and removal of educts in detail

Depicted are the catalysts at the respective temperatures i) under He, which serves as background. ii) Afterwards, EtOH was added to the He flow, iii) followed by addition of O_2. iv) EtOH and O_2 streams were shut off, and the sample under He, including remaining, adsorbed species, is depicted.

Each step was carried out until steady state was reached (after around 20-30 min). It needs to be noted, that this procedure was carried out at multiple temperatures for each catalyst (starting with the lowest temperature) and the pretreatment was done only before the first measurement. Therefore, product species partly remain on the catalysts surface during heating from one temperature-step to the next, at which another spectrum under He was taken and used as new background. This explains some following

absorbance signals being negative: species that had remained on the surface from prior measurements, desorb or react.

4.4.2.1. Rutile

Measurements at 66 °C are depicted in Figure 32 and show mostly ethoxy (black and the bidentate ethoxy signal in red) and EtOH signals (in magenta), whether O_2 is present or not. However, there are also weak signals at 2744 and 2700 cm^{-1} visible, which are ascribed to –CH stretching vibrations of acetaldehyde adsorbed to TiO_2. The negative signal at 1625 cm^{-1} is ascribed to desorption of water due to heating. After reaction, ethoxy as well as molecularly adsorbed EtOH (in magenta) remain on the surface, agreeing with the ethanol TPD results depicted in Figure 27 and the ex-situ ethanol IR studies in 4.3.2 from page 43 onwards.

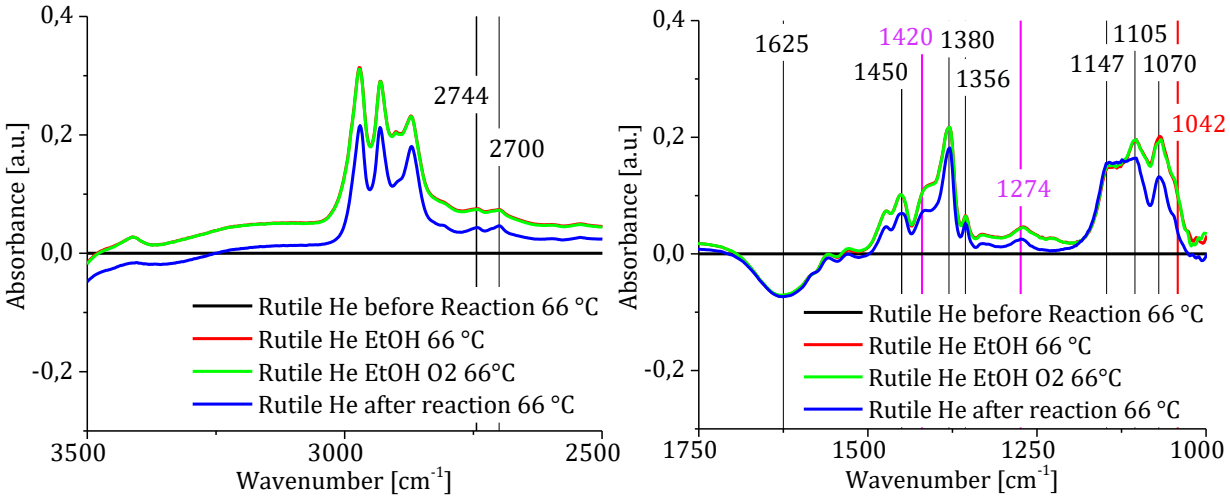

Figure 32 DRIFTS difference spectra of Rutile at 66 °C under He (black, used as background), under EtOH (1.1 mL min^{-1}) diluted in He in red , under EtOH and O_2 (1.1 mL min^{-1} each) diluted in He in green and under He, after reaction, in blue. Molecularly adsorbed EtOH is marked in magenta, ethoxy bidentate in red.

Measurements at 174 °C are shown in Figure 33 and depict similar patterns after introduction of EtOH: signals originating from adsorbed ethoxy (in orange and ethoxy bidentate in red) and EtOH (in magenta, rather weak) rise. After adding oxygen, however, the molecularly adsorbed EtOH and ethoxy groups are oxidized: the signals originating from $EtOH_{ad}$ vanish, while the signals originating from EtO^-_{ad} weaken drastically. Characteristic vibrations of reaction products (depicted in black) arise meanwhile: signals

at 2744, 2700 and 1350 cm^{-1} (CH_3CHO_{ad}), 1520 cm^{-1} (CH_3COOH_{ad}), 1544 and 1443 cm^{-1} ($CH_3COO^-_{ad}$) strongly increase.

After reaction - in absence of EtOH and O_2 - the ethoxy and product signals remain adsorbed. Additionally, a signal arises at 1544 cm^{-1} ($CH_3COO^-_{ad}$), indicating that in presence of EtOH, protonation of $CH_3COO^-_{ad}$ leads to CH_3COOH_{ad}. After removing EtOH from the He flow, more $CH_3COO^-_{ad}$ remain adsorbed. Protonation may happen either directly from EtOH, forming further ethoxy groups, or indirect over hydroxyl groups or even surface atomic hydrogen, as proposed by Liu et al., and depicted in Figure 2. [30]

These results agree with the ethanol TPD (as in Figure 27), which shows desorption peaks rise at above 300 °C.

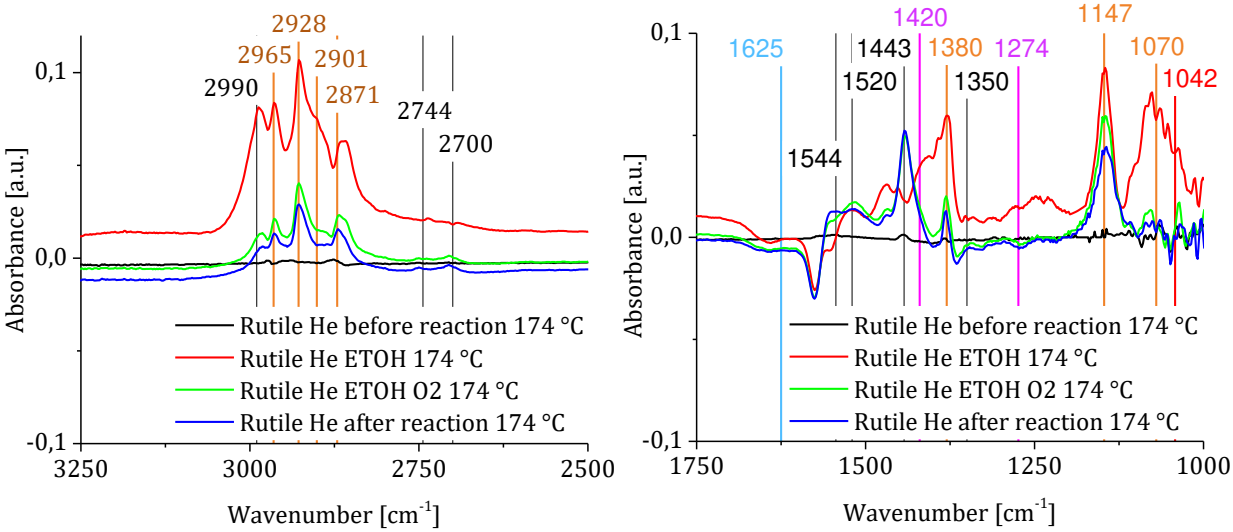

Figure 33 DRIFTS difference spectra of Rutile at 174 °C under He (black, used as background), under EtOH (1.1 mL min^{-1}) diluted in He in red , under EtOH and O_2 (1.1 mL min^{-1} each) diluted in He in green and under He, after reaction, in blue. Molecularly adsorbed EtOH is marked in magenta, ethoxy in orange, except for the bidentate signal, which is red. Reaction products are marked in black.

As depicted in Figure 34, further heating to 324 °C, followed by addition of EtOH leads to negative signals in the region characteristic for adsorbed acetates (1560-1520 cm^{-1} and at 1443 cm^{-1}), indicating desorption of acetate species, presumably due to protonation. The rising ethoxy signals (in orange/red) indicate substitution of the adsorbed acetate specimen by adsorbed ethoxy species. Weak signals at 2744 and 2700 cm^{-1} arise after EtOH introduction, which are ascribed to –CH stretching vibrations of acetaldehyde adsorbed to TiO_2 and therefor indicate dehydrogenation reaction taking place. Upon addition of oxygen to the gas stream, the peak at 1128 cm^{-1} (ethoxy monodentate)

disproportionally weakens, while the other ethoxy signals remain relatively constant. Meanwhile, signals at 3064, 1744, 1700, 1718, 1594 and 1350 cm^{-1} indicate formation of acetaldehyde, adsorbed either as CH_3CHO_{ad} or $CrCHO_{ad}$. Acetate species (1544, 1520, 1443 cm^{-1}) increase likewise.

After reaction, the ethoxy signals almost vanish (due to reaching the desorption temperature, see ethanol TPD in Figure 27) and acetaldehyde signals weaken (2744 and 2700 cm^{-1}), while the acetate (1544, 1520, 1443 cm^{-1}) and crotonaldehyde signals (3064, 1594 cm^{-1}) intensify.

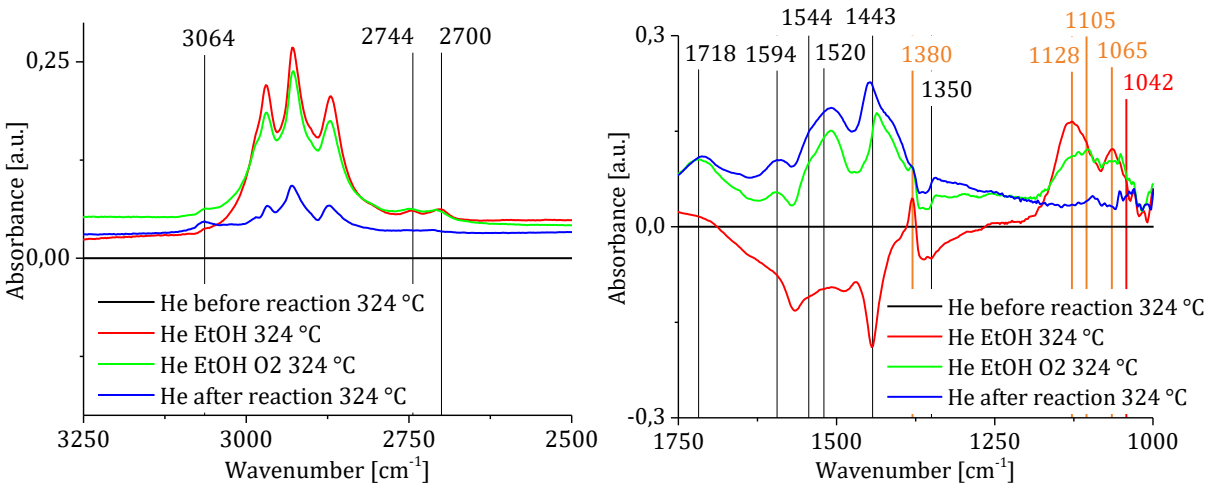

Figure 34 DRIFTS difference spectra of Rutile at 324 °C under He (black, used as background), under EtOH (1.1 mL min^{-1}) diluted in He in red , under EtOH and O_2 (1.1 mL min^{-1} each) diluted in He in green and under He, after reaction, in blue. Ethoxy groups are marked in orange, except for the bidentate signal, which is in red. Reaction products are marked in black.

At 365 °C, again, EtOH addition leads to positive signals in the ethoxy region and at 2744 and 2700 cm^{-1} (CH_3CHO_{ad}) and negative signals in the acetate's characteristic region– indicating, that even at temperatures this high, acetate species remain on the Rutile surface (see Figure 35). Consequently, acetates remaining on the catalysts surface until (at least) 365 °C must be the species responsible for the CO_2 peak at 430 °C in the TPD in Figure 27. For a better understanding, the spectrum taken at 365 °C after reaction is depicted in Figure 36, using a spectrum of the clean catalyst (taken right after pretreatment) as background – the main signals are ascribed to acetate groups. Signals due to acetaldehyde/ crotonaldehyde are found as well, however, there is no sign of ethoxy groups left on the surface. This supports the mechanism proposed by Liu et al. in 2009 (depicted in Figure 1) and contradicts the mechanism suggested by Jørgensen et al.

in 2007 (Figure 2). [29] [30] The latter mechanism was, however, suggested for reaction in the liquid phase.

Upon addition of oxygen, the ethoxy signals weaken and the acetate species form. Weak signals originating from acetaldehyde and/or crotonaldehyde are present as well, however much weaker than at lower temperatures. Taking the quantitative analysis of the effluent gases into account, this however is not due to lesser production of acetaldehyde. Instead, acetaldehyde desorbs immediately.

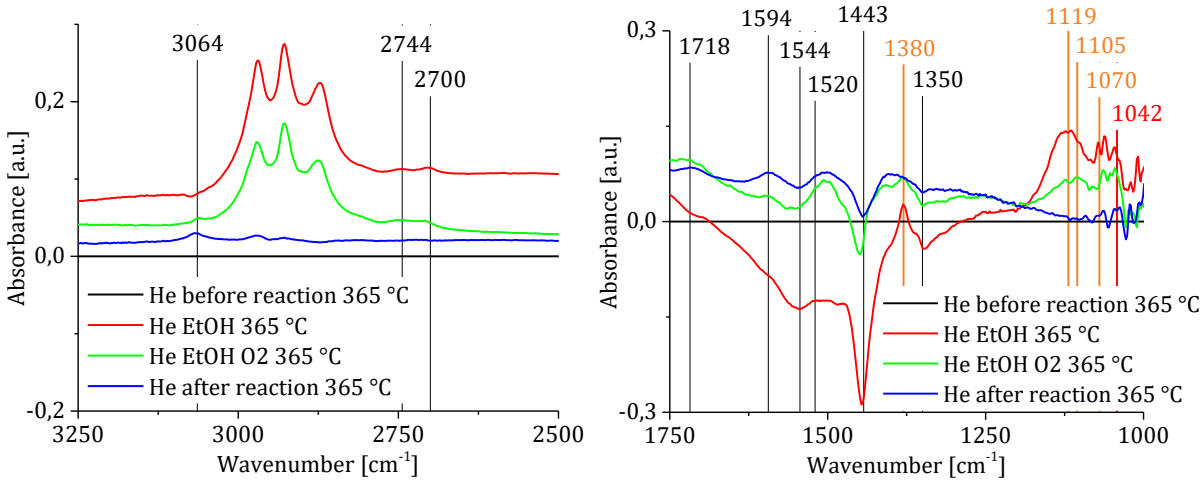

Figure 35 DRIFTS difference spectra of Rutile at 365 °C under He (black, used as background), under EtOH (1.1 mL min^{-1}) diluted in He in red , under EtOH and O_2 (1.1 mL min^{-1} each) diluted in He in green and under He, after reaction, in blue. Ethoxy groups are marked in orange, except for the bidentate signal, which is in red. Reaction products are marked in black.

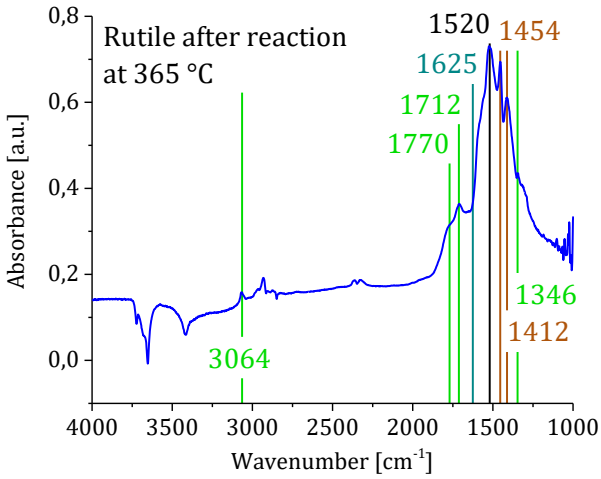

Figure 36 DRIFTS difference spectra of Rutile at 365 °C under He, after reaction. As background, a spectrum taken after pretreatment was used. One (negative) water signal is marked in blue, CH_3CHO/CrCHO signals are marked in green, overlapping acetate/acetaldehyde signals in brown and the main species – acetate – is marked in black.

Summary – steady state in-situ DRIFTS measurements over Rutile

All in all, adsorbed acetate species are not found at 66 °C, but at 174 °C, 324 and 365 °C. Signals arising from acetaldehyde, however, are already found at 66 °C as well as at the higher temperatures. After reaction, (under He flow only) acetaldehyde species remain on the catalysts surface at 66 °C and 174 °C, but desorb at 324 °C and 365 °C. Acetate species, however, are documented to remain on the surface even at 365 °C and must therefore be the responsible species causing the CO_2 peak at 430 °C in the ethanol TPD (Figure 27). However, adsorbed acetate species are easily substituted by ethoxy species, once EtOH is introduced, likely due to protonation and desorption as acetic acid. Ethoxy species remain on the surface at 66 °C, 174 °C and partly at 324 °C, agreeing with the ethanol TPD in Figure 27. Product formation from dehydrogenation (formation of the reaction products in absence of oxygen) is first noted at 324 °C.

4.4.2.2. 5 wt% Au on Rutile

At 66 °C, after introducing EtOH diluted in He, signals owing to the presence of adsorbed ethoxy (in Figure 37 marked in orange and red), EtOH (magenta), but also acetate and acetaldehyde (in black) arise, meaning that dehydrogenation reaction already takes place at 66 °C (in contrast to plain Rutile, where it was first noticed at 324 °C). Signals originating from EtO^-_{ad} weaken slightly upon oxygen introduction, while products' signals rise slightly. The peak at 3064 cm^{-1} ($CrCHO_{ad}$) is not found, signals at 2744 and 2700 cm^{-1} (CH_3CHO_{ad}) are solely indicated by a weak shoulder before and after oxygen introduction. Peaks at 1447, 1400 and 1350 cm^{-1} (adsorbed acetaldehyde and/or acetate species) however, rise relatively strongly upon oxygen addition.

After reaction, under He only, ethoxy and EtOH signals drop significantly (but don't vanish completely), while acetate and acetaldehyde signals rise slightly. The strongest increase show the peaks at 1693 (adsorbed acetaldehyde) and 1450 cm^{-1} (adsorbed acetaldehyde or acetate).

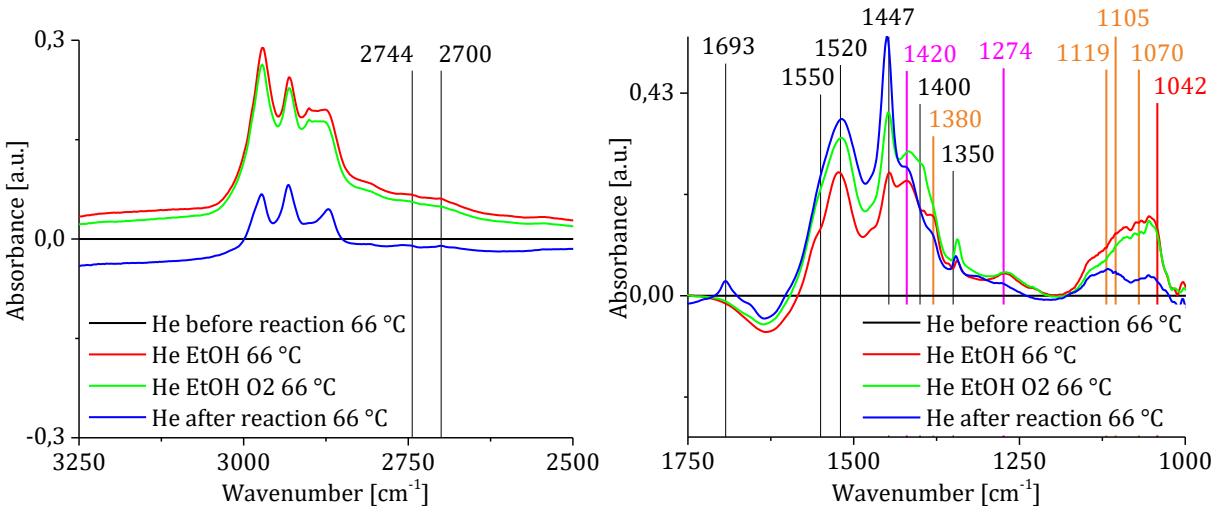

Figure 37 DRIFTS difference spectra of 5 wt% Au Rutile at 66 °C under He (black, used as background), under EtOH (1.1 mL min^{-1}) diluted in He in red , under EtOH and O_2 (1.1 mL min^{-1} each) diluted in He in green and under He, after reaction, in blue. Ethoxy groups are marked in orange, except for the bidentate signal, which is in red. Molecularly adsorbed EtOH is marked in magenta and reaction products in black.

At 174 °C, following EtOH introduction, the ethoxy and acetaldehyde (at 2744 and 2700 cm^{-1}) signals rise, while the acetate signals weaken - suggesting ethoxy groups substitute residual acetate groups from the surface. With oxygen introduction, ethoxy signals weaken slightly (especially ethoxy monodentate at 1147 cm^{-1}) and reaction products' signals rise – mainly around 1725 cm^{-1} (acetaldehyde and/or acetic acid), 1630 and 1594 cm^{-1} (both crotonaldehyde), 1455 cm^{-1} (acetaldehyde and/ or acetate) and 1260 cm^{-1} (acetaldehyde and/or crotonaldehyde). The priorly main peak at around 1450 cm^{-1} stays in the negative, meaning during reaction at 174 °C is less acetate formed than there was remaining from the measurements at 66 °C, supposedly due to acetaldehyde remaining on the surface for a shorter while and desorbing earlier (compare ethanol TPD in Figure 27).

After reaction, ethoxy signals weaken (but do not vanish), crotonaldehyde signals intensify (1594 cm^{-1}) while acetaldehyde signals weaken (1260 cm^{-1}) and those signals around 1725 cm^{-1} (acetaldehyde and/or crotonaldehyde) intensify slightly. The acetate signals increase rather strongly but remain in the slight negative.

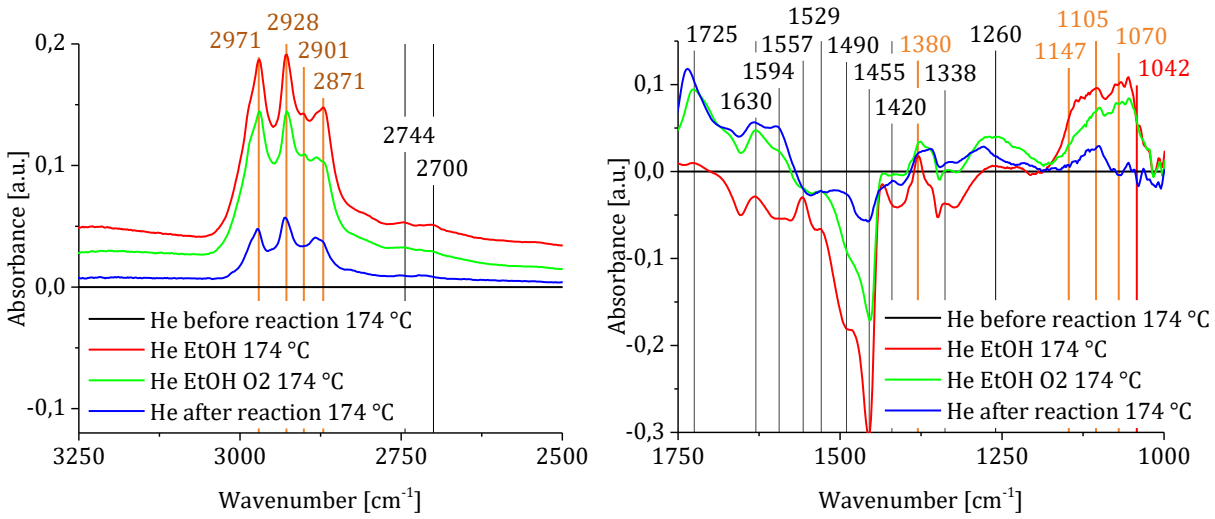

Figure 38 DRIFTS difference spectra of 5 wt% Au Rutile at 174 °C under He (black, used as background), under EtOH (1.1 mL min^{-1}) diluted in He in red , under EtOH and O_2 (1.1 mL min^{-1} each) diluted in He in green and under He, after reaction, in blue. Reaction products are marked in black and ethoxy groups in orange, except for the bidentate signal, which is in red.

At 365 °C, EtOH introduction again leads to rising ethoxy signals (in orange/ red), while signals at 1570 -1520 cm^{-1} (acetates) and 1450 cm^{-1} (acetates and/ or acetaldehyde) drop significantly below zero, meaning once again substitution of acetate species with ethoxy species. A positive signal is found at 1770 cm^{-1}, which is ascribed to CH_3COOH_{ad} and therefore supports the suggestion, that the presence of ethanol leads to protonation of acetate groups. Formation of acetic acid, especially at elevated temperatures, was also shown in 4.2.3.. After oxygen is introduced, the ethoxy signals weaken strongly, while the acetate signals rise back to the level (and slightly above) before EtOH introduction. Additionally, an increase in the region around 1725 cm^{-1} (acetic acid or acetaldehyde) is found. After reaction, the ethoxy signals vanish completely, while acetaldehyde/ acetic acid species weaken, but remain (partly) on the surface. About as much acetate species are found to be on the surface as there were before the reaction.

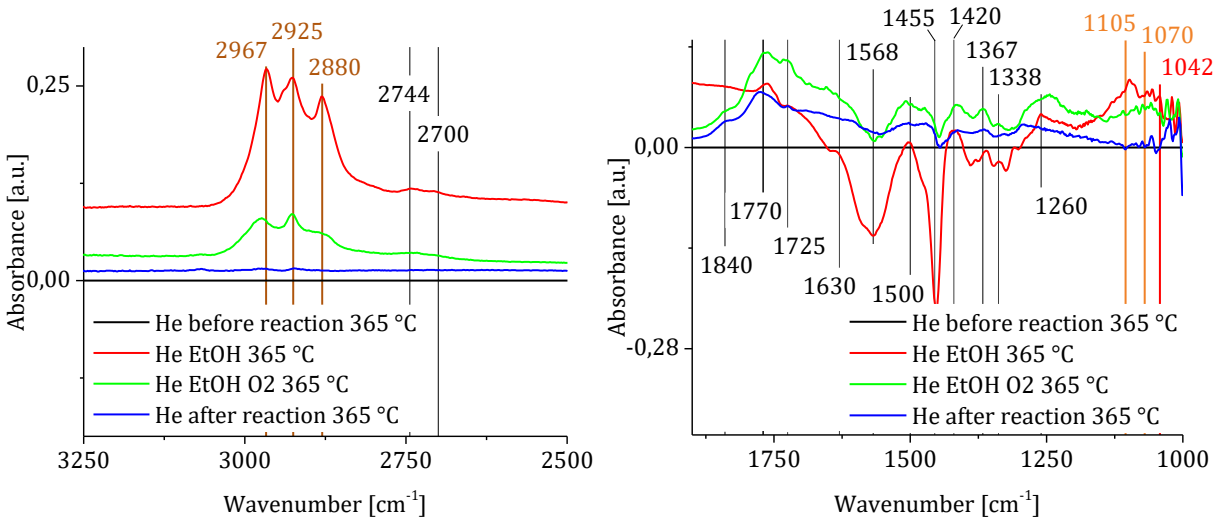

Figure 39 DRIFTS difference spectra of 5 wt% Au Rutile at 365 °C under He (black, used as background), under EtOH (1.1 mL min^{-1}) diluted in He in red , under EtOH and O_2 (1.1 mL min^{-1} each) diluted in He in green and under He, after reaction, in blue. Reaction products are marked in black and ethoxy groups in orange, except for the bidentate signal, which is in red.

Summary – steady state in-situ DRIFTS measurements over Au Rutile

Dehydrogenation reaction produces acetaldehyde and acetate groups at 66 °C already.

Acetate signals are the most intense at 66 °C, then slightly decrease at 174 °C (while acetaldehyde or acetic acid increased) to slightly increase again at 365 °C. This can be explained by an interplay of the smaller chance of acetate formation due to less coverage of acetaldehyde, and on the other hand, the increased reaction rate at higher temperatures.

Ethoxy species and acetaldehyde remain adsorbed after reaction at 66 °C and 174 °C, but desorb completely at 365 °C. Acetic acid and acetate groups remain on the catalysts surface even after reaction at 365 °C and are likely to be responsible for the CO_2 peak in the TPD (Figure 27) at 376 °C.

4.4.2.3. 2 wt% Au 1 wt% Ag Rutile

Measurements on the Au Ag Rutile catalyst were started at 187 °C, for the spectra see Figure 40: EtOH addition leads to an increase of ethoxy (in orange and red), EtOH (in magenta, agreeing with the ex-situ ethanol TPD FTIR studies in 3.5), acetaldehyde, acetic acid and acetate species (both in black). Upon O_2 addition, signals originating from ethoxy,

EtOH and the majority of acetaldehyde remain constant, while the ones at 1658 and 1443 cm^{-1} rise disproportionally. Both are ascribed to acetaldehyde and/or acetate species.

After reacion, signals of molecularly adsorbed ethanol vanish and ethoxy signals weaken, while acetaldehyde and acetate species remain on the catalysts surface. Signals originating from acetaldehyde remain constant, while signals at 1555 and 1443 cm^{-1} increase and the 1520 cm^{-1} peak decreases – possibly due to a shift from acetic acid to acetate species.

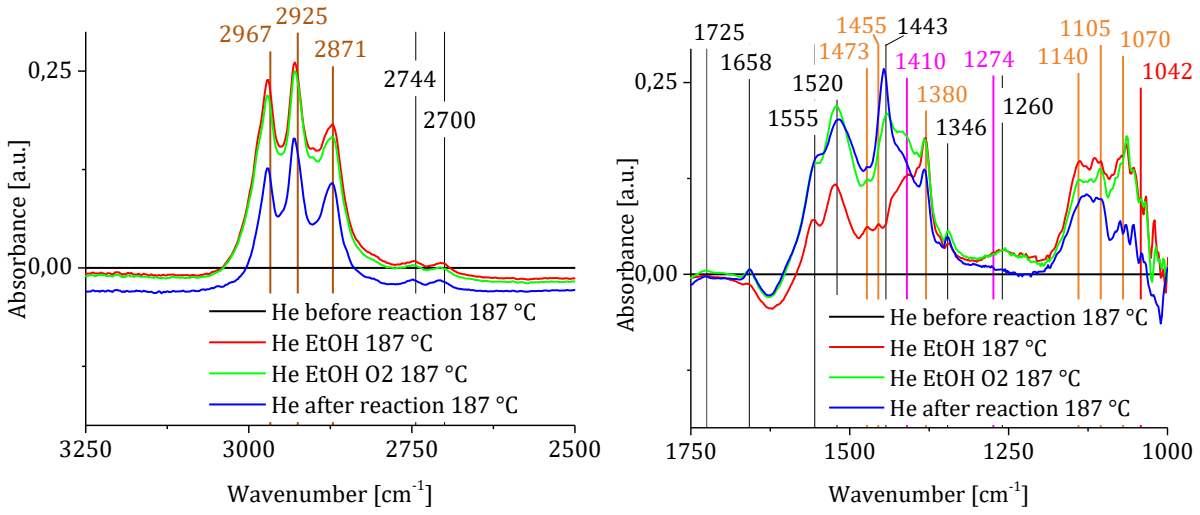

Figure 40 DRIFTS difference spectra of 2 wt% Au 1 wt% Ag Rutile at 187 °C under He (black, used as background), under EtOH (1.1 mL min^{-1}) diluted in He in red , under EtOH and O_2 (1.1 mL min^{-1} each) diluted in He in green and under He, after reaction, in blue. Reaction products are marked in black and ethoxy groups in orange, except for the bidentate signal, which is in red. Molecularly adsorbed EtOH in magenta.

At 325 °C, ethanol addition leads to an increase of ethoxy signals (but not of molecularly adsorbed ethanol, agreeing with the results of the ex-situ measurements in 4.3.2 from page 43 onwards). A shoulder at 2750 – 2700 cm^{-1} indicates adsorption of acetaldehyde. Characteristic vibrations of acetate species deliver strongly negative signals. Introduction of oxygen then leads to a strong decrease in ethoxy signals. A peak indicating crotonaldehyde arises at 3064 cm^{-1}, the shoulder at 2750 – 2700 cm^{-1} (signalling adsorbed acetaldehyde on TiO_2) remains. Furthermore, there is a strong increase of signals in the region 1900 – 1250 cm^{-1}, indicating an extensive formation of acetaldehyde/ crotonaldehyde, acetic acid and acetate species.

After reaction, the ethoxy and acetaldehyde signals vanish, while acetate and crotonaldehyde remain adsorbed.

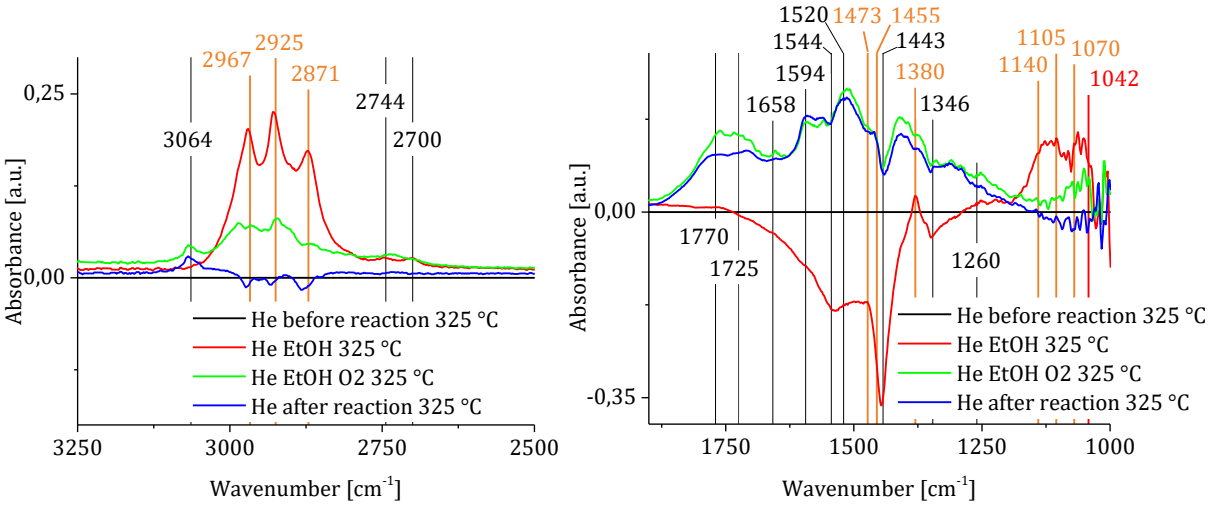

Figure 41 DRIFTS difference spectra of 2 wt% Au 1 wt% Ag Rutile at 325 °C under He (black, used as background), under EtOH (1.1 mL min^{-1}) diluted in He in red , under EtOH and O_2 (1.1 mL min^{-1} each) diluted in He in green and under He, after reaction, in blue. Reaction products are marked in black and ethoxy groups in orange, except for the bidentate signal, which is in red.

Summary – steady state in-situ DRIFTS measurements over Au Ag Rutile

Dehydrogenation reaction at 187 °C mostly delivers acetaldehyde, while a strong rise in acetate species is noted once oxygen is added to the reaction. Ethanol adsorbs in its molecular form at a temperature as high as 187 °C, agreeing with the ex-situ ethanol TPD IR studies (as discussed in 3.5).

At 365 °C, an extensive overlay of different signals is noted. After reaction, both ethoxy and acetaldehyde species desorb, while crotonaldehyde and acetates remain adsorbed. The signals of crotonaldehyde are weak, likewise the CH_3CHO peak at 409 °C in the TPD. Acetate species keep delivering intense signals, and can be accounted to the CO_2 peak at 438 °C in the TPD (see Figure 27).

4.4.2.4. Discussion

Altogether, comparison of Rutile, Au Rutile and Au Ag Rutile leads to the conclusion that the metal addition increases the formation of acetaldehyde and acetate, both in dehydrogenation and oxidative dehydrogenation conditions. Besides the increased

activity, the vastly different desorption behavior of ethoxy and acetaldehyde species from the catalysts surface influences the product distribution.

Acetate species remain adsorbed onto the respective catalyst up to the highest temperatures reached (325 or 365 °C), while the ethoxy species desorb in absence of EtOH. Therefore, those acetate species must be responsible for the CO_2 peaks in the ethanol TPDs (Figure 27). Once EtOH is added back into the He stream, ethoxy groups substitute acetate groups (at least partly), possibly due to proton transfer from EtOH to acetate (directly or indirectly, e.g. via hydroxyl groups or surface atomic hydrogen) resulting in adsorbed ethoxy and acetic acid. Acetic acid mostly desorbs and was detected in the gas phase at the exit of the IR cell. Ethoxy groups dehydrogenate to acetaldehyde, which in presence of oxygen partly condensates to crotonaldehyde. Further oxidation of acetaldehyde leads to acetate groups. However, quantitative analysis of the effluent gases shows, that the vast majority of acetaldehyde desorbs, before acetate groups can form – hence the relatively weak signals of acetaldehyde/ crotonaldehyde (compared to signals of ethoxy or acetate groups). Oxygen is beneficial for ethoxy dehydrogenation, however not necessary: product formation of acetaldehyde, acetic acid and acetates also takes place -to a smaller extent - in the absence of oxygen. Addition of oxygen furthermore promotes the formation of crotonaldehyde, explaining why crotonaldehyde was not observed in the ex-situ FTIR ethanol TPD in 4.3.2. Once crotonaldehyde is formed, it appears to be more stable than acetaldehyde on the catalysts surface, at times remaining adsorbed after reaction, while acetaldehyde desorbs.

Reaching the desorption temperature of acetaldehyde from TiO_2 makes formation of acetic acid improbable, explaining Figure 14 in 4.2.3, where catalytic screenings demonstrate, how selectivity towards acetaldehyde rises with rising temperature – for Au Ag TiO_2 to a higher extent than for Au TiO_2 (Figure 15). Lesser formation of acetic acid at high temperatures over Au Ag TiO_2 can therefore be explained due to less coverage of acetaldehyde on the surface. This suggestion is supported by the TPD (Figure 27): the CH_3CHO peak at 409 °C on Au Ag Rutile is remarkably smaller than the respective peak at 365 °C on Au Rutile. Majority of acetaldehyde desorbs from Au Ag Rutile at below 200 °C, while on Au Rutile, a considerable fraction remains adsorbed up to 365 °C.

4.4.3. Modulation Excitation measurements

Owing to the difficulty of distinguishing and interpreting the different signals in *3.6 In-situ DRIFTS Measurements*, modulation excitation measurements were initiated, intending to differentiate overlaying peaks from one another.

However, depletion and accumulation of conduction band electrons in TiO_2 due to different reaction conditions hindered the interpretation of the results to its full extent. The extent of accumulation of electrons can be decreased by adsorbed electron-scavengers such as gasphase O_2 or adsorbed –OH or H_2O, making clear that oscillating educt-streams and oscillating product formation will affect the background absorbance periodically. The TiO_2 background therefore dominates the phase sensitive detection.

Further results of the MS on-line surveillance are depicted in the appendix on pages 105 to 107.

0.8 wt% Au 4.2 wt% Ag Aurolite – 175 °C

Figure 42 gives an overview of the phase-sensitive detection over the entire measured region of 4000 – 900 cm^{-1}. The oscillating background absorption leads to a massive hump between 3000 and 1600 cm^{-1}.

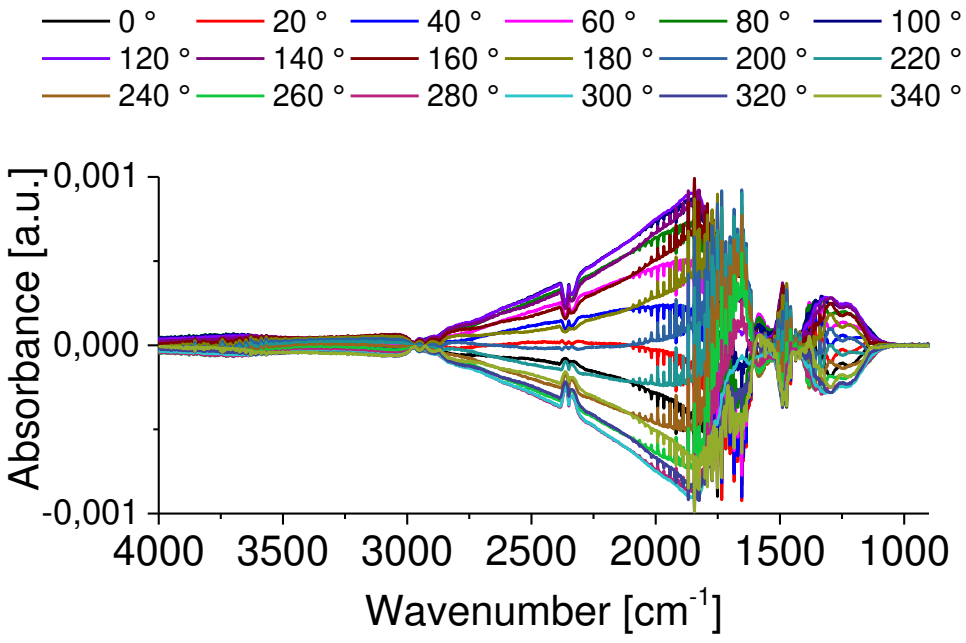

Figure 42 MES with 0.8 wt% Au 4.2 wt% Ag Aurolite at 175 °C: He EtOH O_2 (1st half period) vs He EtOH H_2 (2nd half period); one half-period lasted 101 s. Phase sensivite detection (PSD) analysis

Focusing on the region between 2000 – 1200 cm^{-1} reveals, that the rotational modes of gas-phase water dominate the spectra. Phase sensitive detection (PSD) shows, that there are no rotational modes visible at phase delays of 120 and 300 ° - indicating its out-of-phase angles. The strongest, positive signals are therefore found at a phase-delay of 210 °. Water is a reaction product of the oxidative dehydrogenation and likely to adsorb to the catalysts surface. Within the 101 s of the first half-period, surface coverage will steadily increase until the surface is more and more saturated, resulting in more gas-phase water at the end of the first half-period. The solenoid valves redirected gas flows at phase shifts of 0 and 180 °. Due to the gas-line and cell volume, the exchange of the reaction atmosphere is slightly time-delayed. The maximum of gas-phase water may therefore indicate the actual end of the oxidative half-period for the catalyst.

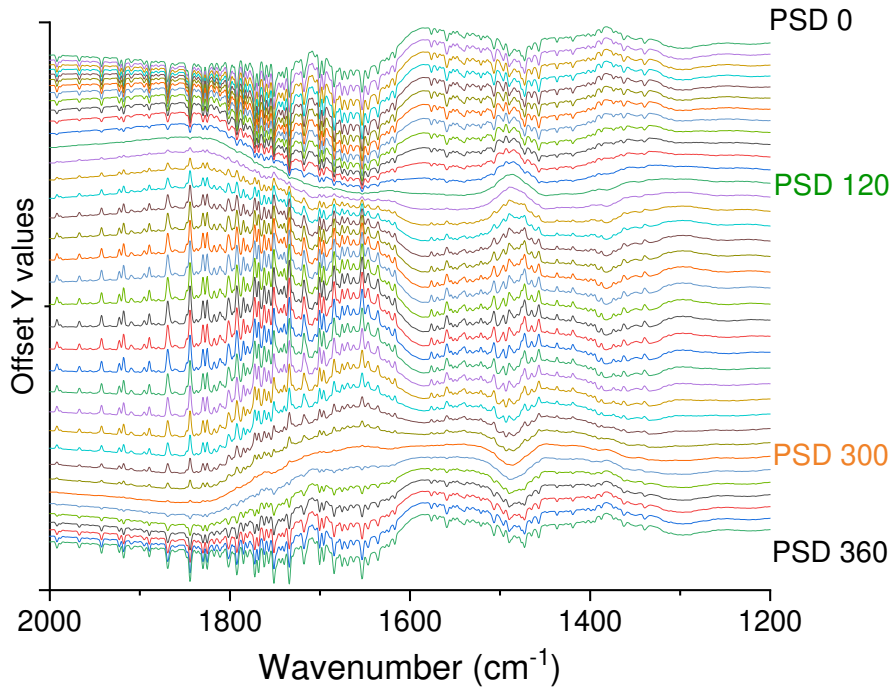

Figure 43 MES with 0.8 wt% Au 4.2 wt% Ag Aurolite at 175 °C: He EtOH O_2 (1st half period) vs He EtOH H_2 (2nd half period); one half-period lasted 101 s. Phase sensitive detection (PSD) in detail between 2000 - 1200 cm^{-1}

The IR region of interest of spectra at certain phase delays are portrayed in Figure 44. The strongest oscillations are found in the 1725-1750 cm^{-1} region (CH_3COOH_{ad} or CH_3CHO_{ad}), 1660 (CH_3CHO_{ad} or $CrCHO_{ad}$), 1622 (H_2O_{ad}), 1490 (possibly EtO^-_{ad}), 1383 (EtO^-_{ad} or $CrCHO_{ad}$) and in the region between 1350 and 1150 cm^{-1} (accumulation of EtO^-_{ad}, $CrCHO_{ad}$, CH_3CHO_{ad} signals). In-phase angles of all measured wavenumbers are depicted in the

appendix in Figure 75 on page 105. However, due to the overlay of the oscillations of the background absorbance and the rotational modes of the gas-phase water, those depicted in-phase-angles are impaired and cannot be taken into account for mechanistic considerations.

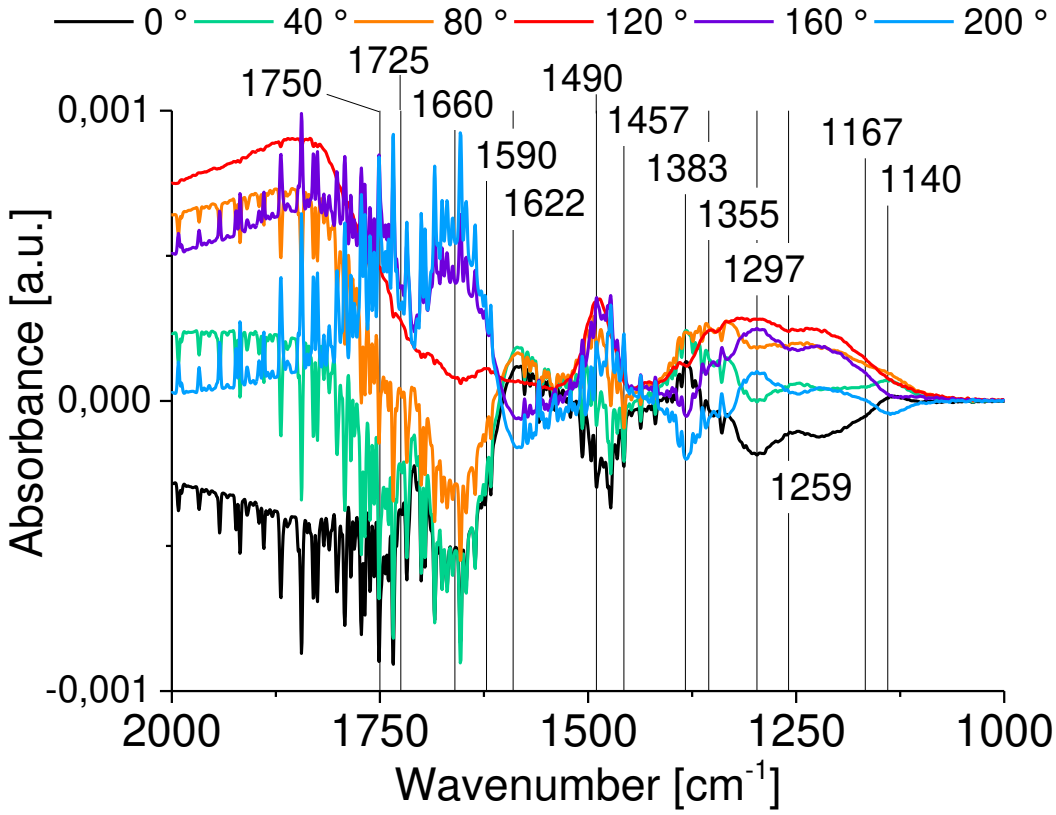

Figure 44 MES with 0.8 wt% Au 4.2 wt% Ag Aurolite at 175 °C: He EtOH O_2 (1st half period) vs He EtOH H_2 (2nd half period); one half-period lasted 101 s; spectra of certain phase shifts between 2000 and 1000 cm^{-1}

0.8 wt% Au Aurolite – 175 °C

Figure 45 shows, similarly to Au Ag Aurolite, that the oscillating background absorption between 3000 and 1600 cm^{-1} dominates the phase sensitive detection.

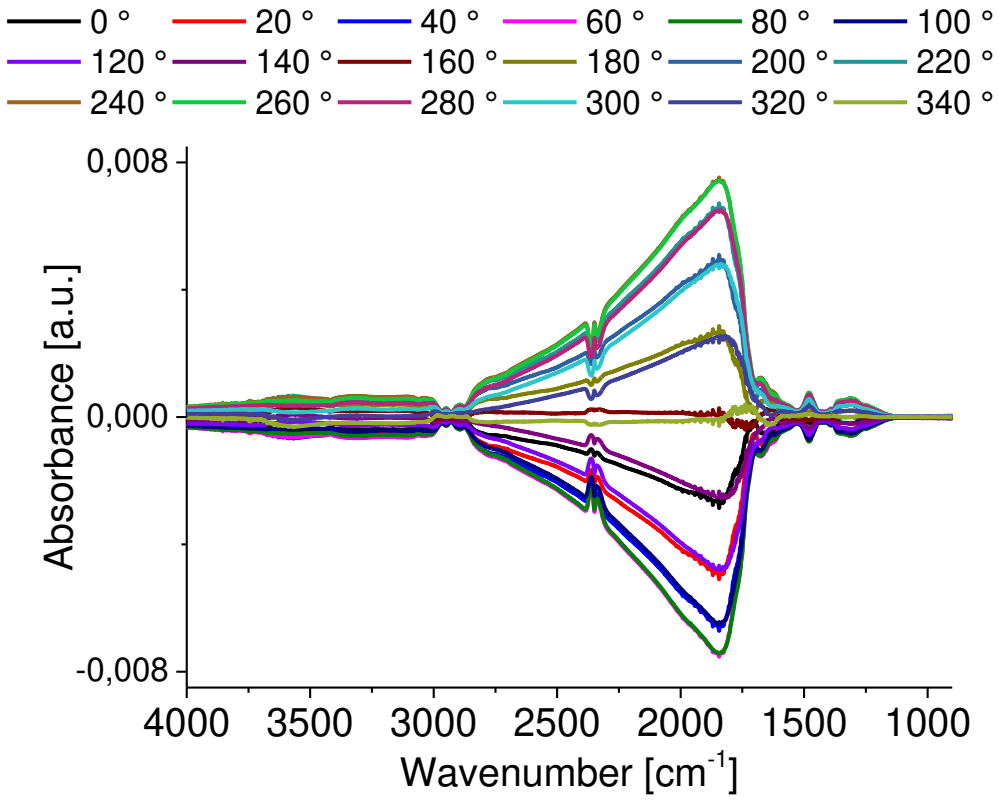

Figure 45 MES with 0.8 wt% Au Aurolite: He EtOH O_2 (1st half period) vs He EtOH H_2 (2nd half period); one half-period lasted 101 s.

Gas-phase water signals are present, however appear much weaker than in Au Ag Aurolite, either due to less product formation (also shown in kinetic screenings) or due to the background oscillating stronger (possibly due to electronic situation, which impacts reducibility of TiO_2 or rather the formation of conduction-band electrons). The out-of-phase angle for the gas-phase water (= phase delay without visible gas-phase water) is between 90 ° and 100 °, the in-phase angle (with positive signals) is therefore between 180 ° and 190 °.

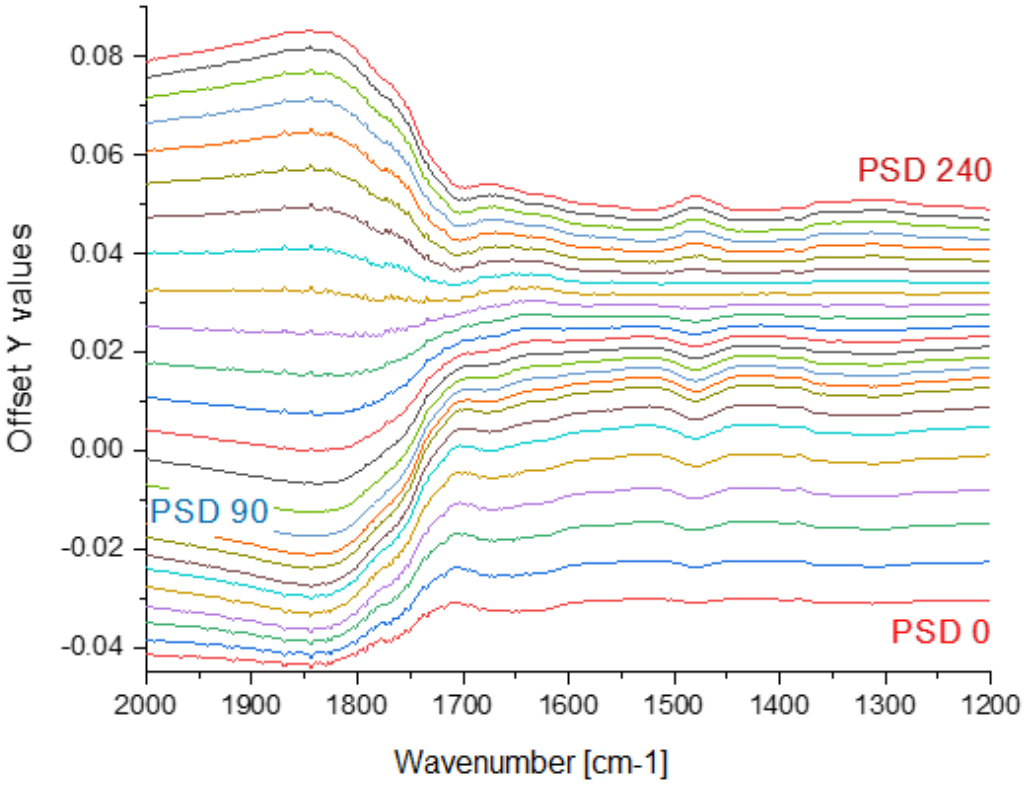

Figure 46 MES with 0.8 wt% Au Aurolite: He EtOH O_2 (1st half period) vs He EtOH H_2 (2nd half period); one half-period lasted 101 s. Phase sensitive detection (PSD) in detail between 2000 - 1200 cm^{-1}

The in-phase angles plotted over the respective wavenumbers are shown in Figure 47. Given that for the ν_a (CH_3) at 2973 cm^{-1} and the ν_s (CH_3) at 2871 cm^{-1} strongly different in-phase angles are calculated, indicates, that the oscillating background absorption compromises the in-phase angles.

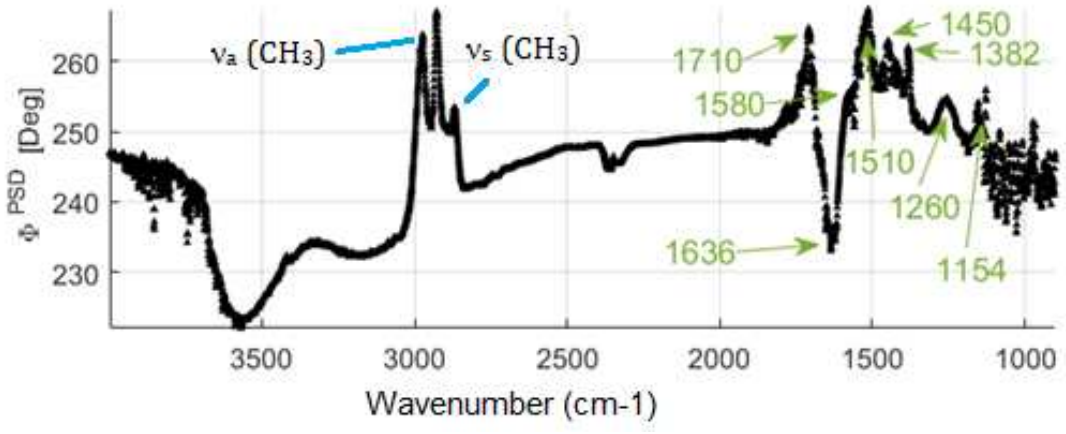

Figure 47 MES with 0.8 wt% Au Aurolite: He EtOH O_2 (1st half period) vs He EtOH H_2 (2nd half period); one half-period lasted 101 s. in-phase angles of phase-sensitive-detection for each wavenumber

The IR region of interest is portrayed in more detail in Figure 48. The strongest oscillations are found at 1706 cm^{-1} (CH_3CHO_{ad}), 1667 (CH_3CHO_{ad}), 1625 (H_2O_{ad}), 1475 (EtO^-_{ad}), 1383 (EtO^-_{ad} or $CrCHO_{ad}$) and in the region between 1365 and 1150 cm^{-1} (accumulation of EtO^-_{ad}, $CrCHO_{ad}$, CH_3CHO_{ad} signals).

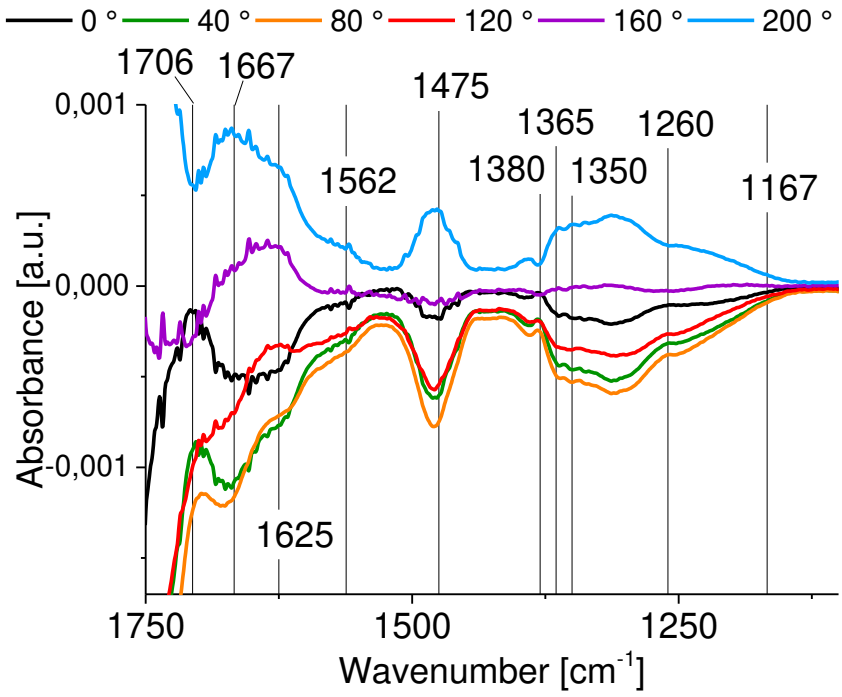

Figure 48 MES with 0.8 wt% Au Aurolite: He EtOH O_2 (1st half period) vs He EtOH H_2 (2nd half period); one half-period lasted 101 s. Spectra of certain phase shifts between 1800 and 1100 cm^{-1}

P25 – 175 °C

Figure 49 gives an overview of the phase-sensitive detection over the entire measured region of 4000 – 900 cm^{-1} for P25 and gives a very different picture than Au Aurolite and Au Ag Aurolite have given. Indeed, on P25 still is a rise in background absorption between 3000 and 1600 cm^{-1} reported, however, the rise is much weaker than what it is in the samples with added Au and Ag. Apparently, the TiO_2 gets less reduced in absence of Au activating H_2.

The strongest oscillating signals arise from adsorbed water – as weakly bound hydroxyl groups on the TiO_2 surface, causing O-H stretching vibrations between 3500 and 3000 cm^{-1} and causing H-O-H bending at 1625 cm^{-1}. Both deliver the weakest signals at a phase delay of 20 °, then steadily rise in the EtOH and O_2 atmosphere until they reach their

maxima at 200 °, and then weaken again in the EtOH and H_2 atmosphere. Due to water being a major reaction side-product of oxidative dehydrogenation, it builds up and accumulates under the oxidative condition. In presence of O_2 oxidative dehydrogenation dominates leading to acetaldehyde and water production, whereas in absence of O_2, dehydrogenation of ethanol to acetaldehyde and hydrogen is the main pathway.

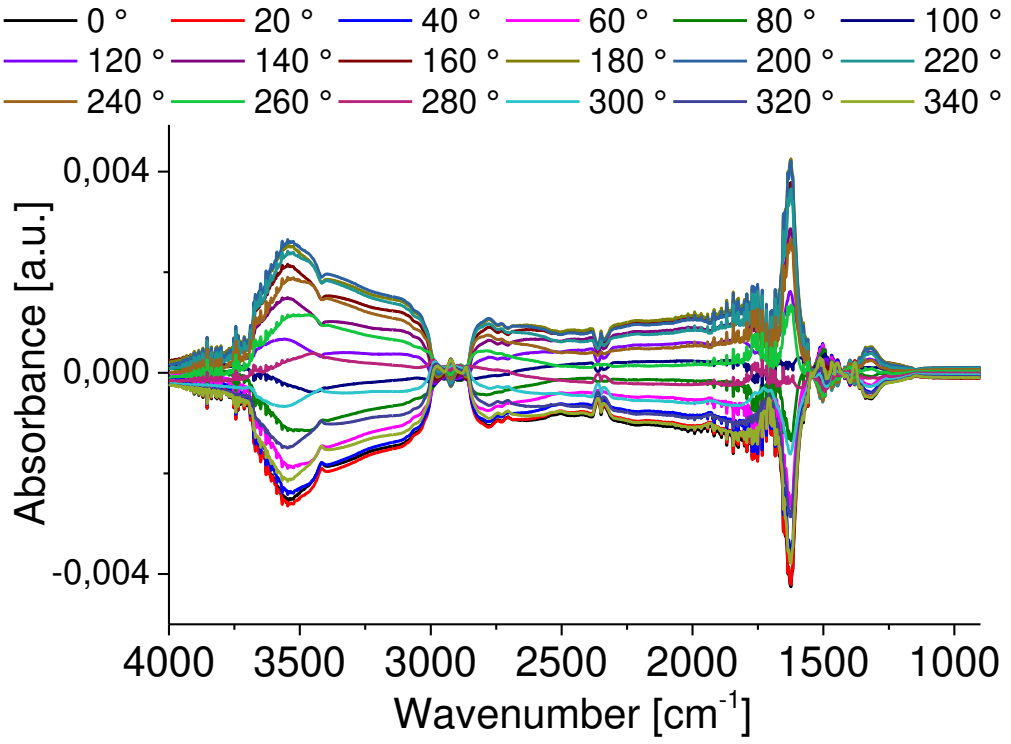

Figure 49 MES with P25 at 175 °C: He EtOH O_2 (1st half period) vs He EtOH H_2 (2nd half period); one half-period lasted 101 s. Overview over the entire measured IR region 4000 – 900 cm^{-1}.

Gas-phase water dominates the region between 2000 and 1400 cm^{-1}, as it is depicted in more detail in Figure 50. The spectra at 120 ° phase delay shows no rotational modes of gas-phase water (= out-of-phase angle), therefore means, that the in-phase-angle for formation of gas-phase water is 210 ° and is therefore slightly behind the in-phase-angle of adsorbed water (200 °).

Taking a look at Figure 51 reveals more detailed information of the highly interesting 1600 – 1200 cm^{-1} region. The spectra at 200 ° phase delay – where oxidative conditions come to an end and product concentration has reached its maximum – shows lows for EtO^-_{ad} signals and highs at 1750 (ν_a(CO)/CH_3COOH_{ad}), 1625 (δ (H_2O)/H_2O_{ad}), 1420 ($\delta_{as}(CH_3)$/ CH_3CHO_{ad} or ν_s (COO)/ $CH_3COO^-_{ad}$), 1400, 1365 ($\delta_s(CH_3)$/CH_3CHO_{ad}), 1356

($\delta(CH_3) + \delta(CH)/ CH_3CHO_{ad}$), 1338 ($\delta s(CH_3)/ CH_3CHO_{ad}$) and a broad signal between 1370 and 1270 cm^{-1}. The spectra at 120 ° is particularly interesting, since the absence of gas-phase water facilitates the interpretation of the spectra and peaks appear, that are overlooked in the other spectra: one peak at 1533 (ν_a (COO)/ $CH_3COO^-_{ad}$) and a peak at 1488 cm^{-1} which has not been assigned.

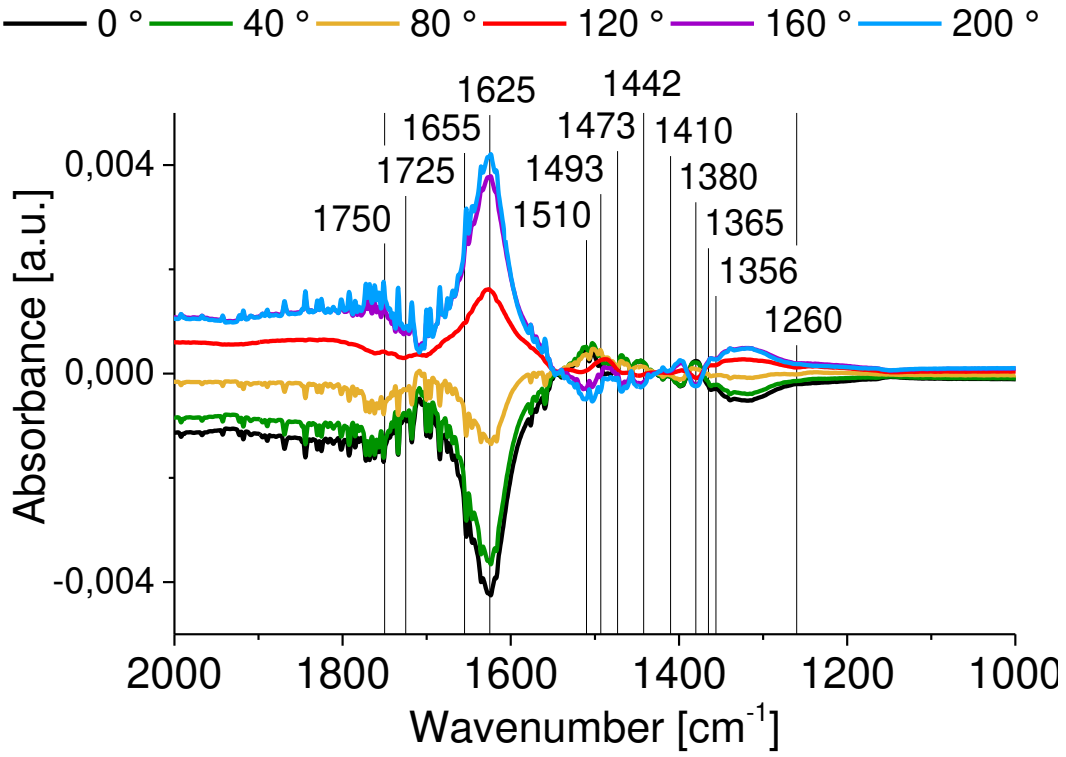

Figure 50 MES with P25 at 175 °C: He EtOH O_2 (1st half period) vs He EtOH H_2 (2nd half period); one half-period lasted 101 s. Spectra of certain phase shifts between 2000 and 1000 cm^{-1}

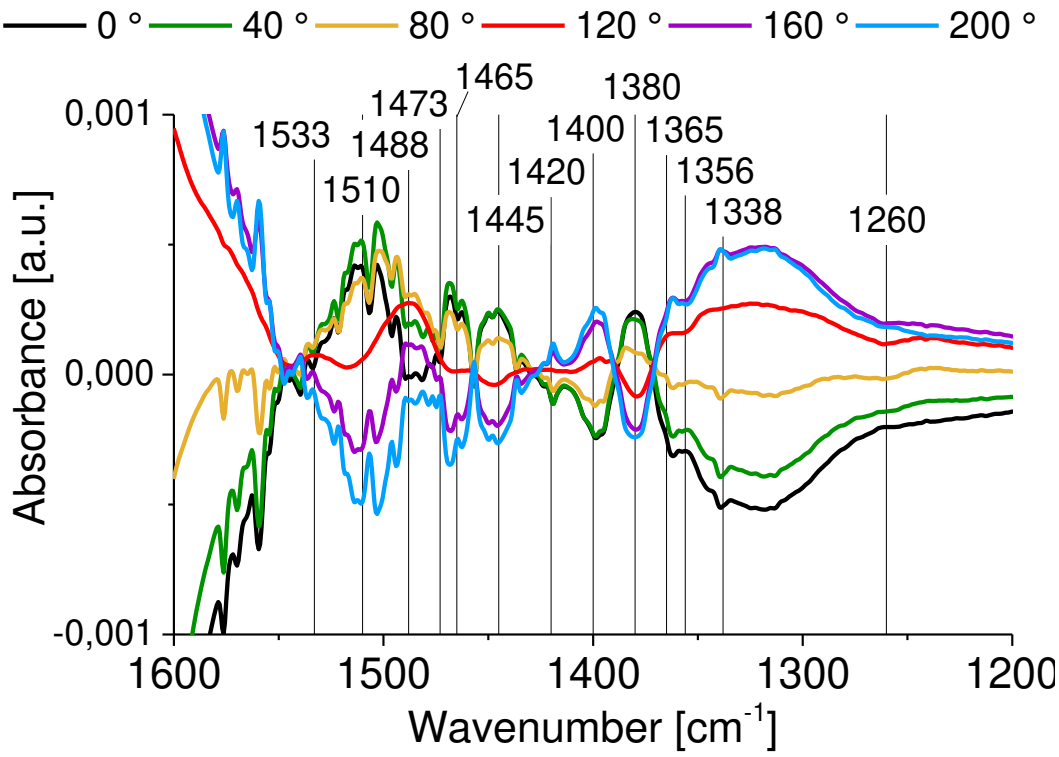

Figure 51 MES with P25 at 175 °C: He EtOH O_2 (1st half period) vs He EtOH H_2 (2nd half period); one half-period lasted 101 s. Spectra of certain phase shifts between 1600 and 1200 cm^{-1}.

Figure 52 shows the in-phase-angles of P25 at 175 °C. Interestingly, for ν_a (CH_3) at 2973 and ν_s (CH_3) at 2871 cm^{-1} it is found at 300 °, while for ν_a (CH_2) at 2930 cm^{-1} it is 350 °. Further EtO_{ad} signals (1450 and 1380 cm^{-1}) are found at a similar phase shift: 0-10 °. Ethoxy signals have their maximum in the 2nd half period due to less of it being used in reaction. The signal at 1510 cm^{-1} (ν_a (COO) of adsorbed carboxyl species) appears with a slightly higher phase shift, indicating protonation of adsorbed acetate species once oxidative conditions are applied. The rest of the products signals comes with a phase shift of around 200 °.

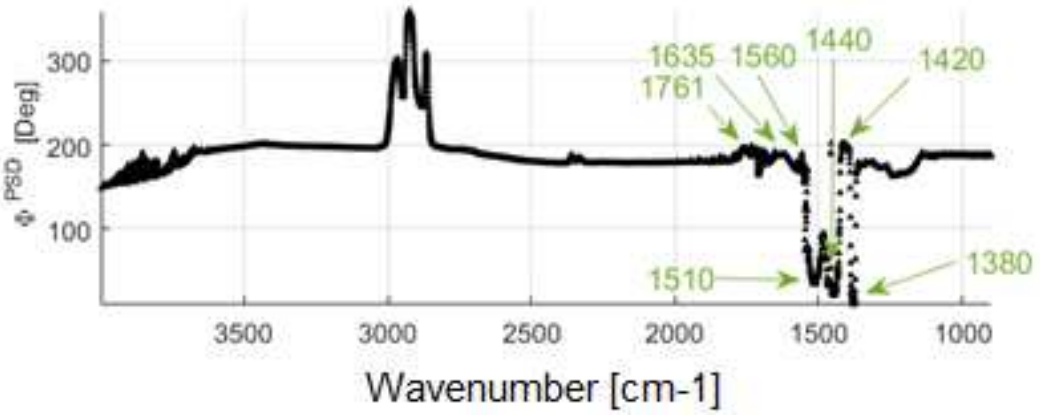

Figure 52 MES with P25 at 175 °C: He EtOH O_2 (1st half period) vs He EtOH H_2 (2nd half period); one half-period lasted 101 s. In-phase angles of phase-sensitive-detection for each wavenumber

0.8 wt% Au 4.2 wt% Ag Aurolite – 325 °C

The overview of phase-sensitive detection in Figure 53 again reveals a strong up-and-down of the background absorption between 3000 and 1600 cm^{-1}. However, product signals are -unsurprisingly- much stronger than at 175 °C. Gas-phase water is out-of-phase at 190 ° and in-phase at 100 ° phase delay.

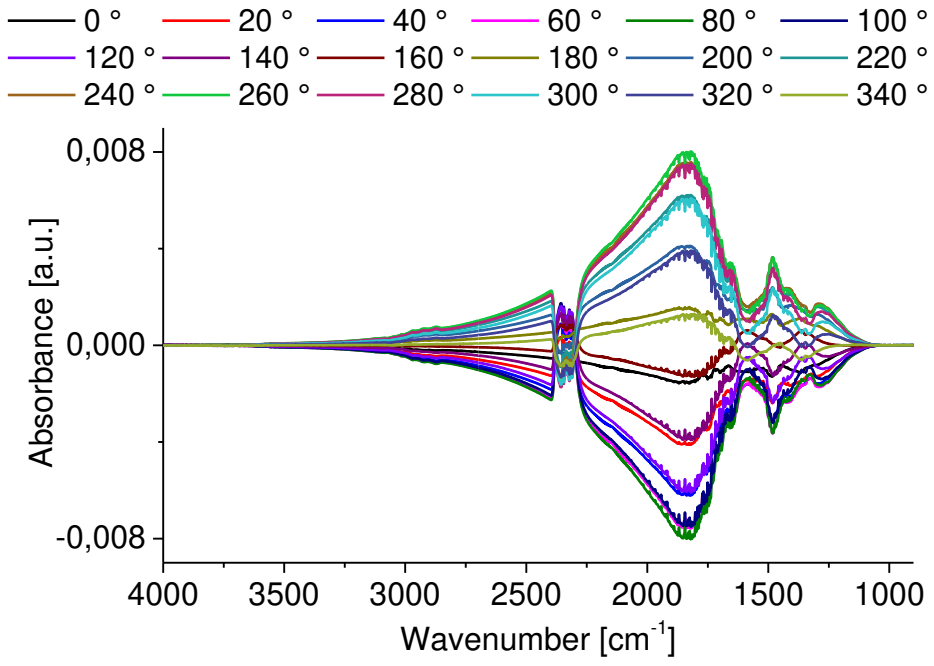

Figure 53 MES with 0.8 wt% Au 4.2 wt% Ag Aurolite at 325 °C: He EtOH O_2 (1st half period) vs He EtOH H_2 (2nd half period); one half-period lasted 101 s. Overview over the entire measured IR region 4000 – 900 cm^{-1}

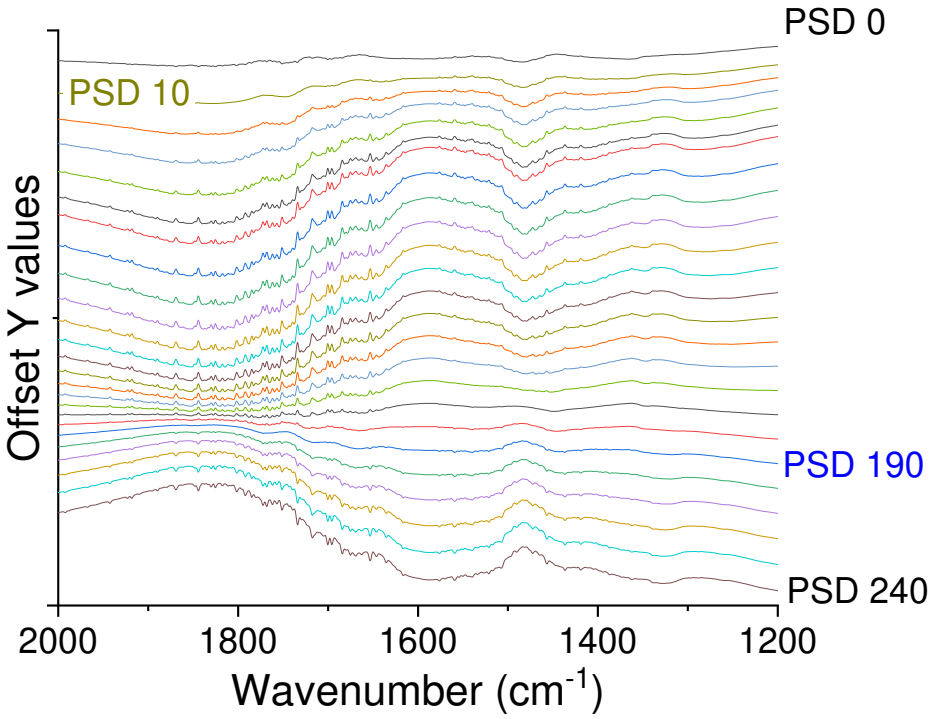

Figure 54 MES with 0.8 wt% Au 4.2 wt% Ag Aurolite at 325 °C: He EtOH O_2 (1st half period) vs He EtOH H_2 (2nd half period); one half-period lasted 101 s. Phase sensitive detection (PSD) in detail between 2000 - 1200 cm^{-1}

The in-phase angles of each wavenumber are depicted in Figure 55 and show a phase delay of gas-phase CO_2 of around 100 ° (like gas-phase water). Signals at 1588 (ν (C=C) / $CrCHO_{ad}$), 1363 ($\delta(CH)/CH_3CHO_{ad}$) and 1329 ($\delta_s(CH_3)$/ CH_3CHO_{ad}) appear at the same phase-shift of around 225-230 °.

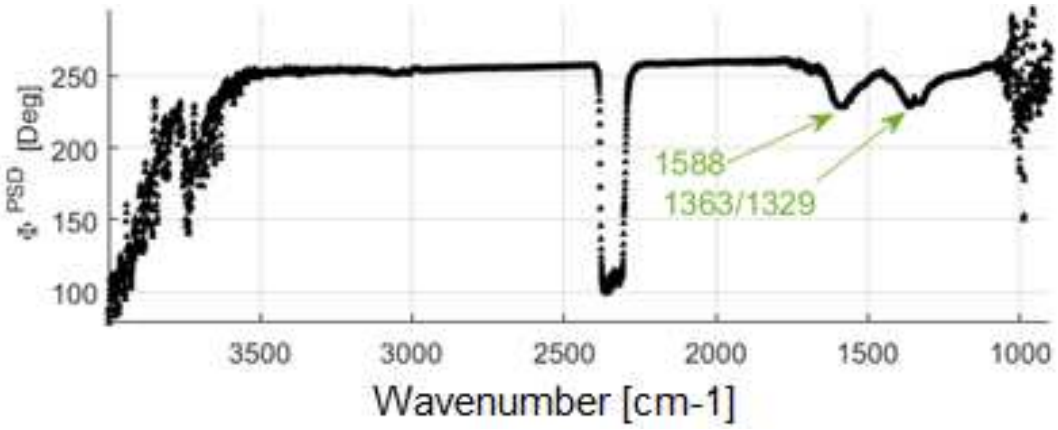

Figure 55 MES with 0.8 wt% Au 4.2 wt% Ag Aurolite at 325 °C: He EtOH O_2 (1st half period) vs He EtOH H_2 (2nd half period); one half-period lasted 101 s. In-phase angles of phase-sensitive-detection for each wavenumber

Taking a closer look at Figure 56 indicates, that the above discussed in-phase-angles, are compromised by the background absorption. The signal at 1594 cm^{-1} (ν (C=C) / $CrCHO_{ad}$) for example, is clearly more established at 120 and 160 ° phase delay. However, due to the oscillating background absorption, the strongest signal is measured at around 250 ° (see Figure 55). Generally, product formation is stronger in the first half-period of measurements, due to the presence of oxygen. However, the oxidative atmosphere leads to a depletion of conduction band electrons and therefore a lowering of the background absorption, making the product peaks hard to identify and even harder to assign a phase shift to them. The signals at 1588, 1363 and 1329 cm^{-1}, which are calculated to have the same phase shift (see Figure 55) are hard to recognize in Figure 56.

Signals at 1750 (ν_a(CO) / CH_3COOH_{ad}), 1725 (ν(C=O)/ CH_3COOH_{ad} and CH_3CHO_{ad}), 1691 (ν(C=O)/CH_3CHO_{ad}), 1656 (ν (C=O) / $CrCHO_{ad}$), 1594 (ν (C=C) / $CrCHO_{ad}$), 1485 (?), 1443 ($\delta_{as}(CH_3)$/ CH_3CHO_{ad}), 1355 ($\delta(CH_3)$, δ(CH)/ CH_3CHO_{ad}), 1338 ($\delta_s(CH_3)$/ CH_3CHO_{ad}), 1260 cm^{-1} (η^2(CO) / CH_3CHO_{ad} or δ(CH) / $CrCHO_{ad}$) are found. However, phase shifts cannot be ascribed.

Adsorbed ethoxy signals are merely very weakly found, indicating immediate dehydrogenation to acetaldehyde.

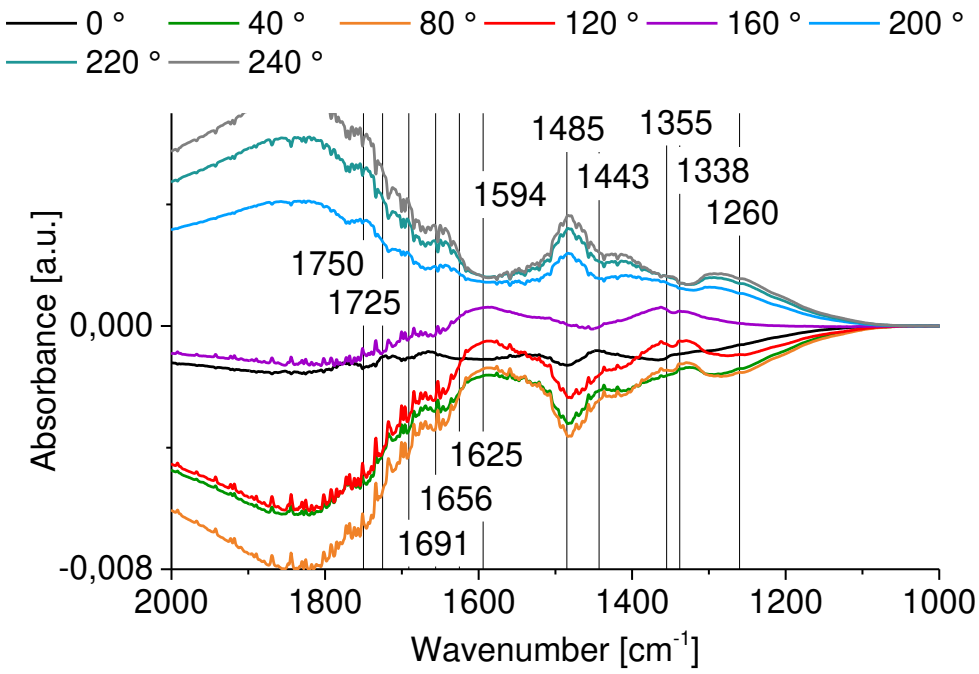

Figure 56 MES with 0.8 wt% Au 4.2 wt% Ag Aurolite at 325 °C: He EtOH O_2 (1st half period) vs He EtOH H_2 (2nd half period); one half-period lasted 101 s. Spectra of certain phase shifts between 1600 and 1200 cm^{-1}.

0.8 wt% Au Aurolite – 325 °C

Background absorbance dominates the phase-sensitive detection, as shown in Figure 57. Hardly any product signals are visible besides the immense hump. Closer examination reveals gas-phase water with in in-phase-angle of 100 ° (see Figure 58).

Figure 60 shows product signals (at 1750, 1725 and 1691 cm^{-1} from acetic acid and acetaldehyde) merely as shoulders in the immense rise of background absorption, making a proper calculation of in-phase-angles impossible. The in Figure 59 depicted in-phase-angles are therefore once again compromised by the depletion/formation of conduction-band electrons in TiO_2.

Figure 61 merely shows an accumulation of adsorbed ethoxy species rising in the 2nd half-period.

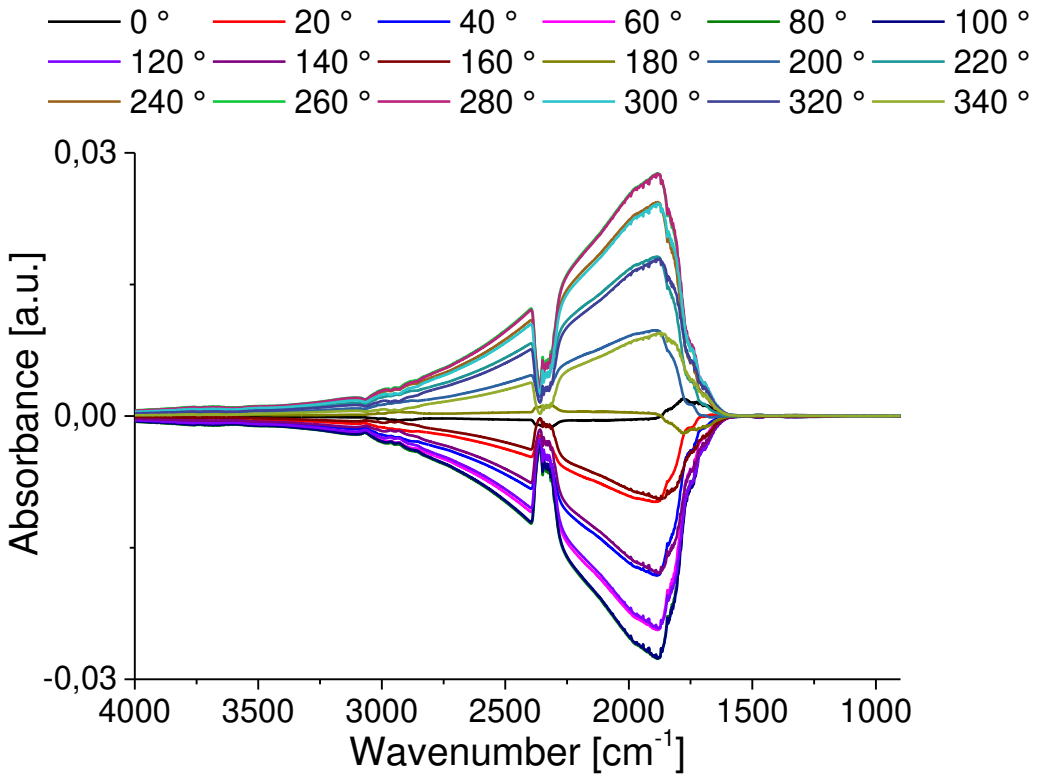

Figure 57 MES with 0.8 wt% Au Aurolite at 325 °C: He EtOH O_2 (1st half period) vs He EtOH H_2 (2nd half period); one half-period lasted 101 s.

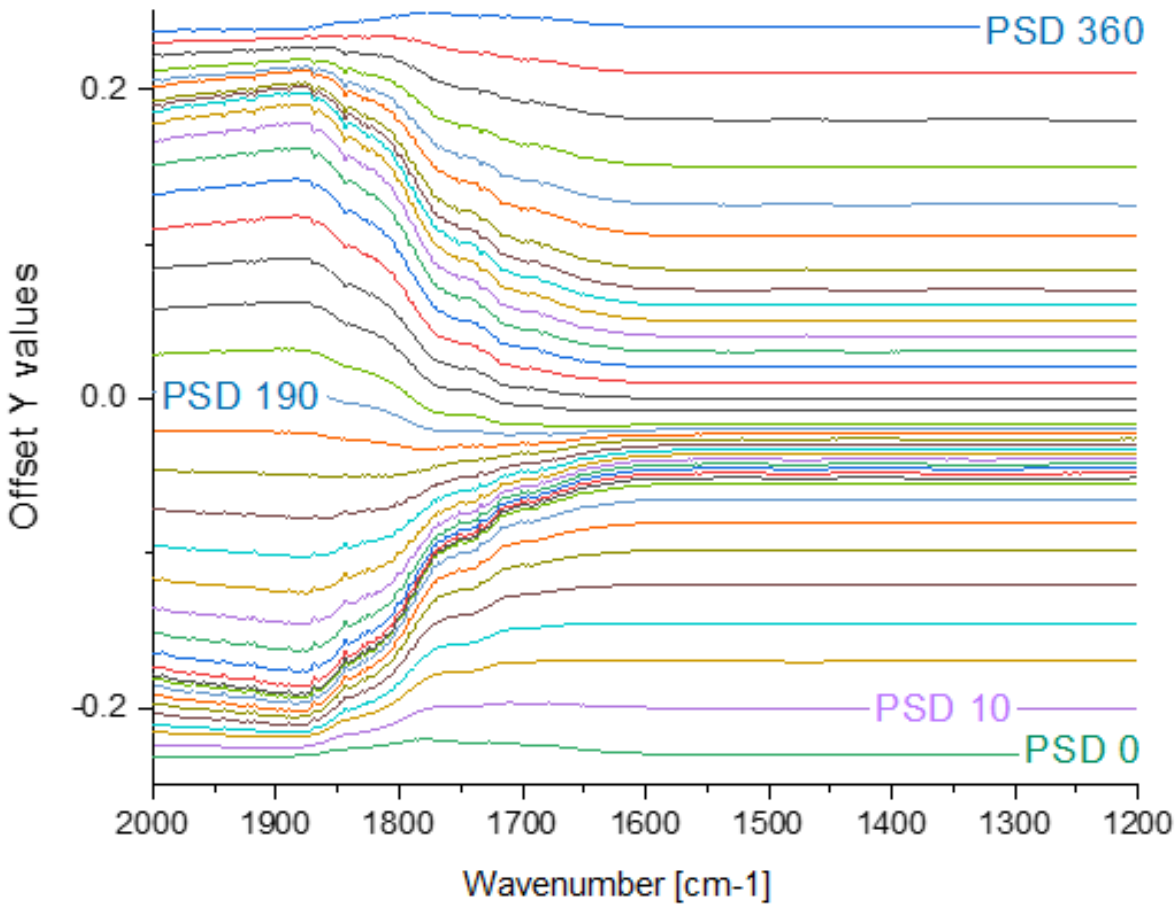

Figure 58 MES with 0.8 wt% Au Aurolite at 325 °C: He EtOH O_2 (1st half period) vs He EtOH H_2 (2nd half period); one half-period lasted 101 s. Phase sensitive detection (PSD) in detail between 2000 - 1200 cm^{-1}

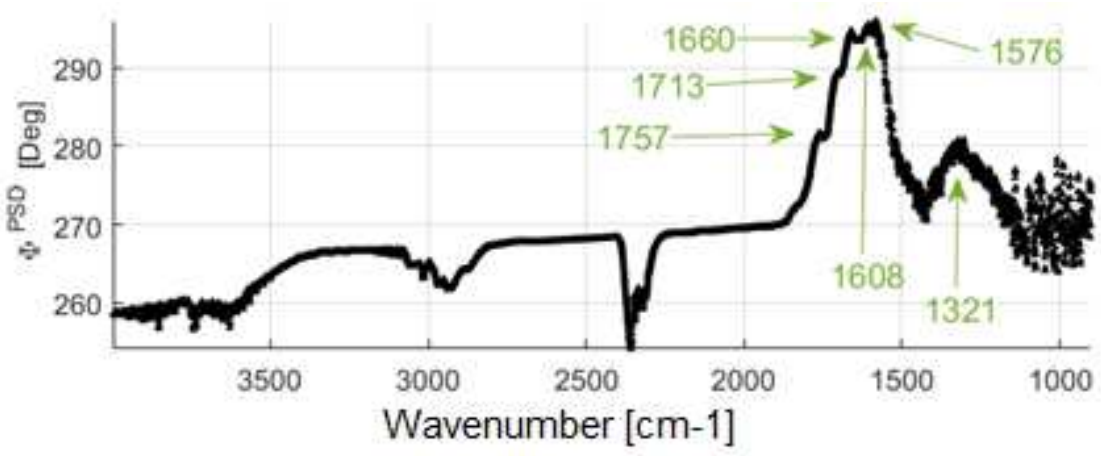

Figure 59 MES with 0.8 wt% Au Aurolite at 325 °C: He EtOH O_2 (1st half period) vs He EtOH H_2 (2nd half period); one half-period lasted 101 s. In-phase angles of phase-sensitive-detection for each wavenumber.

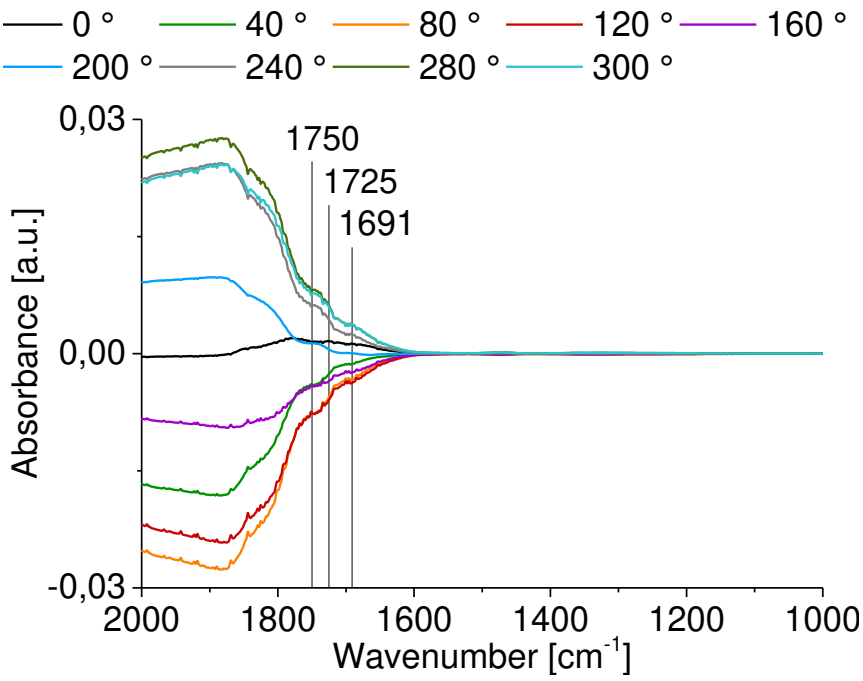

Figure 60 MES with 0.8 wt% Au Aurolite at 325 °C: He EtOH O_2 (1st half period) vs He EtOH H_2 (2nd half period); one half-period lasted 101 s. Spectra of certain phase shifts between 2000 and 1000 cm^{-1}.

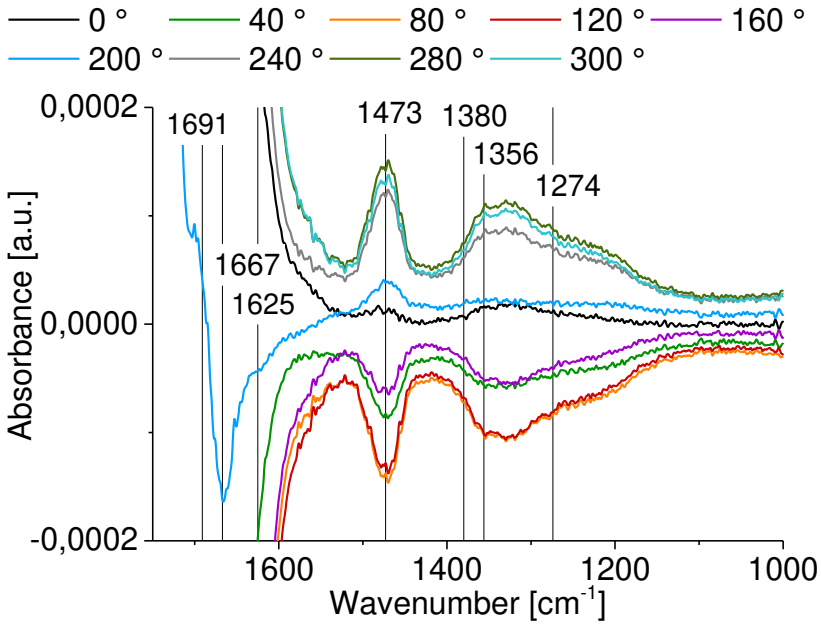

Figure 61 MES with 0.8 wt% Au Aurolite at 325 °C: He EtOH O_2 (1st half period) vs He EtOH H_2 (2nd half period); one half-period lasted 101 s. Spectra of certain phase shifts between 1750 and 1000 cm^{-1}

Results of the MS on-line observation are depicted in Figure 77. It shows that m/z 29, 43, 61 and 70, which are all caused by acetaldehyde, ethyl acetate and acetic acid, are in tune.

The maximum of those reaction products is followed by the maximum of m/z 32 (molecular oxygen) and slightly afterwards m/z 44 (CO_2).

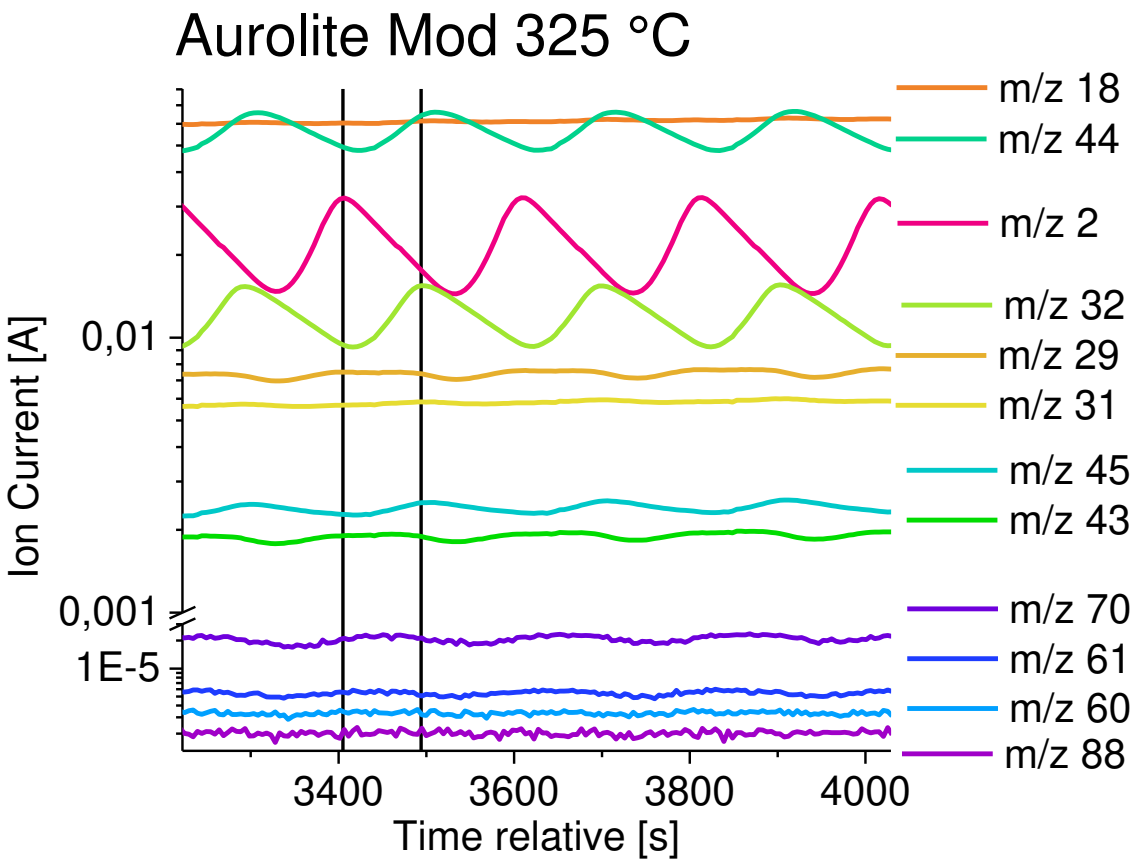

Figure 62 Normalized ion current signals of MS detection during MES with 0.8 wt% Au Aurolite at 325 °C: He EtOH O_2 (1st half period) vs He EtOH H_2 (2nd half period); one half-period lasted 101 s; different m/z values are depicted in varying colours.

P25 – 325 °C

In contrast to the P25 measurements at 175 °C (where only minimal background absorption is reported), the spectra at 325 °C is dominated by the up-and-down from background absorption, similarly to the sample with Au and Ag added. The rotational modes of gas-phase water are not visible.

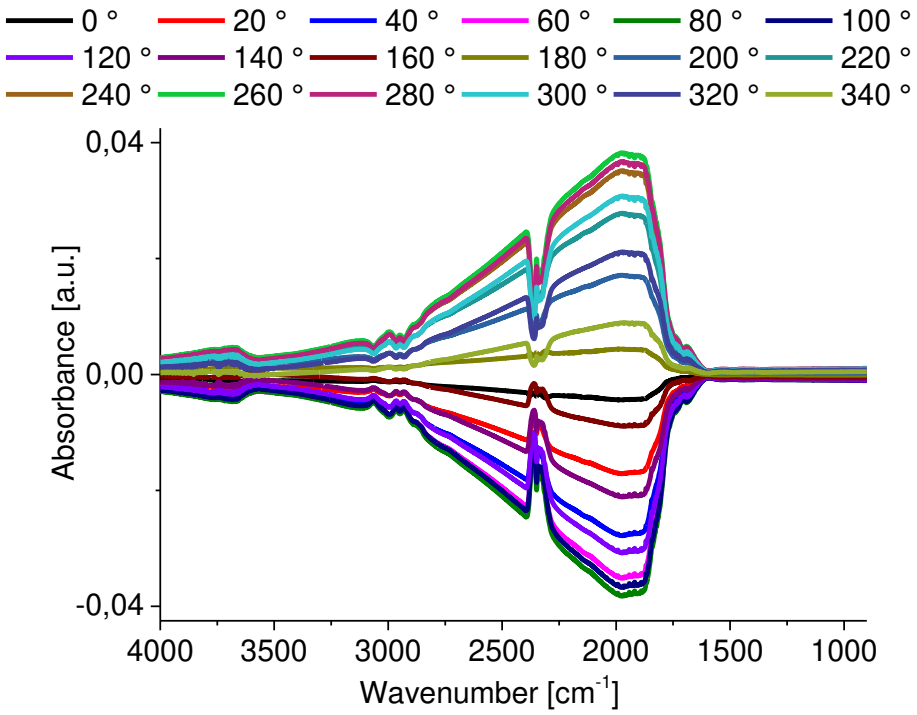

Figure 63 MES with P25 at 325 °C: He EtOH O_2 (1st half period) vs He EtOH H_2 (2nd half period); one half-period lasted 101 s.

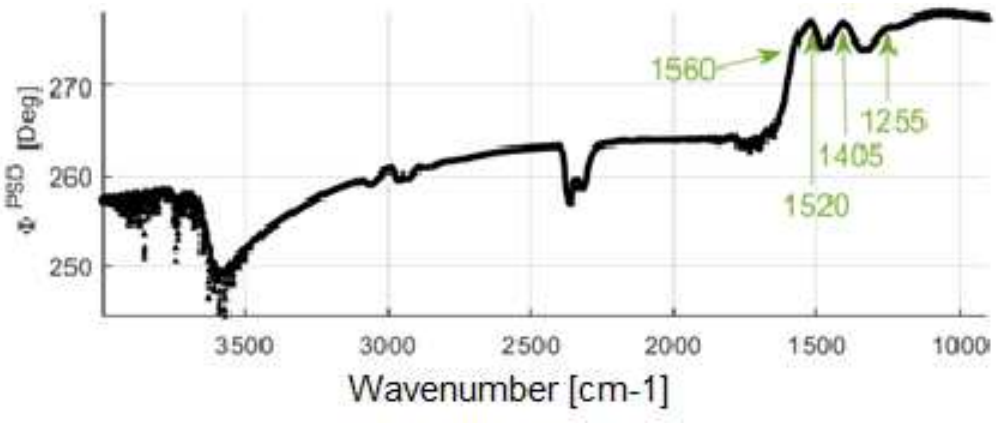

Figure 64 MES with P25 at 325 °C: He EtOH O_2 (1st half period) vs He EtOH H_2 (2nd half period); one half-period lasted 101 s. In-phase angles of phase-sensitive-detection for each wavenumber.

Similarly to Au Aurolite, Figure 65 shows product signals (at 1750, 1725 and 1691 cm^{-1} from acetic acid and acetaldehyde) merely as shoulders in the immense rise of background absorption, hindering a proper calculation of in-phase-angles. The in-phase-angles depicted in Figure 66 are therefore once again compromised by the depletion and formation of conduction-band electrons in TiO_2.

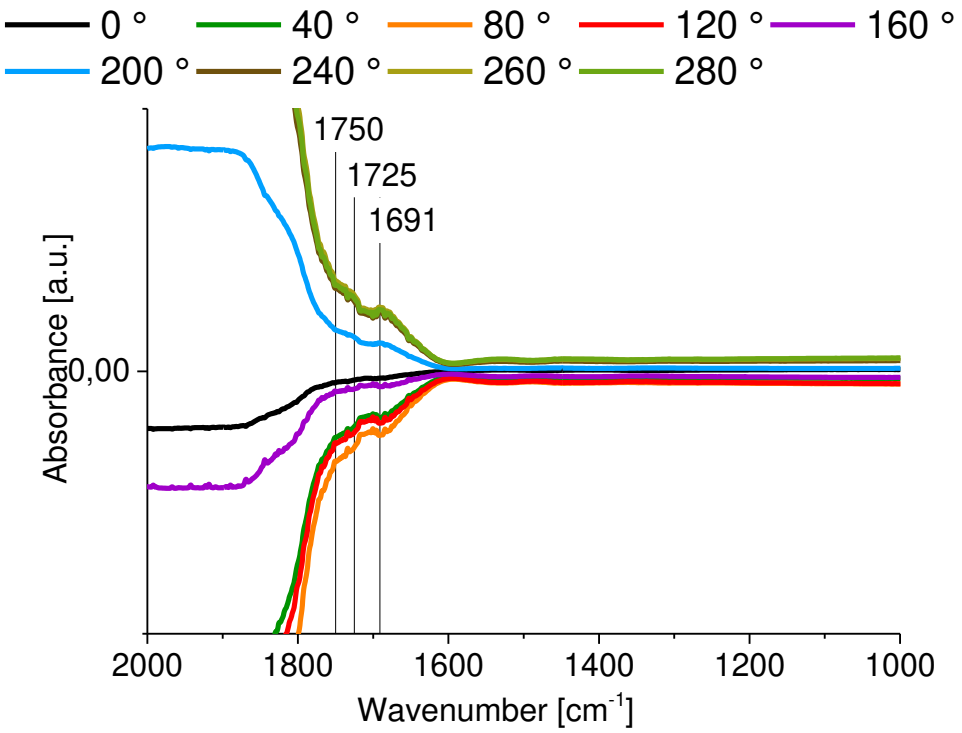

Figure 65 MES with P25 at 325 °C: He EtOH O_2 (1st half period) vs He EtOH H_2 (2nd half period); one half-period lasted 101 s. Spectra of certain phase shifts between 2000 and 1000 cm^{-1}.

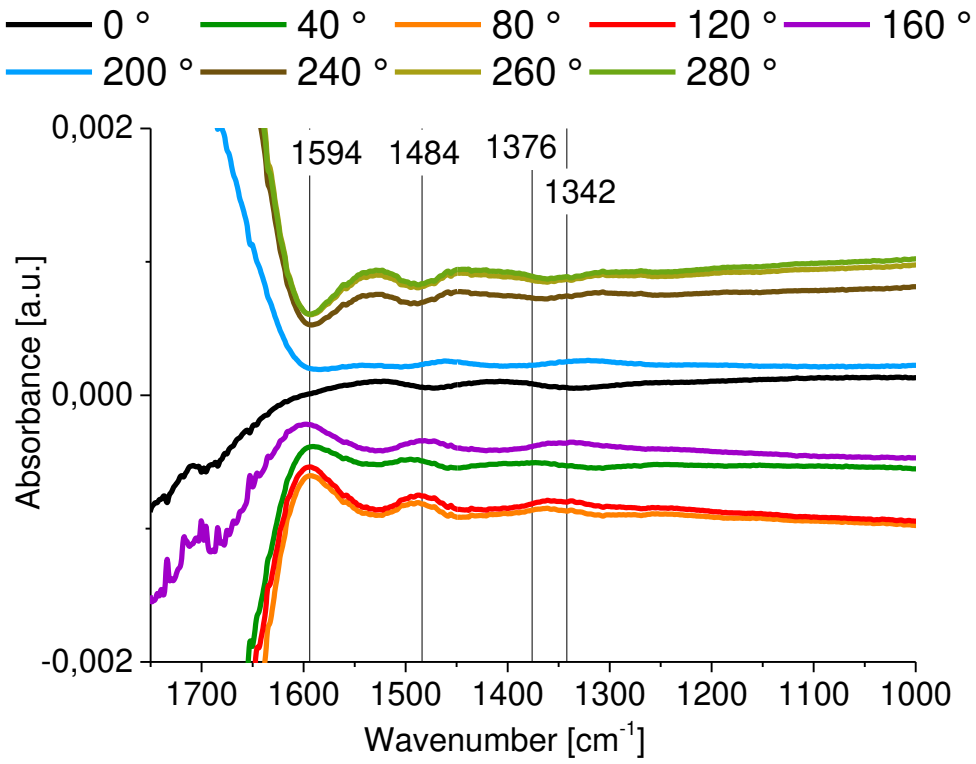

Figure 66 MES with P25 at 325 °C: He EtOH O_2 (1st half period) vs He EtOH H_2 (2nd half period); one half-period lasted 101 s. Spectra of certain phase shifts between 1750 and 1000 cm^{-1}.

4.4.3.1. Discussion

The oscillating formation and depletion of conduction band electrons in TiO_2 inhibited seizing the mighty possibilities of modulation excitation measurements to their full extent. The power of MES –highlighting only those signals that oscillate with the reaction– became void when the background absorbance turned out to oscillate much more intense than the reaction products. Moreover, rotational modes of gas-phase water overlaid signals, hindering their interpretation further.

The measurements on P25 at 175 °C reveal the most useful spectra. The background oscillates significantly weaker on pure TiO_2 than when Au or Ag are added, demonstrating the immense effect of the presence of Au and Ag on conduction band electrons in TiO_2. The phase-sensitive detection allows to differ educt and product signals, uncovering product peaks at 1750 (ν_a(CO)/CH_3COOH_{ad}), 1625 ($\delta(H_2O)/H_2O_{ad}$), 1533 (ν_a (COO)/ $CH_3COO^-_{ad}$), 1488, 1420 ($\delta_{as}(CH_3)$/ CH_3CHO_{ad} or ν_s (COO)/ $CH_3COO^-_{ad}$), 1400, 1365 ($\delta_s(CH_3)/CH_3CHO_{ad}$), 1356 ($\delta(CH_3)$ + δ(CH)/ CH_3CHO_{ad}), 1338 ($\delta s(CH_3)$/ CH_3CHO_{ad}) and a broad signal between 1370 and 1270 cm^{-1}. Comparison of in-phase angles reveals that for ν_a (CH_3) at 2973 and ν_s (CH_3) at 2871 cm^{-1} it is found at 300 °, while for ν_a (CH_2) at 2930 cm^{-1} it is found later, at 350 °.

4.5. (S)MSI in Au Ag TiO_2

4.5.1. O_2 Chemisorption dependent on reduction temperature

The oxidative step was carried out as usual, the reductive step was then carried out at either 200 °C or 300 °C. The adsorbed volume of oxygen was measured with the TCD detector and is directly correlated with the surface of the silver particles on the catalysts surface. The results are listed in Table 5.

Measurements were carried out directly after one another, without dismounting the sample inbetween. Therefore, metal loading variations within one catalysts' batch and errors in sample preparation as reason for the deviations can be ruled out. Measurements carried out directly after one another show good reproducibility, with exception of B4 and B5, which will be discussed later on.

Table 5 Oxygen adsorption volumes on 0.8 wt% Au 4.2 wt% Ag Aurolite and 0.7 wt% Au 7.3 wt% Ag, reduced at either 200 °C or 300 °C.

Catalyst	Sample weight (mg)	Label of measurement	Reduction Temperature (°C)	Adsorbed O_2 Volume (mm^3)
0.8 % Au 4.2 % Ag	108,8	A1	200	13,0
		A2	300	7,8
		A3	300	7,6
0.7 % Au 7.3 % Ag	59,6	B1	No Pretreatment	-0,6
		B2	200	30,1
		B3	200	30,8
		B4	300	17,6
		B5	300	13,3
		B6	300	13,9

For both catalysts, one trend becomes clear: is the reductive step carried out at an increased temperature, then the adsorbed volume of oxygen decreases. This phenomenon can be explained by either i) sintering of the silver particles or ii) migration of a TiO_2 layer on top of the metal particles.

i. Sintering of silver particles would lead to larger particles and therefore a smaller total surface
ii. Migration of a TiO_2 layer onto the metal particles (as it is reported in literature as *SMSI effect* and explained in 2.2.2 on page 11) would also decrease the total metal surface

Addressing i): Why would sintering happen during the reductive step in the first place? The oxidative step is carried out at 400 °C, so one would instinctively assume, that sintering –if it took place- would happen during this step to a much larger degree than during the significantly cooler reductive step (happening at 300 °C or 200 °C). However, as reduction is an exothermic process, locally, the temperature might be much higher than what is measured by the thermal sensor. Moreover, the surface free energy is larger for metallic Ag than for oxidic AgO_x, which might explain enhanced sintering under reducing atmosphere in order to minimize the surface energy. Thus, further measurements were required to reveal absence or presence of sintering.

The relatively large difference in adsorbed O_2 volume between measurements B4 and B5 can be attributed to i) sintering or ii) SMSI not having reached a steady state after B4 and continuing during B5.

4.5.1.1. XRD Measurements

A reference with a silver loading of 10 wt% Ag on P25 was synthesized and pretreated as follows: the oxidation step was carried out as usual. The reductive step was either carried out at 200 °C or at 300 °C. After that, O_2 chemisorption measurements were carried out.

Following the powder XRD, the Rietveld refinements were performed using Highscore Plus (PANalytical). For the sample reduced at 200 °C, an Ag crystallite size of 80 Å and for the sample reduced at 300 °C a crystallite size of 90 Å was calculated, the respective rietveld refinements are depicted in the appendix on the pages 103 and 104. The results are shown in Figure 67.

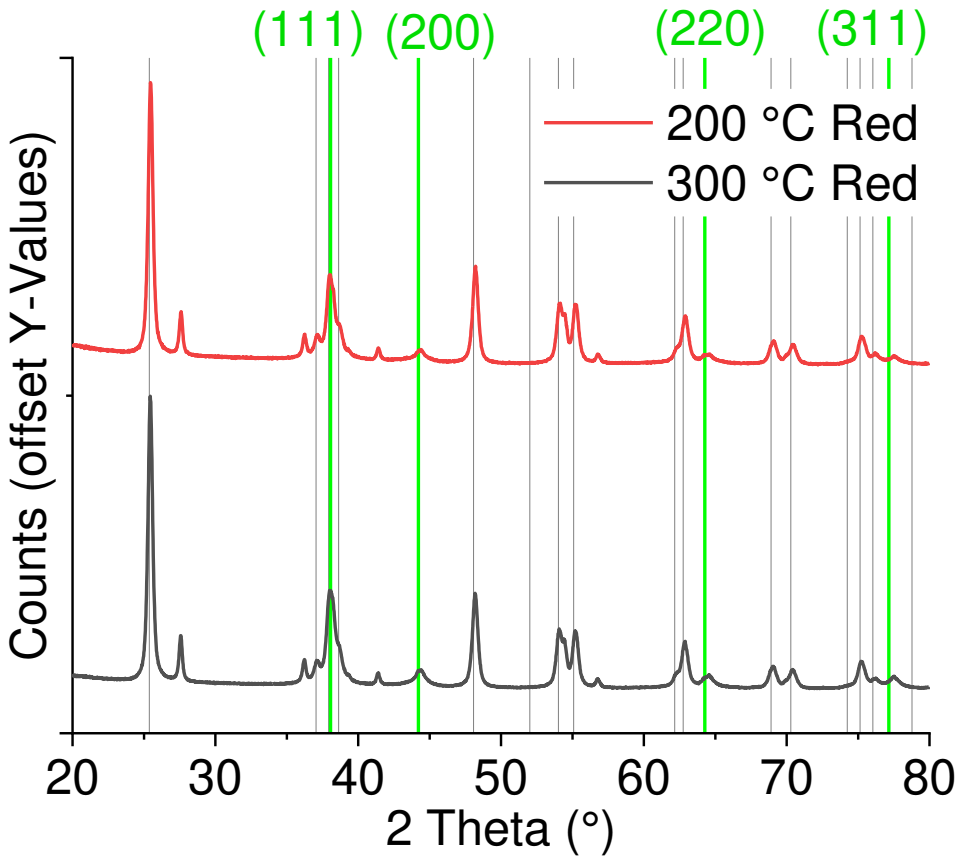

Figure 67 XRD powder patterns of 10 wt% Ag P25, reduced at 200 °C (in red) and at 300 °C (in black). In green are the reflexes of silver nanoparticles (reference code 04-001-2617), in grey the signals of titanium oxide (00-064-0863). The Bragg reflections at 38.06 °, 44.22 °, 64.27 ° and 77.16 ° correspond to (111), (200), (220) and (311). [50]

4.5.2. CO Adsorption sites

CO adsorption on references and catalysts repeatedly displayed a striking phenomenon: When gold on P25 is tested, the CO will adsorb on metallic gold. A peak at 2102 cm^{-1} is the consequence. However, as soon as silver is added onto the catalyst, the gold peak is no longer observable (see Figure 68). Two possible explanations for the disappearance of the gold peak are considered: either i) Ag or Ag_xO covers the Au or ii) a layer of suboxidic TiO_2 migrates onto the metal particles (as it is reported in literature as *SMSI effect* and explained in 2.2.2 on page 11). The list of peak assignments can be found in Table 6.

For Au Aurolite and the Au Ag Aurolite batch, there is a shoulder at 2165 cm^{-1} visible, which is ascribed to CO adsorbed on γ-Ti^{4+} sites. The relatively strong appearance can be reasoned by the low temperature during those measurements, owing to the strong temperature-dependency of the CO adsorption on γ-Ti^{4+} sites. [19] On 0.8 wt% Au 2.5/4.2 wt% Ag Aurolite, the mentioned shoulder at 2165 cm^{-1} is accompanied by another one at 2156 cm^{-1}, which is ascribed to the interaction of CO with residual OH groups located on TiO_2 defect sites. [51]

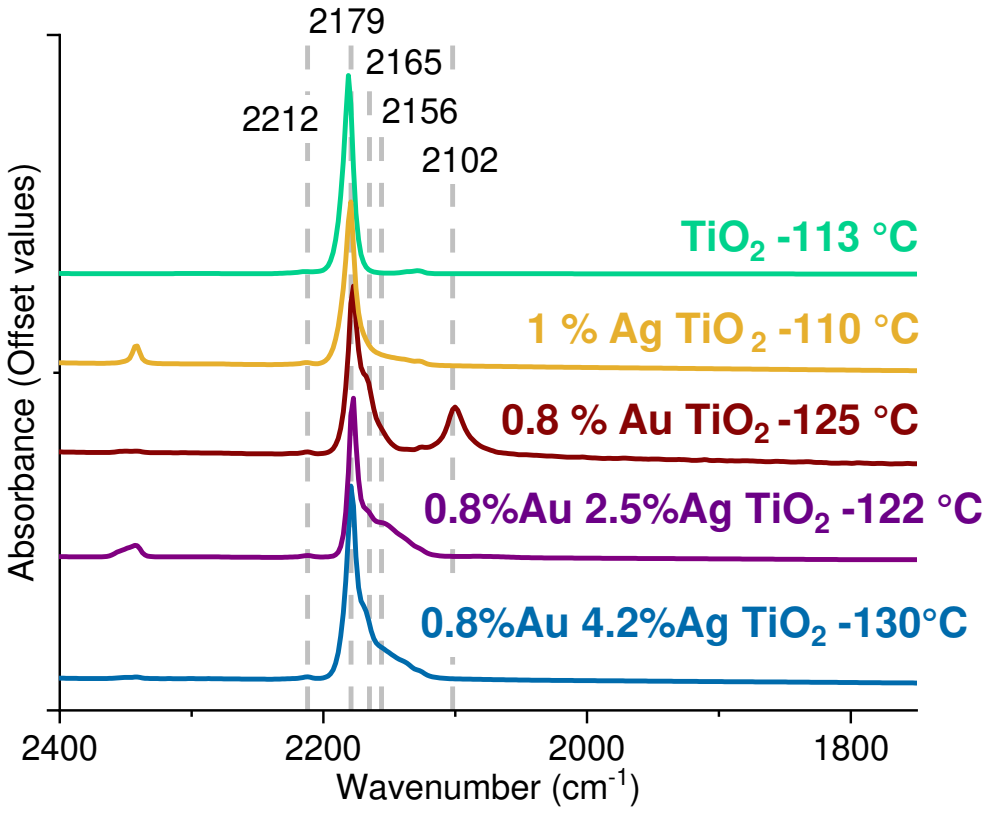

Figure 68 Adsorption of 5 mbar CO in the FTIR transmission cell on P25, 1 wt% Ag P25, 10 wt% Ag P25, Aurolite and the 0.8 wt% Au 4.2 wt% Ag Aurolite catalyst.

Table 6 CO Adsorption peak assignment

Measured wavenumbers (cm^{-1})	Adsorbens / References
2102	CO adsorbed on Au(0) / 2105 [52] / 2098 [53]
2156	few residual OH groups located on TiO_2 defect sites/ 2156-2158 [51]
2160-2165	CO adsorbed on $Ag^{\delta+}$ sites exposed at the surface of an Ag_xO layer fully covering the support / 2161 [52] *or* CO Adsorption on γ-Ti^{4+} on (001) and (112) and edges (101) x (011) anatase face / 2165 [19]
2179	CO adsorption on β-Ti^{4+}: most stable anatase face: (101) and (100) / 2179 [19]
2212	CO adsorption on α-Ti^{4+} sites: highly acidic Ti Lewis sites exhibiting very low coordination, e.g. located on edges, steps, and corners; faces (110), (111), (113) and edges of (110) face / 2212 [19]
2342	CO_2 adsorbed to Anatase / 2344 [51]

4.5.2.1. CO adsorption on β-Ti^{4+} and γ-Ti^{4+}

Due to measuring a peak at 2342 cm^{-1} -which is ascribed to CO_2 adsorbed to anatase [51]- it was assumed, that CO_2 must derive from incompletely reduced Ag ($Ag^{\delta+}$): CO reduces the residual AgO_x to Ag^0 and CO_2 is formed. The CO_2 peak was especially established in the catalyst with a 0.7 wt% Au and 7.3 wt% Ag loading, indicating that the reduction of Ag is incomplete when not all the Ag is in close contact with Au.

Therefore, the 0.7 wt% Au 7.3 wt% Ag Aurolite catalyst was chosen for the following measurements. The reductive step was once carried out as usual and once carried out more extensively: instead of reducing at 300 °C for 30 min under 50 mbar H_2, 200 mbar H_2 were introduced into the cell, and reduction was carried out at 350 °C for 3.5 h, before cooling down and exposure to 5 mbar CO. The following spectra were taken under 5 mbar CO, over the course of 10 min. The results are depicted in Figure 69.

Firstly, the most striking effect of the more extensive reduction is the lack of the CO_2 peak, which suggests that the above assumption is true, and the silver was not entirely reduced after the regular pretreatment. However, it is entirely reduced with the alternatively carried out pretreatment. Even when reducing the residual $Ag^{\delta+}$, there is still no CO adsorbed to Au^0 peak visible, excluding coverage of Au by Ag_xO as possible explanation for disappearance of the gold peak.

Secondly, when taking a closer look, another effect is noticeable: the signal at 2160 cm^{-1} becomes vastly stronger, after the more extensive reduction. As listed in Table 6, there are two possible explanations for a signal at that wavenumber: either CO adsorption on i) $Ag^{\delta+}$ sites or on ii) γ-Ti^{4+}. Firstly, as the signal turned out significantly stronger, after the reduction was carried out more extensively and the Ag was successfully reduced – it clearly supports the second explanation. Secondly, when taking the temperature into account, it shows that the lower the temperature is, the stronger the signal at 2160 cm^{-1} gets, which agrees with what was found in literature for the γ-Ti^{4+} sites. [19]

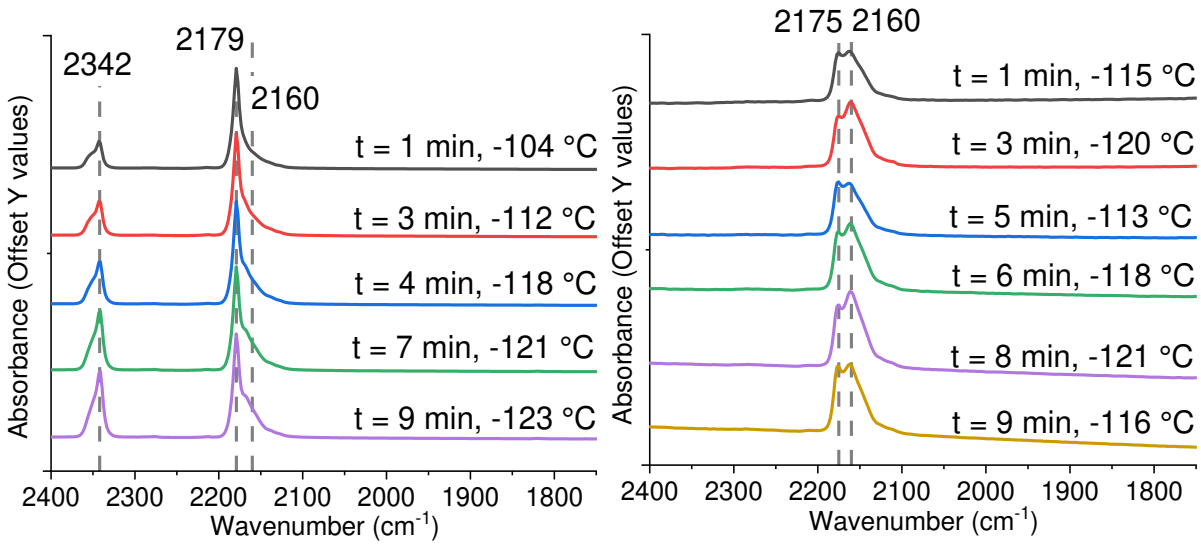

Figure 69 CO Adsorption on 0.7 wt% Au 7.3 wt% Ag Aurolite. Left side: after regular pretreatment. Right side: after more extensive reduction.

4.5.3. Catalytic activity dependent on reduction temperature

Catalytic activity showed no difference between reduction at 200 °C (R200) and reduction at 300 °C (R300) as it is depicted in Figure 70 and Figure 71, where EtOH conversion (in %) is plotted over the reaction time (in h). Measurements at 200 °C were carried out 4 times (M1 to M4), while measurements at 300 °C were carried out twice each.

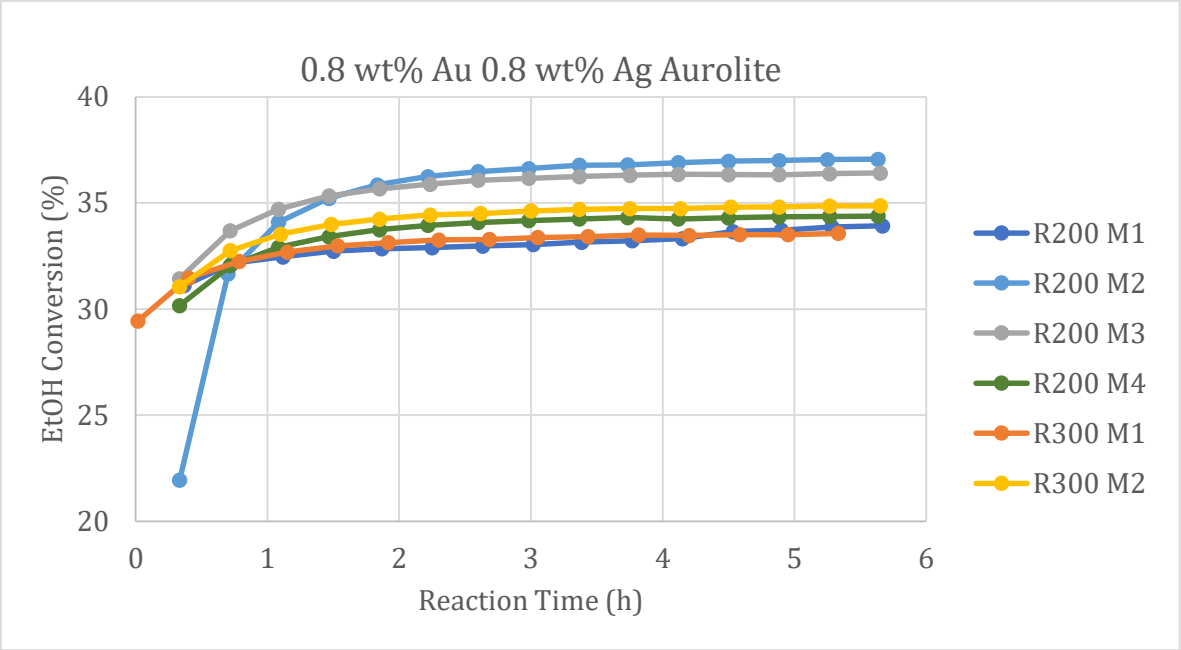

Figure 70 EtOH conversion (%) over reaction time (h) after reducing the 0.7 wt% Au 7.3 wt% Ag Aurolite catalyst at either 200 °C (R200) or 300 °C (R300).

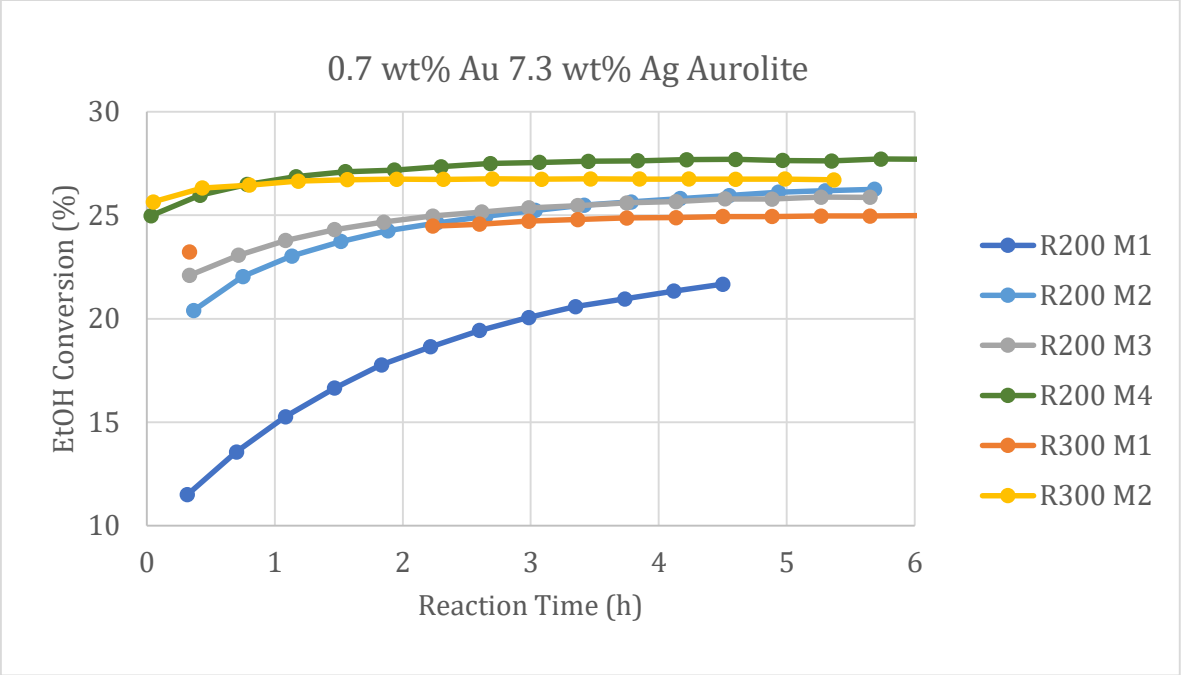

Figure 71 EtOH conversion (%) over reaction time (h) after reducing the 0.7 wt% Au 7.3 wt% Ag Aurolite catalyst at either 200 °C (R200) or 300 °C (R300).

4.5.4. Discussion

The results of O_2 chemisorption measurements demonstrate, that the temperature of reduction has significant impact on the accessible silver surface. According to XRD results, the crystallites differ from 8 nm to 9 nm in size, which is classified as insignificant difference. Either, the crystallites sintered, but re-dispersed during the presence of oxygen of the chemisorption pulses, or SMSI is the reason for the decrease of measured silver surface.

CO adsorption carried out in the FTIR transmission cell shows, that as soon as silver is present on the catalyst, gold is not measured to be on the surface anymore. This can be due to coverage of gold by either Ag, Ag_xO or TiO_x. Coverage of Ag_xO was ruled out by carrying out a more extensive reduction, and therefore reducing residual $Ag^{\delta+}$ to Ag^0. CO adsorption after the more extensive reduction also shows a remarkable increase of the signal originating from γ-Ti^{4+} sites. Those are reported to derive from highly acidic Ti Lewis sites e.g. located on edges, steps and corners [19] – again hinting towards SMSI (migration of a suboxidic TiO_x layer on top of the metal particles would lead to a high concentration of low coordinated sites on substoichiometric TiO_{2-x}). Additionally, for the catalysts with silver loading of > 1 wt%, there are peaks measured, that are accounted to residual OH groups located on TiO_2 defect sites. Summarizing, highly acidic Ti Lewis sites - e.g. located on edges, steps and corners- as well as OH groups located on TiO_2 defect sites, appear once silver is added to the catalysts. This indicates a modification of the TiO_2 surface by addition of silver, concluding that migration of a suboxidic TiO_x layer is most likely the reason for the disappearance of the gold peak.

Recalling the results of *4.3.1 EtOH Adsorption Sites* – where it was shown, that silver addition leads to adsorption of ethoxy in its bidentate form – are also hinting towards SMSI: a suboxidic TiO_x layer (on top of the metal particles) would also increase the probability of bidentate instead of monodentate adsorption.

However, there is no impact on the catalytic activity, whether reduction takes place at 200 °C or at 300 °C, suggesting, that the effect leading to reduced O_2 chemisorption – whether it is sintering or SMSI- reaches some kind of steady state at the given reaction conditions.

5. Conclusion and Outlook

Silver was added to the commercial catalyst "Aurolite" (0.8 wt% Au on an anatase/rutile mixture) by incipient wetness technique. Batches with four different silver loadings were synthesized: 0.8, 2.5, 4.2 and 7.3 wt% Ag were added onto Aurolite. TEM images result in a mean particle diameter of 5 nm, EDX images show bimetallic particles.

Performance-wise, addition of silver to Aurolite appears beneficial in selective oxidation of ethanol to acetaldehyde: catalytic activity and selectivity for acetaldehyde both increase with the silver loading. Benefits of the silver-addition however flatten out. From the catalyst containing 4.2 wt% Ag to the catalyst with 7.3 wt% Ag loading little to no performance-improvement is detected. At low temperatures of reaction (< 225 °C), a reference catalyst with a higher Au metal loading (2.8 wt% Au 1 wt% Ag Rutile) outperforms the Aurolite batch. Gold is known to show high activity at low temperatures, the increased activity below 225 °C is therefore most likely due to the higher gold content in the reference.

With silver-addition, the reactions apparent activation energy steadily rises. This is ascribed to (partial) coverage of the gold NP by silver and TiO_{2-x}. Silver addition also leads to a significant decrease of the oxygen reaction order, indicating a higher availability of activated oxygen in the presence of silver on TiO_2. The 4.2 wt% Ag catalyst delivers values between 0.0 and 0.1 for the oxygen reaction order, indicating oxygen is almost activated to its full extent and further addition of silver becomes more and more pointless.

FTIR measurements monitoring ethanol adsorption and desorption on and from Rutile, 5 wt% Au Rutile and 1 wt% Au 2 wt% Ag Rutile were carried out (both values are nominal values, LA-ICP-MS measurements resulted that the actual metal loading is significantly lower: 2.8 wt % Au instead of the 5 wt% Au were reported in the past [2]) and resulted in differing adsorption behavior of ethanol on the non-metallic, mono- and bimetallic Rutile catalysts. Compared to plain Rutile, 5 wt% Au Rutile shows slightly more bidentate adsorbed ethoxy species onto titania. On 1 wt% Au 2 wt% Ag Rutile the presence of bidentate adsorbed ethoxy species strongly increases. As described in more detail in *2.2 Oxygen activation and the role of titanium oxide and silver* from page 10 onwards, oxygen vacancy formation on the TiO_2 surface is known to be facilitated in the perimeter of Au NP. [17] Furthermore, encapsulation of Ag NP supported on TiO_2 by amorphous TiO_{2-x}

layers has been reported. [24] The higher concentration of oxygen vacancies on the TiO_2 surface is therefore ascribed to be the reason for the increased amount of bidentate adsorbed ethoxy groups to titania.

Ethoxy species adsorbing to an increased degree in their bidentate form might also be part of the reason for the increased apparent activation energies: By Pauling scale, the electronegativity of Ti is 1.54, while for C it values 2.55 and for O 3.44. When oxygen is bound to a Ti atom on the one side and C on the other, then it will withdraw more electron density from the O-Ti bonds and therefore less from the O-C bond. In a bidentate adsorbed ethoxy molecule, the C atom will be charged slightly less positively than in its monodentate counterpart – which will to some extent hinder the β-H-elimination, which is rate-limiting in the investigated reaction.

In-situ DRIFTS measurements helped shedding light onto the reaction mechanism: EtOH adsorbs in its ethoxy form to titania, then reacts to acetaldehyde, which mostly desorbs instantly. Otherwise, acetaldehyde either couples with ethoxy to ethyl acetate and desorbs, or oxidizes to acetate species, which remain adsorbed until high temperatures unless they are protonated. Once acetate species get protonated (which happens in the presence of EtOH), the produced acetic acid desorbs. If the acetates are not protonated, they decompose and desorb as CO_2 at above 350 °C. Under reaction conditions however, this does likely not happen, since EtOH is present and acetate groups will be protonated and desorb as acetic acid. Moreover, in presence of oxygen, adsorbed acetaldehyde also condensates to crotonaldehyde, which then remains on the TiO_2 surface slightly longer than the acetaldehyde itself.

Working at elevated temperatures is therefore not only beneficial for the reaction rate, but also the selectivity towards acetaldehyde: reaching the desorption temperature of acetaldehyde from the catalyst surface is critical for improved selectivity. At 400 °C, an ethanol conversion of 99.7 % with a selectivity towards acetaldehyde of 99 % is achieved with the 0.8 wt% Au 4.2 wt% Ag TiO_2 catalyst.

In accordance with literature reports, our oxygen chemisorption results, the XRD diffractograms and their rietveld refinement, and the results of FTIR monitored EtOH adsorption lead to the conclusion, that partial coverage (or even encapsulation) of the Ag by amorphous TiO_{2-x} takes place during the reductive step of pretreatment at 300 °C in 5 % H_2 in He. Owing to the bimetallic character of the particles. Au will be affected by the

migration of TiO_{2-x} as well - this is supported by the FTIR monitored CO adsorption results. During reaction conditions, a regression of the TiO_{2-x} layer and an altervalent state may be reached, explaining the indifference in the catalytic behavior, whether reduction is carried out at 300 °C or 200 °C.

Following the assumed migration of TiO_{2-x} layers onto the bimetallic Au Ag NP owing to the presence of silver, the stepwise silver addition between 0.8 wt% and 7.3 wt% leads to extended migration of TiO_{2-x} onto the bimetallic Au Ag NP, increasing the concentration of oxygen vacancies in the perimeter of the NP. The addition of silver is shown to be beneficial for the reaction rate. The increase of metal-support interface or rather oxygen vacancy concentration is therefore beneficial for the reaction rate as well, even though it includes a reduced accessibility of metal surface area.

Drawing a connection from the extended research about the Au-assisted Mars-van Krevelen mechanism in CO oxidation over Au TiO_2 catalysts (CO adsorbs on the Au nanoparticles, which then reacts with activated surface lattice oxygen species at the perimeter of the Au TiO_2 interface. At last, those interface sites get replenished by dissociative adsorption of O_2 [14] [15] [16] [17]), it appears that the strongly increased metal-support interface (due to the presence of silver) is the cause for the decrease of the oxygen reaction order. Activation of oxygen is accordingly not ascribed to merely silver alone, but more to the interaction of the Ag-TiO_2 and Au-TiO_{2-x} interface.

For future investigations, UV-VIS measurements to determine charge-transfer between Au and TiO_2, Ag and TiO_2, Au and Ag and TiO_2 will be of interest, whereas a comparison of anatase and rutile might shatter light onto why rutile leads to a more active catalyst in the selective oxidation of ethanol to acetaldehyde over Au Ag NP on TiO_2.

Literaturverzeichnis

[1] M. Eckert, „Acetaldehyde," in *Ullmann's Encyclopedia of Industrial Chemistry*, Weinheim, Wiley-VCH, 2007.

[2] A. Nagl und K. Föttinger, *Selective Oxidation of Ethanol on Modified Supported Au Catalysts: From Fundamental Understanding to Improved Performance,* TU Vienna: Doctoral Dissertation, 2019.

[3] S. Mostrou-Moser, J. A. Van Bokhoven, S. E. Pratsinis und K. Föttinger, *Oxidation of aqueous ethanol to acetic acid over heterogeneous catalysts,* ETH Zurich, 2020.

[4] N. Zheng und G. D. Stucky, „A General Synthetic Strategy for Oxide-Supported Metal Nanoparticle Catalysts," *J. Am. Chem. Soc.,* Nr. 128, pp. 14278-14280, 2006.

[5] Y. Guan und E. Hensen, „Ethanol dehydrogenation by gold catalysts: The effect of the gold particle size and the presence of oxygen," *Applied Catalysis A: General,* pp. 49-56, 2009.

[6] C. W. Corti, R. J. Holliday und D. T. Thompson, „Commercial aspects of gold catalysis," *Apllied Catalysis A: General,* Nr. 291, pp. 253-261, 2005.

[7] Y. Guan und E. J. M. Hensen, „Ethanol dehydrogenation by gold catalysts: The effect of the gold particle size and the presence of oxygen," *Applied Catalysis A: General,* Nr. 361, pp. 49-56, 2009.

[8] M. Rothensteiner, K. Föttinger und G. Rupprechter, *Selective Oxidation of Ethanol on Supported AuAg Bimetallic Catalysts,* Vienna: Master Diploma Thesis, 2012.

[9] S. Biella und M. Rossi, „Gas phase oxidation of alcohols to aldehydes or ketones catalysed by supported gold," *The Royal Society of Chemistry,* pp. 378-379, 2003.

[10] B. Zope, D. Hibbitts, M. NEurock und R. Davis, „Reactivity of the Gold/Water Interface During Selective Pxidation Catalysis," *Science,* Nr. 6000, pp. 74-78, 01 Oct 2010.

[11] X. Deng, B. K. Min, A. Guloy und C. M. Friend, „Enhancement of O2 Dissociation on Au(111) by Adsorbed Oxygen: Implications for Oxidation Catalysis," *J. Am. Chem. Soc.,* Nr. 127, pp. 9267-9270, 2005.

[12] S. McClure, T. Kim, J. Stiehl, P. Tanaka und C. Mullin, „Adsorption and Reaction of Nitric Oxide with Atomic Oxygen Covered Au(111)," *J. Phys. Chem. B,* Nr. 108, pp. 17952-17958, 2004.

[13] A. Abad, P. Concepción, A. Corma und H. García, „A Collaborative Effect between Gold and a Support Induces the Selective Oxidation of Alcohols," *Angew. Chem. Int. Ed.,* Nr. 44, pp. 4066-4069, 2005.

[14] D. Widmann und J. Behm, „Active Oxygen on a Au/TiO2 Catalyst: Formation, Stability, and CO Oxidation Activity," *Angew. Chem. Int.,* Nr. 50, pp. 10241-10245, 2011.

[15] H. Kim und G. Henkelman, „CO Oxidation at the Interface of Au Nanoclusters and the Stepped- CeO2(111) Surface by the Mars–van Krevelen Mechanism," *J. Phys. Chem. Lett.,* Nr. 4, pp. 216-221, 2013.

[16] D. Widmann und R. Behm, „Dynamic surface composition in a Mars-van Krevelen type reaction: CO oxidation on Au/TiO2," *Journal of Catalysis,* Nr. 357, pp. 263-273, 2018.

[17] P. Schlexer, D. Widmann, R. Behm und G. Pacchioni, „CO oxidation on a Au/TiO2 nanoparticle catalyst via the Au-Assisted Mars-van Krevelen Mechanism," *ACS Catalysis,* Nr. 8, pp. 6513-6525, 2018.

[18] D. Goodman, „''Catalytically active Au on Titania'': yet another example of a strong metal support interaction (SMSI)?," *Catalysis Letters,* Nr. 99, January 2005.

[19] K. I. Hadjiivanov und D. G. Klissurski, „Surface Chemistry of Titania (Anatase) and Titania-supported Catalysts," *Chemical Society Reviews,* 1996.

[20] M. Grabchenko, G. Mamontov, Zaikovskii V.I., V. La Parola, L. Liotta und O. Vodyankina, „The role of metal–support interaction in Ag/CeO2 catalysts for CO and soot oxidation," *Applied Catalysis B: Environmental,* Nr. 260, pp. 118-048, 2020.

[21] W. Figueiredo, G. Della Mea, M. Segala, D. Baptista, C. Escudero, V. Pérez-Dieste und F. Bernardi, „Understanding the Strong Metal–Support Interaction (SMSI) Effect in CuxNi1−x/CeO2 (0 < x < 1) Nanoparticles for Enhanced Catalysis," *ACS Appl. Nano Mater.,* Nr. 2, pp. 2599-2573, 2019.

[22] Q. Fu, T. Wagner, S. Olliges und H. Carstanjen, „Metal-Oxide Interfacial Reactions: Encapsulation of Pd on TiO2 (110)," *J. Phys. Chem. B,* Nr. 109, pp. 944-951, 2005.

[23] U. Diebold, „The surface science of titanium dioxide," *Surface Science Reports,* Nr. 48, pp. 53-229, 2003.

[24] P. Claus und H. Hofmeister, „Electron Microscopy and Catalytic Study of Silver Catalysts: Structure Sensitivity of the Hydrogenation of Crotonaldehyde," *J. Phys. Chem. B,* Nr. 103, pp. 2766-2775, 1999.

[25] W. Grünert, A. Brückner, H. Hofmeister und P. Claus, „Structural Properties of Ag/TiO2 Catalysts for Acrolein Hydrogenation," *J. Phys. Chem. B,* Nr. 108, pp. 5709-5717, 2004.

[26] G. Mamontov, M. Grabchenko, V. Sobolev, V. Zaikovskii und O. Vodyankina, „Ethanol dehydrogenation over Ag-CeO2/SiO2 catalyst: Role of Ag-CeO2 interface," *Applied Catalysis A: General,* Nr. 528, pp. 161-167, 2016.

[27] J. Liu, A. Wang, Y. Chi, H. Lin und C. Mou, „Synergistic Effect in an Au-Ag Alloy Nanocatalyst: CO Oxidation," *The Journal of Physical Letters B,* Nr. 109, pp. 40-43, 2005.

[28] M. C. Holz, K. Tölle und M. Muhler, „Gas-phase oxidation of ethanol over Au/TiO2 catalysts to probe metal–support interactions," *Catal. Sci. Technol.,* Nr. 4, pp. 3495-3504, 2014.

[29] B. Jørgensen, S. E. Christiansen, M. L. D. Thomsen und C. H. Christensen, „Aerobic oxidation of aqueous ethanol using heterogeneous gold catalysts: Efficient routes to acetic acid and ethyl acetate," *Journal of Catalysis,* Nr. 251, pp. 332-337, 2007.

[30] X. Liu, B. Xu, J. Haubrich, R. J. Madix und C. M. Friend, „Surface-Mediated Self-Coupling of Ethanol on Gold," *J. AM. CHEM. SOC.,* Nr. 131, pp. 5757-5759, 2009.

[31] A. Rismanchian, Y.-W. Chen und S. S. Chuang, „In situ infrared study of photoreaction of ethanol on Au and Ag/TiO2," *Catalysis Today,* Nr. 264, pp. 16-22, 2016.

[32] Z. Yu und S. S. Chuang, „In situ IR study of adsorbed species and photogenerated electrons during photocatalytic oxidation of ethanol on TiO2," *Journal of Catalysis,* Nr. 246, pp. 118-126, 2007.

[33] M. Buchalska, M. Kobielusz, A. Matuszek, M. Pacia, S. Wojtyla und W. Macyk, „On Oxygen Activation at Rutile- and Anatase-TiO2," *ACS Catal.,* Nr. 5, pp. 7424-7431, 2015.

[34] M. Latschka und K. Föttinger, *Kinetic Studies on Bimetallic Au Nanoparticles,* Vienna: Bachelor Thesis, 2017.

[35] M. Rothensteiner, K. Föttinger und G. Rupprechter, *Selective Oxidation of Ethanol on Supported AuAg Bimetallic Catalysts,* Vienna, 2012.

[36] T. Bürgi und A. Baiker, „Attenuated Total Reflection Infrared Spectroscopy of Solid Catalysts Functioning in the Presence of Liquid-Phase Reactants," *Adv. Catal.,* Nr. 50, p. 227–283, 2006.

[37] A. Urakawa, R. Wirz, T. Bürgi und A. Baiker, „ATR-IR Flow-Through Cell for Concentration Modulation Excitation Spectroscopy: Diffusion Experiments and Simulations," *J. Phys. Chem. B,* Nr. 107, pp. 13061-13068, 2003.

[38] D. A. Panayotov und J. T. Yates Jr., „Depletion of conduction band electrons in TiO2 by water chemisorption – IR spectroscopic studies of the independence of Ti–OH frequencies on electron concentration," *Chemical Physics Letters,* Nr. 410, pp. 11-17, 2005.

[39] T. Bezrodna, G. Puchkovska, V. Shymanovska, J. Baran und H. Ratajczak, „IR-analysis of H-bonded H2O on the pure TiO2 surface," *Journal of Molecular Structure,* Nr. 700, pp. 175-181, 2004.

[40] A. Nagl und K. Föttinger, *Selective Oxidation of Ethanol on Modified Supported Au Catalysts: From Fundamental Understanding to Improved Performance,* TU Vienna, 2019.

[41] W.-C. Wu, C.-C. Chuang und J.-L. Lin, „Bonding Geometry and Reactivity of Methoxy and Ethoxy Groups Adsorbed on Powdered," *J. Phys. Chem. B,* Nr. 104, pp. 8719-8724, 2000.

[42] G. A. M. Hussein, N. Sheppard, M. I. Zaki und R. B. Fahim, „Infrared Spectroscopic Studies of the Reactions of Alcohols over," *J. CHEM. SOC. FARADAY TRANS.,* Nr. 87(16), pp. 2661-2668, 1991.

[43] J. Raskó, A. Hancz und A. Erdöhelyi, „Surface species and gas phase products in steam reforming of ethanol on TiO2 and Rh/TiO2," *Applied Catalysis A: General,* Nr. 269, pp. 13-25, 2004.

[44] M. Singh, N. Zhou, D. K. Paul und K. J. Klabunde, „IR spectral evidence of aldol condensation: Acetaldehyde adsorption over TiO2 surface," *Journal of Catalysis,* Nr. 260, pp. 371-379, 2008.

[45] R. Nakamura, K. Ueda und S. Sato, „In Situ Observation of the Photoenhanced Adsorption of Water on TiO2 Films by Surface-Enhanced IR Absorption Spectroscopy," *Langmuir,* Bd. 17, Nr. 8, pp. 2298-2300, 2001.

[46] J. E. Rekoske und M. A. Barteau, „Competition between Acetaldehyde and Crotonaldehyde during Adsorption and Reaction on Anatase and Rutile Titanium Dioxide," *Langmuir,* Nr. 15, pp. 2061-2070, 1999.

[47] J. Rasko, T. Kecskés und J. Kiss, „FT-IR and mass spectrometric studies on the interaction of acetaldehyde with TiO2-supported noble metal catalysts," *Applied Catalysis A: General,* Nr. 287, pp. 244-251, 2005.

[48] W. Rachmady und M. A. Vannice, „Acetic Acid Reduction by H2 over Supported Pt Catalysts: A DRIFTS and TPD/TPR Study," *Journal of Catalysis,* Nr. 207, pp. 317-330, 2002.

[49] D. Kozlov, E. Paukshtis und E. Savinov, „The comparative studies of titanium dioxide in gas-phase ethanol photocatalytic oxidation by the FTIR in situ method," *Applied Catalysis B: Environmental,* Nr. 24, pp. L7-L12, 2000.

[50] A. M. Awwad, N. M. Salem und A. O. Abdeen, „Green synthesis of silver nanoparticles using carob leaf extract and its antibacterial activity," *International Journal of Industrial Chemisty (IJIC),* Nr. 4:29, 2013.

[51] L. Mino, G. Spoto und A. Ferrari, „CO2 Capture by TiO2 Anatase Surfaces: A Combined DFT and FTIR Study," *J. Phys. Chem. C,* Nr. 118, pp. 25016-25026, 2014.

[52] F. Boccuzzi, A. Chiorino, M. Manzoli, D. Andreeva, T. Tabakova, L. Ilieva und V. Iadakiev, „Gold, silver and copper catalysts supported on TiO2 for pure hydrogen production," *Catalysis Today,* Nr. 75, pp. 169-175, 2002.

[53] F. Menegazzo, M. Manzoli, A. Chiorino, F. Boccuzzi, T. Tabakova, M. Signoretto, Pinna F. und N. Pernicone, „Quantitative determination of gold active sites by chemisorption and by infrared measurements of adsorbed CO," *Journal of Catalysis,* Nr. 237, pp. 431-434, 2006.

[54] K. Rintramee, K. Föttinger, G. Rupprechter und J. Wittayakun, „Ethanol adsorption and oxidation on bimetallic catalysts containing platinum and base metal oxide supported on MCM-41," *Applied Catalysis B: Environmental,* Nr. 115-116, pp. 225-235, 2012.

[55] D. Baurecht und U. Fringeli, „Quantitative modulated excitation Fourier transform infrared spectroscopy," *REVIEW OF SCIENTIFIC INSTRUMENTS,* Nr. 72, pp. 3782-3792, 2001.

[56] H. Liu, A. Kozlov, A. Kozlova, T. Shido, K. Asakura und Y. Iwasawa, „Active Oxygen Species and Mechanism for Low-Temperature CO Oxidation Reaction on a TiO2-Supported Au Catalyst Prepared from Au(PPh3)(NO3) and As-Precipitated Titanium Hydroxide," *Journal of Catalysis,* Nr. 185, pp. 252-264, 1999.

Appendix

a. Details for Kinetic Measurements

GC Settings

An Agilent 7890A GC was used for on-line analysis of the product stream. 1000 µL of sample were introduced at 110°C, the inlet was operated in splitless mode and the carrier gas flow (He) was kept at 6 mL min^{-1}. For 4.5 min, the column was held at 40 °C, followed by a rapid heating (100 °C min^{-1}) to 200 °C was conducted, where it was kept for 11 min. The GC was equipped with an FID and a TCD detector. The FID Detector was set at 250 K with a 40 mL min^{-1} H_2 and 400 mL min^{-1} synthetic air flow. The TCD was set at 220°C with a 20 mL min^{-1} reference flow. The molar concentration of each component was determined using linear regression of calibration standards. This GC program was optimized for speed, allowing an injection every 23 minutes.

Flow Settings for Reaction Order Measurements

Table 7 Flow settings for the determination of oxygen reaction orders

$EtOH/O_2$ ratio	O_2 flow [mL min^{-1}]	EtOH flow [mL min^{-1}]	Total flow [mL min^{-1}]	p_{EtOH} [kPa]	p_{O2} [kPa]
1/0.5	0.55	1.10	50.64	2.2	1.1
1/1	1.10	1.10	51.18	2.2	2.2
1/1.5	1.70	1.10	51.79	2.1	3.3
1/2	2.20	1.10	52.29	2.1	4.3
1/2.5	2.70	1.10	52.79	2.1	5.2
1/4	4.40	1.10	54.49	2.0	8.2

Table 8 Flow settings for the determination of EtOH reaction orders

O_2/EtOH ratio	O_2 flow [mL min^{-1}]	EtOH flow [mL min^{-1}]	Total flow [mL min^{-1}]	p_{EtOH} [kPa]	p_{O2} [kPa]
5/0.25	5	0.26	49.73	0.5	10
5/0.60	5	0.62	50.00	1.2	10
5/1.1	5	1.10	50.00	2.2	10
5/1.65	5	1.64	50.00	3.3	10
5/2.2	5	2.21	50.21	4.5	10

b. Rietveld Refinement of XRD diffractograms for particle size evaluation

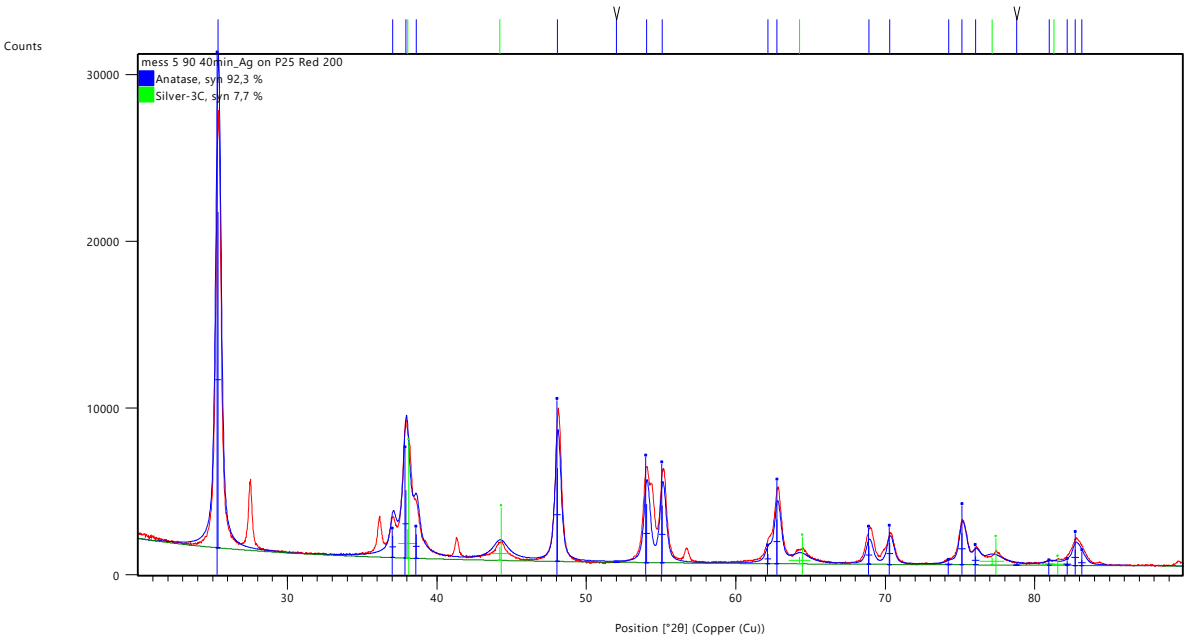

Figure 72 Rietveld Refinement for P25 with 10 wt% Ag reduced at 200 °C

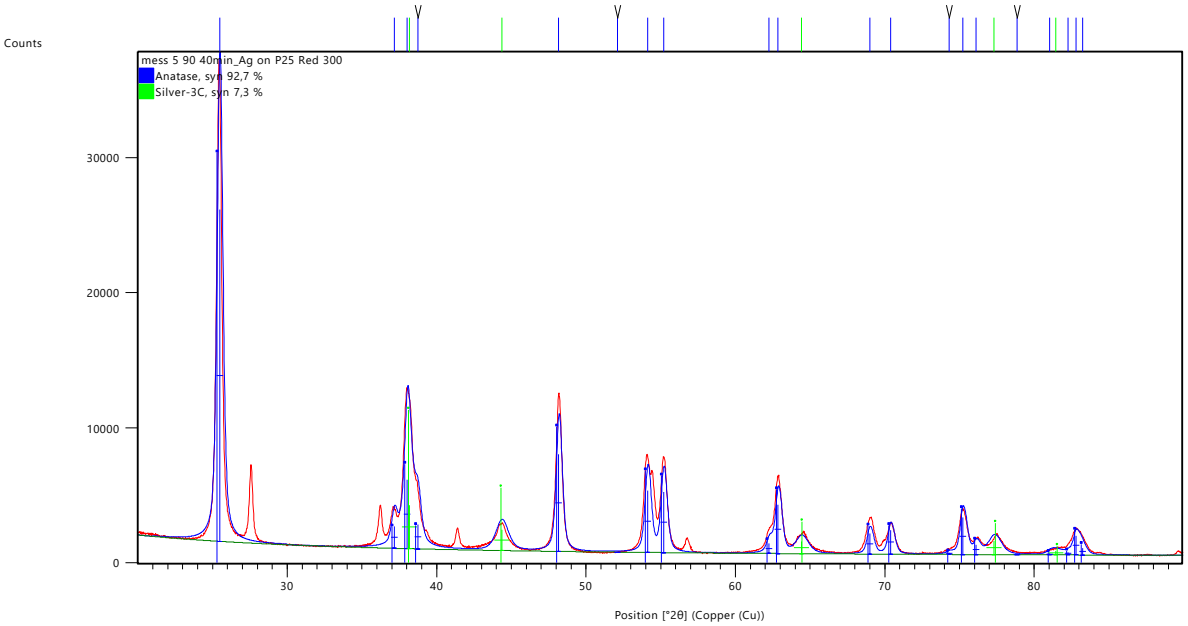

Figure 73 Rietveld Refinement for P25 with 10 wt% Ag reduced at 300 °C

c. Modulation excitation spectroscopy

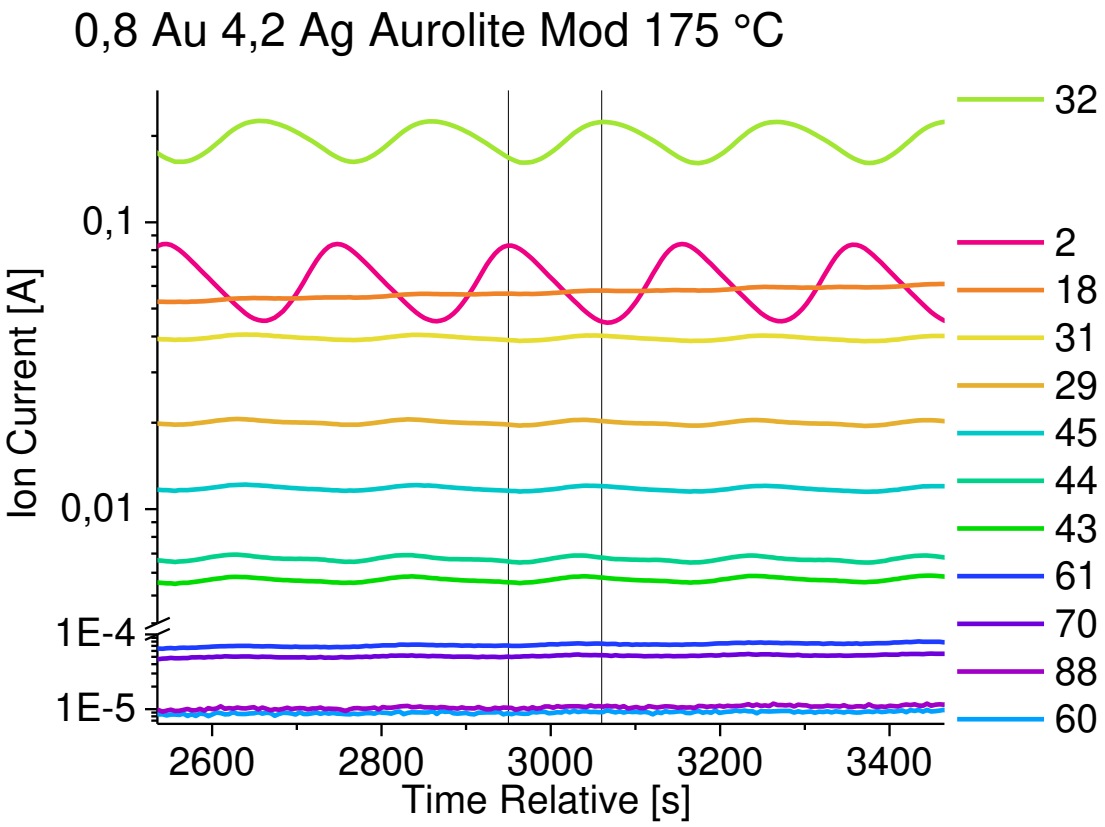

Figure 74 Normalized ion current signals of MS detection during MES with 0.8 wt% Au 4.2 wt% Ag Aurolite at 175 °C: He EtOH O_2 (1st half period) vs He EtOH H_2 (2nd half period); one half-period lasted 101 s; different m/z values are depicted in varying colours.

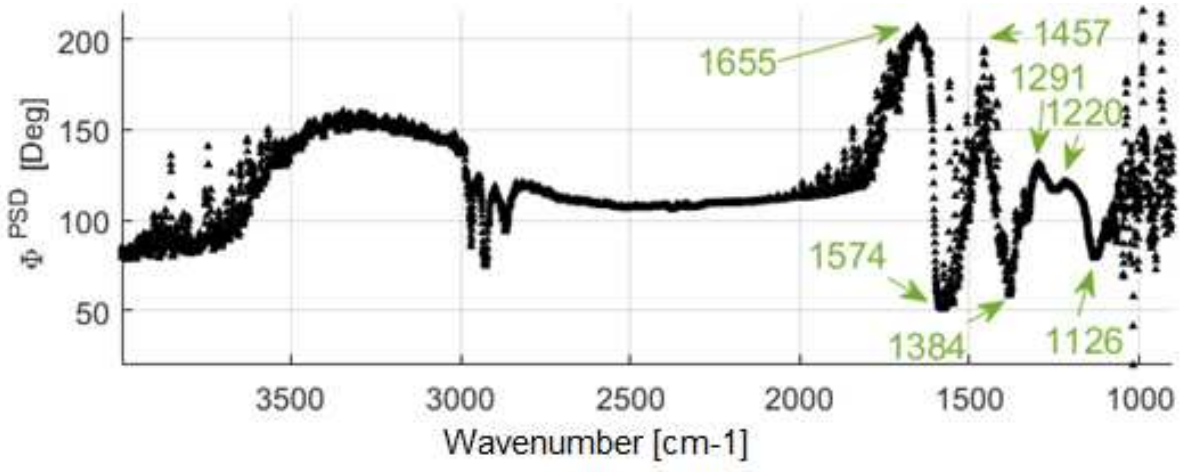

Figure 75 MES with 0.8 wt% Au 4.2 wt% Ag Aurolite at 175 °C: He EtOH O_2 (1st half period) vs He EtOH H_2 (2nd half period); one half-period lasted 101 s; in-phase angles for each wavenumber.

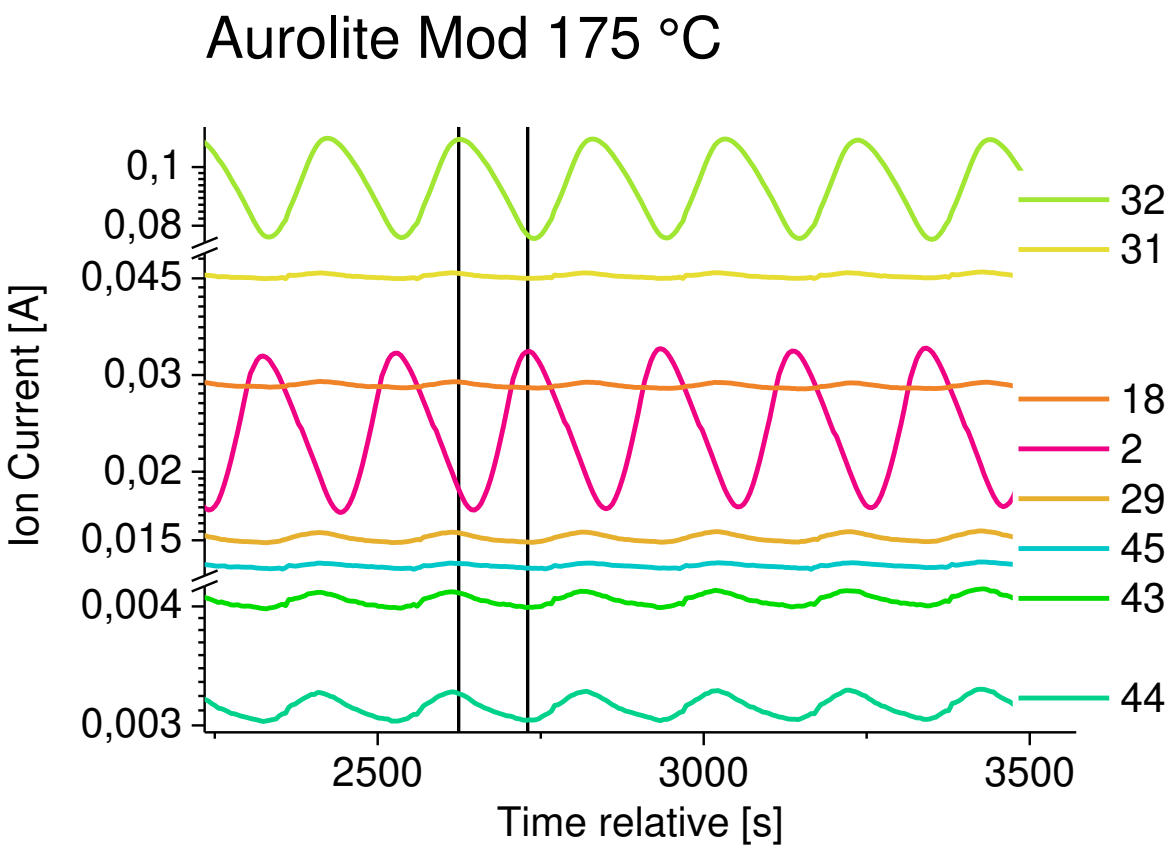

Figure 76 Normalized ion current signals of MS detection during MES with 0.8 wt% Au Aurolite at 175 °C: He EtOH O_2 (1st half period) vs He EtOH H_2 (2nd half period); one half-period lasted 101 s; different m/z values are depicted in varying colours.

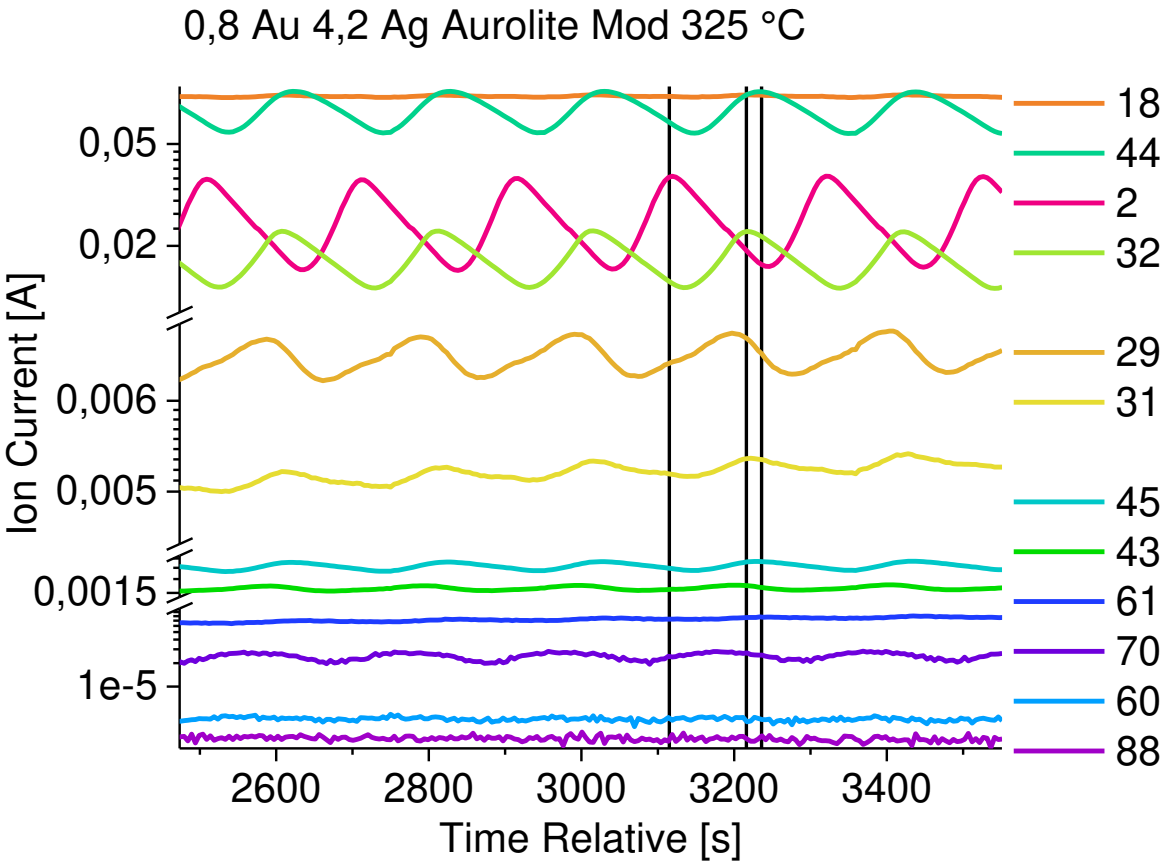

Figure 77 Normalized ion current signals of MS detection during MES with 0.8 wt% Au 4.2 wt% Ag Aurolite at 325 °C: He EtOH O_2 (1st half period) vs He EtOH H_2 (2nd half period); one half-period lasted 101 s; different m/z values are depicted in varying colours.